

Dynamic Analysis of a Drill-string under Deterministic and Random Excitations

by

©Hongyuan Qiu

A Thesis submitted to the School of Graduate Studies in partial fulfillment of the
requirements for the degree of

Master of Engineering

Department of Engineering and Applied Science

Memorial University of Newfoundland

October 2014

St. John's

Newfoundland

AUTHOR'S DECLARATION

I hereby declare that I am the sole author of this thesis. This is a true copy of the thesis, including any required final revisions, as accepted by my examiners. I understand that my thesis may be made electronically available to the public.

Abstract

Drill-strings are slender structures used to dig into the rock in search of oil and gas. Failures of drill-strings are time and money consuming and therefore the dynamics of drill-strings must be investigated and carefully controlled.

In the thesis, a dynamic model of the drill-string that is suitable for predicting axial, torsional and lateral vibrations is built using Euler-Bernoulli beam theory. The drill-string is driven by a DC motor on the top and is subjected to distributed loads due to its own weight as well as bit/formation interaction. The model is axial-torsional, lateral-torsional coupled. Under deterministic excitations, the model captures stick-slip behavior in drilling operation. Analysis on its negative effect on drilling performance is made, and potential mitigation measures are also discussed. In random model, the excitations to the drill-bit are modeled as combination of deterministic and random components. Monte Carlo (MC) simulation is employed to obtain the statistics of the response. Two cases of random excitation with different intensities are investigated. The results from MC simulation are compared against that from deterministic case.

Secondly, the thesis focuses on the drill-string torsional vibration and its stick-slip analysis. A finite element model of the drillstring with inclusion of both deterministic and random excitations is also developed. Simulation is carried out under certain parameters and it is shown that in deterministic case the torsional vibration may

behave stick-slip. With change of some parameters, bifurcation and chaos of the system are observed. In the random case, Monte Carlo simulation and path integration method are used to capture the probabilistic information of the response. The results of path integration match well to those of deterministic cases.

Although there are some limitations, this thesis will help the author better understand drill-string downhole behaviors and lay a foundation for further research work.

Keywords: Drill-string, Finite element model, Stick-slip, Random excitation, Path integration

Acknowledgements

The author would like to acknowledge the input and support from many people.

First of all, the author would like to express his special thanks to his close relatives for their supports.

Then, the author would like to express his thanks to his supervisor, Dr. James Yang, for his professional supervision, critical discussions and immeasurable contributions during the last two years. Without his guidance and ideas, this work will never be completed. As a respected supervisor, Dr. James Yang is also a trustworthy friend and an easy-going person. The author would also like to express his thanks to Dr. Geoff Rideout for the valuable advice and help during his studies.

The author would like to express his thanks to the friends he made here. It is the friendship that relieves the homesick, brings the happiness and offers warmly help.

Finally, the author would like to express his sincere gratitude to the faculty, staff, and students of the Department of Engineering and Applied Science for making his study at MUN such a great experience.

Notes on Units of Dimensions

The drilling industry normally uses imperial units to report the relative parameters while International System of Units (SI) is employed in some research. In this thesis, SI units are mainly used and other units will be converted. Table 1 shows the conversion between Centimetre–Gram–Second unit system (CGS) and SI unit system for some quantities related in this reasearch.

Table 1: Conversion between CGS and SI units in Mechanics

Quantity	Symbol	CGS unit	Equivalent in SI units
Length/Position	L/x	cm	$10^{-2}m$
Mass	m	g	$10^{-3}Kg$
Time	t	s	$1s$
Force	F	$dyne$	$10^{-5}N$
Pressure	P	Bar	$10^{-1}Pa$
Dynamic Viscosity	μ	$Poise$	$10^{-1}Pa \cdot s$

Table of Contents

AUTHOR’S DECLARATION	ii
Abstract	iii
Acknowledgments	v
Notes on Units of Dimensions	vi
Table of Contents	x
List of Tables	xi
List of Figures	xiv
List of Symbols, Nomenclature or Abbreviations	xv
1 Introduction	1
1.1 Overview of a Rotary Drill Rig Systems	1
1.1.1 Drill-string	3
1.1.2 Drill-bit	3
1.1.3 Drilling fluid	5
1.1.4 Hoisting system	5
1.1.5 Power generation system	6

1.1.6	Well blowout preventer	6
1.1.7	Measurement while drilling equipment	6
1.2	Down-hole Vibration	6
1.2.1	Axial vibration	7
1.2.2	Torsional vibration	8
1.2.3	Lateral vibration	8
1.2.4	Coupled vibrations	9
1.3	Brief Introduction of the Thesis	10
1.3.1	Objective and significance	11
1.3.2	Methodology	11
1.3.3	Limitations	11
1.4	Conclusion	11
2	Literature Review	12
2.1	Drill-string finite element model	12
2.2	Bit-bounce and stick-slip vibration research	14
2.3	Downhole uncertainty research review	19
2.4	Remarks	22
3	Finite Element Model	23
3.1	Euler-Bernoulli Beam	23
3.2	Simple Simulation	25
3.2.1	Model Introduction	25
3.2.2	Simulation Results and Conclusion	26
3.3	Covariance Matrix Solution to Linear Drill-string System	30
4	Stochastic and Deterministic Vibration Analysis on Drill-string with Finite Element Method	33

4.1	Dynamic Model	35
4.1.1	Dynamic model and deterministic excitations	35
4.1.2	Initial deformed condition	39
4.1.3	Model simplification	39
4.2	Simulation Setup and Results	40
4.2.1	Deterministic results	40
4.2.2	Monte Carlo Simulation for Random Case	46
4.2.3	Random Response Statistics	50
4.3	Conclusion Remarks	56
5	Stick-slip Analysis of a Drill-string under Deterministic and Stochastic Circumstances	57
5.1	Dynamic Model	58
5.1.1	Finite Element Model	58
5.1.2	Dynamic Equation	60
5.2	Solution Strategy	62
5.3	Results from Deterministic Excitations	63
5.3.1	Stick-slip	63
5.3.2	Bifurcation and Chaos	65
5.4	Results Considering Random Components	68
5.5	Conclusions	70
6	Stick-slip Analysis of a Drill-string Using Path Integration	73
6.1	Dynamic Model	73
6.2	System Dimensionless	76
6.3	Path Integration	77
6.3.1	Brief introduction	77

6.3.2	Numerical procedure	79
6.3.3	Calculation method for purely slip case	80
6.3.4	Calculation method for stick-slip case	81
6.4	Simulation Results	85
6.4.1	Simulation results of purely slip case	85
6.4.2	Simulation results of stick-slip case	87
6.5	Conclusions	92
7	Conclusion and Recommendations	93
7.1	Achievements	93
7.2	Recommendations for Future Work	94
	Bibliography	95
	Appendix A	101
	Appendix B	102

List of Tables

1	Conversion between CGS and SI units in Mechanics	vi
6.1	Deterministic results of x and v	86
6.2	Probability of slip and stick at each point	92
7.1	Drill-string data.	101

List of Figures

1.1	Basic Elements of a Drill Rig System [3]	2
1.2	A tricone bit [5]	4
1.3	A PDC bit [6]	4
1.4	Hoisting system [7]	5
1.5	Modes of vibration in drill-string [11]	7
1.6	BHA whirl phenomenons [11]	9
1.7	Drill-string vibration mechanisms, after [14]	10
2.1	The model introduced in [20]	14
2.2	Simplified drill-string model in [22]	15
2.3	Drill-string model describing the torsional behaviour in [23]	16
2.4	Sketch of a simplified model of the drilling system in [24]	17
2.5	Simplified model of the drilling system in [25]	18
2.6	Excitation models for BHA with a tricone bit (a) and a PDC bit (b)	20
2.7	Sketch of the system analyzed in [33]	21
3.1	Degrees of freedom of an element	24
3.2	Axial displacement of the beam (Matlab Result)	27
3.3	Axial displacement of the beam (Abaqus Result)	27
3.4	Lateral displacement of the beam (Matlab Result)	28

3.5	Lateral displacement of the beam (Abaqus Result)	28
3.6	Torsional displacement of the beam (Matlab Result)	29
3.7	Torsional displacement of the beam (Abaqus Result)	29
4.1	The simplified model of the system	34
4.2	Desired table speed is 15 <i>rad/s</i> and stick-slip is detected	41
4.3	Increasing desired table speed from 15 <i>rad/s</i> to 30 <i>rad/s</i>	41
4.4	Time-based axial stress of each element	42
4.5	Time-based torsional surface stress of each element	43
4.6	Increasing <i>ratio</i> from 0.6 to 0.8	44
4.7	Bit trajectory when desired table speed is 15 <i>rad/s</i>	45
4.8	Bit trajectory when desired table speed is 30 <i>rad/s</i>	46
4.9	System response under deterministic excitation	49
4.10	System response with white noise ($S_0 = 200$)	50
4.11	System response with white noise ($S_0 = 2000$)	51
4.12	Mean bit speed (MC, $S_0 = 200$)	51
4.13	Bit speed standard deviation (MC, $S_0 = 200$)	52
4.14	Mean bit speed (MC, $S_0 = 2000$)	52
4.15	Bit speed standard deviation (MC, $S_0 = 2000$)	53
4.16	σ for bit axial displacement (MC, $S_0 = 200$)	54
4.17	σ for bit y direction (MC, $S_0 = 200$)	54
4.18	σ for bit z direction (MC, $S_0 = 200$)	55
5.1	The simplified model of the system	58
5.2	Stick-slip is detected in model 1	63
5.3	Stick-slip is detected in model 2	64
5.4	Stick-slip is eliminated by increasing the ground speed to 55 <i>rad/s</i>	65

5.5	Friction coefficients induced bifurcation	66
5.6	Frequency induced bifurcation	66
5.7	Damping induced bifurcation	67
5.8	Chaos is detected when u_2 is 0.14, u_1 is 0.2 and w is 1 <i>rad/s</i>	68
5.9	Mean relative bit speed (rad/s) and the corresponding phase plane	69
5.10	Phase plane for all MC samples	70
5.11	Probability density estimate of the bit	71
5.12	Probability density estimate of the bit displacements when bit changes between stick and slip	72
6.1	The simplified model of the system	74
6.2	Stick-slip response after making the system dimensionless	77
6.3	The figure for describing purely slip case	80
6.4	The figure for explaining calculation method for stick-slip case	82
6.5	Evolution of probability density at (a) $9\frac{1}{4}T$; (b) $9\frac{2}{4}T$; (c) $9\frac{3}{4}T$; (d) $10T$	85
6.6	Contour of the corresponding probability density distribution	86
6.7	Evolution of probability density at (a) P_0 ; (b) P_1 ; (c) P_2 ; (d) P_3	88
6.8	Contour of the corresponding probability density distribution	89
6.9	Evolution of probability density at (a) P_4 ; (b) P_5 ; (c) P_6 ; (d) P_7	90
6.10	Contour of the corresponding probability density distribution	91
7.1	Monte Carlo simulation and stochastic central difference method result1	103
7.2	Monte Carlo simulation and stochastic central difference method result2	103
7.3	Monte Carlo simulation of duffing oscillator ($k = 1$)	104
7.4	Monte Carlo simulation of duffing oscillator ($k = 100$)	105
7.5	Monte Carlo simulation of duffing oscillator ($k = 100$, sample = 10000)	105

List of Symbols, Nomenclature or Abbreviations

For chapter 4

$l_e = 50$ For drillpipe

$l_e = 20$ For drillcollar

$J = 1.754 \times 10^{-5} m^4$ For drillpipe

$J = 2.648 \times 10^{-4} m^4$ For drillcollar

$g = 9.84 m/s^2$ Gravity Acceleration

$G = 7.6923 \times 10^{10} N/m^2$ Drill-string shear modulus

$E = 210 Gpa$ Drill-string elastic modulus

$\rho = 7850 kg/m^3$ Drill-sting density

$E_0 = 4 \times 10^{10} N/m^2$ Rock elastic modulus

$\nu = 0.25$ Poisson ratio

$G_0 = 1.6 \times 10^{10} N/m^2$ Rock shear modulus

$r_0 = 0.2$ Foundation diameter

$\rho_0 = 2100 kg/m^3$ Rock density

$k_c = 4.27 \times 10^9 N/m$ Rock stiffness

$c = 1.05 \times 10^6$ Rock damping coefficient

$m = 500 kg$ Stabilizer mass

$k = 10 \text{ MN/m}$ Stabilizer stiffness

$r = 0.03 \text{ m}$ Eccentric distance of stabilizer mass

w Average bit speed

$r_b = 0.22$ Bit radius

$L = 0.005 \text{ H}$ Motor inductance

$R_m = 0.01 \text{ } \Omega$ Armature resistance

$K_m = 6 \text{ V/s}$ Motor constant

$n = 7.2$ Gear ratio of the gearbox

$\alpha = 0.01$

$\beta = 0.01$

$c_1 = 1.35 \times 10^{-8}$

$c_2 = -1.9 \times 10^{-4}$

$\xi_0 = 1$

$\alpha_1 = 2$

$\alpha_2 = 1$

$\nu = 0.01$

For chapter 5

$G = 7.6923 \times 10^{10} \text{ N/m}^2$ Drill-string shear modulus

$\rho = 7850 \text{ kg/m}^3$ Drill-string density

$l_e = 50 \text{ m}$ For drillpipe

$l_e = 20 \text{ m}$ For drillcollar

$J = 1.754 \times 10^{-5} \text{ m}^4$ For drillpipe

$J = 2.648 \times 10^{-4} \text{ m}^4$ For drillcollar

$\alpha = 0.01$

$\beta = 0.01$

$F = 2 \times 10^4$ N Constant force

$WOB = 4 \times 10^4$ N Constant weight on bit

$r_b = 0.22$ Bit radius

$\omega = 5$ rad/s Frequency of the harmonic excitation, default

$S_0 = 20$ Power spectral density

For chapter 6

$l = 1000$ m Drill-string total length

$G = 7.6923 \times 10^{10}$ N/m² Drill-string shear modulus

$\rho = 7850$ kg/m³ Drill-string density

$J = 1.754 \times 10^{-5}$ m⁴ Polar moment of inertia of the cross section

$\alpha = 0.1$

$\beta = 0.1$

$WOB = 400000$ N Constant weight on bit

$r_b = 0.22$ Bit radius

$k = 1$ dimensionless system stiffness

$c = 0.345$ dimensionless system damping

$m = 1$ dimensionless system mass

$f_0 = 1.4260$

$f_1 = 1.7195$

$f_2 = 0.1853 \sin(1.2778t)$

$e = 0.01$ Numerical calculation threshold

$V = 0.2$

$r = 0.0632$

$r_1 = 0.000637$

Chapter 1

Introduction

Nowadays, natural resources are becoming more and more important in fueling our industrial development. Among them, the crude oil, or petroleum, is the crucial resource in the modern economy. Driven by the development of modern technology, the growth in drilling technology over the 20th century was enormous [1]. After changing from cable tool method to rotary drilling method, the drilling efficiency was largely improved and boreholes can be drilled to much greater depth. It was reported that the deepest holes of all are made for oil, and they sometimes go down to as much as 10000 meters in search of it. Measurement While Drilling (MWD), Rotary Steerable Tools and advanced drill bits made drilling along specified well paths possible [2]. Floating drill ships and marine risers realized human offshore drilling dreams [2].

1.1 Overview of a Rotary Drill Rig Systems

Drill rig system in petroleum industry is normally the massive structure housing equipment used to drill oil, or natural gas exploration and production wells. When it has been decided where to drill, an oil derrick will be put up at the surface. In order to get the oil out, the great length of drill-string, which is rotated by an engine

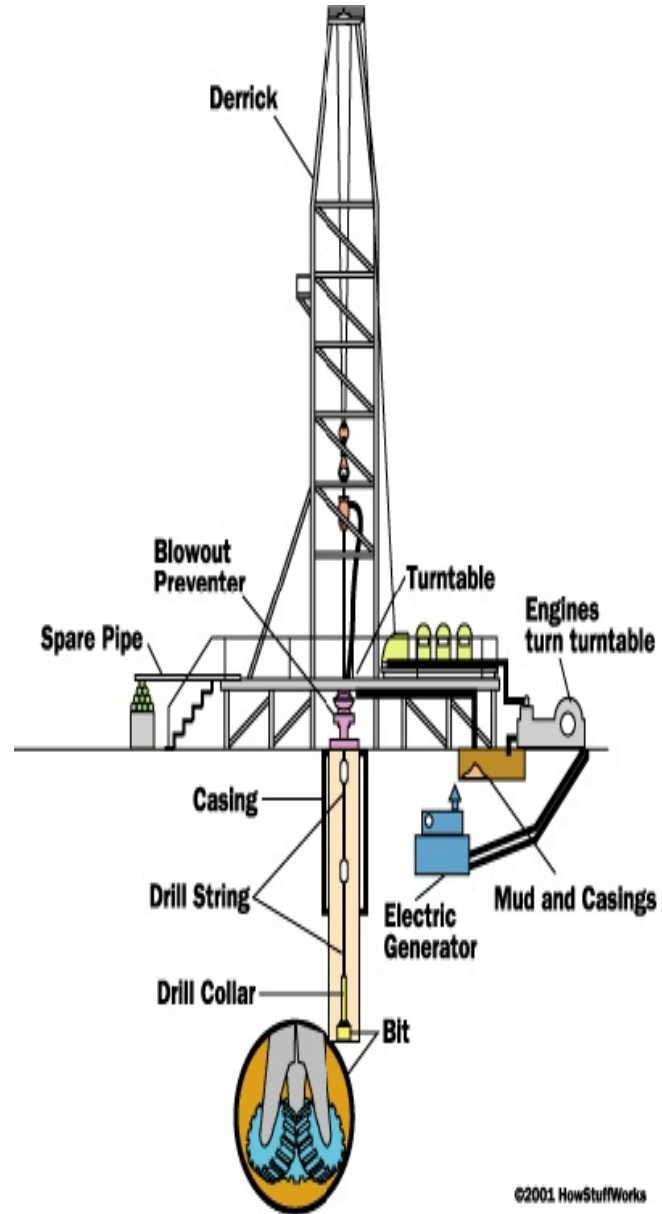


Figure 1.1: Basic Elements of a Drill Rig System [3]

at the top and is fitted with a cutting bit at the bottom, is lowered into the ground. Normally, a drill rig system contains four major components: rotating equipment, circulating system, hoisting system and power generation system. Figure 1.1 shows the basic elements of a drill rig system. The blowout preventer in the figure is the safety system.

1.1.1 Drill-string

The drill-string is the crucial component to rotary drilling. It is usually made up of drill-pipes, drill-collars, stabilizers and drill-bit. It transports the torque from the surface to the bit, affects drilling direction and serves as a conduit for drilling fluid [2]. During drilling operation, the drill-string is subjected to many loads, such as hook load at the top, rotary table driven torque, weight on the bit (WOB), torque on the bit (TOB), drilling fluid buoyancy and gravity force. Extending from the surface to a few hundred meters above the drill-bit, the drill-pipe section normally constitutes most of the drill-string length. During the drilling operation, the hoisting system supports most of the drill-string weight and therefore the drill-pipe section is normally rotating in tension. Placed right above the drill-bit, drill-collars are extra heavy steel pipes providing the necessary WOB to help the bit bore in to the formation. The significant strength of drill-collars helps stabilize the downhole assembly, facilitate straight drilling and protect itself from excessive fatigue or wear.

1.1.2 Drill-bit

Another important component that makes the drilling process possible is the drill-bit. The drill-bit, which fractures the rock and penetrates into the bottom hole formation, is usually subjected to rotary cutting and downward forces. Nowadays, two main kinds of drill-bits used are the roller-cone bits (RC) and polycrystalline diamond compact

bits (PDC). It is the property of the formation (soft or hard) that determines the type of the drill-bit selected. The RC bits possess cones that rotates with respect to their bit axes [4]. Several types of RC bits exist. Among them, two-cone bits are only suitable for soft formations. Four-cone bits are good at drilling large holes. Most of the RC bits are tricone bits. PDC bits are generally used for drilling in soft to medium-hard formations. Unlike RC bits, PDC bits do not have any moving elements. Figure 1.2 and Figure 1.3 show a tricone bit and a PDC bit, respectively.

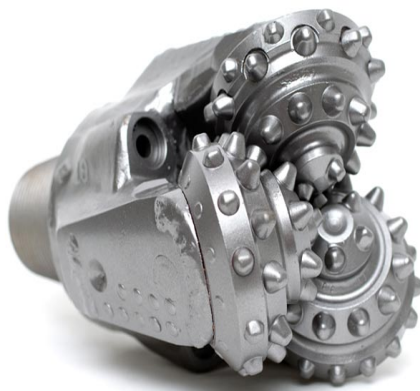


Figure 1.2: A tricone bit [5]



Figure 1.3: A PDC bit [6]

1.1.3 Drilling fluid

As the circulating system proceeds, drilling fluid (also called drilling mud) plays an important role in maintaining well bore stability and keeping drilling pressure balance. Without it, the formation fluids may flow to the surface because of the great pressure generated by the gas or water. By circulating down the drill-string and ejecting from the bit nozzles, the drilling fluid cleans the cuttings around the drill-bit and carries them to the surface.

1.1.4 Hoisting system

The hoisting system enables the installation of an extra length of pipe or a new drill-bit by working as a pulley to lift the traveling block and remove the drill-pipe [7]. It consists of crown block, derrick, traveling block, drilling line and drawworks. A hoisting system is depicted in Figure 1.4.

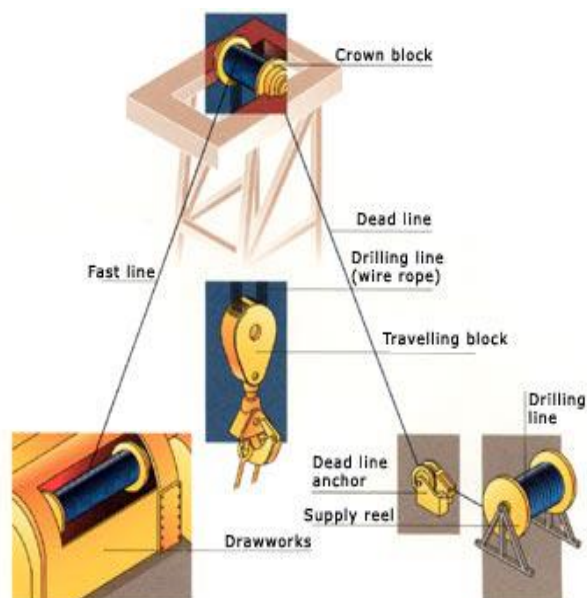


Figure 1.4: Hoisting system [7]

1.1.5 Power generation system

The power supplied for the drill rig system is either generated at the rig site using internal-combustion diesel engines or taken as electric power supply from existing power lines [8].

1.1.6 Well blowout preventer

Blowout preventers (BOPs) are the safety defense for the workers and the well to prevent a blowout. BOPs and associated valves are installed on the top of the casing head before drilling ahead after rigging up. These high-pressure safety valves and associated equipments are designed to shut off the well hole and prevent the escape of the underground fluids or gases and prevent a blowout from occurring [9].

1.1.7 Measurement while drilling equipment

Using accelerometers and magnetometers to measure the inclination and azimuth of the wellbore at certain locations, MWD operators can provide the directional drillers with the accurate and qualified data to allow them to keep the well safely on the planned trajectory. Further more, MWD tools can also provide useful information about the drill-string such as the rotational speed, WOB and TOB, type and severity of downhole vibrations, and mud flow volume [10]. Use of these information allows the operator to drill the well more efficiently.

1.2 Down-hole Vibration

It is well known that downhole vibrations are prevalent causes of drill-string failures. They can decrease rate of penetration (ROP), interfere with MWD tools and even cause premature fatigue of the components. Three primary categories of vibratory

motions exist in rotary oil-well downhole equipment: axial, torsional and lateral. It is found that these three vibration mechanisms usually occur simultaneously while drilling. The modes of vibration in drill-string are depicted in Figure 1.5.

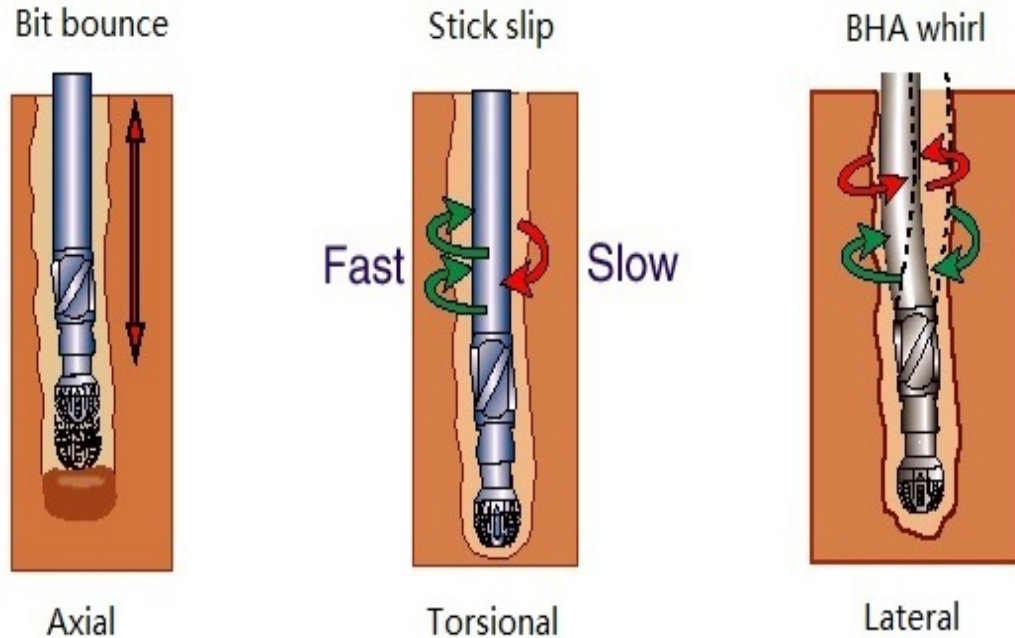


Figure 1.5: Modes of vibration in drill-string [11]

1.2.1 Axial vibration

As can be seen in Figure 1.5, the axial vibration of a drill-string results in the motion of its components parallel to its longitudinal axis. During the process, time-variant WOB is applied to the drill-bit and is usually unpredictable. The bit-formation interaction is the main cause for axial vibration.

One of the axial vibration forms is bit bounce, in which the bit repeatedly lifts off bottom and impacts formation. Bit bounce is likely to happen in near vertical holes when drilling with RC bits due to their type of interaction with the formation. Severe bit-bounce leads to premature bit and bottom hole assembly (BHA) failure and rate

of penetration (ROP) reduction. Sometimes, increasing WOB and adjusting rotation per minute (RPM) can relieve the problem.

1.2.2 Torsional vibration

It is found by downhole measurements that applying a constant rotary speed at the surface does not necessarily lead to a steady rotational motion of the drill-bit. In fact, during a significant fraction of the drilling time, the down-hole torsional speed may experience large amplitude fluctuations due to the torsional flexibility of the drilling assembly [4, 12].

For torsional vibration, the most common phenomenon is stick-slip. Stick-slip happens when the rotation of the drill-string is slowed down (or even stopped) and then suddenly increased when the torque overcomes the anti-torque result from the rock cutting and friction. Stick-slip vibration sometimes happens when drilling in high angle wells with aggressive PDC bits and in the down-hole environment where the BHA to wellbore friction is high [11]. Stick-slip vibration can largely decrease ROP and cause fatigue failure of the drill-bit. Increasing RPM can relieve stick-slip once it is detected.

1.2.3 Lateral vibration

Lateral vibration is considered to be the most destructive and can create large shocks. It may cause uneven drill-string and stabilizer wear and bore-hole wall enlargement. However, paradoxically, lateral vibration is difficult to detect at the surface because it barely travels beyond the neutral point [4]. Increasing WOB and decreasing RPM can diminish the lateral vibration.

An important subset of lateral vibrations is the BHA whirl phenomenon. Most of the BHA will operate in compression as drilling proceeds. This situation causes the

BHA to be a region where buckling and whirling are likely to occur. As explained by Vandiver et al: " If the center of gravity of the drill collar is not initially located precisely on the centerline of the hole, then as the collar rotates, a centrifugal force acts at the center of gravity, causing the collar to bend" [13]. The BHA whirl can be qualified as forward or backward whirl depending on whether the BHA rotates around the wellbore with the same direction as the driving rotation or not, as can be clearly seen in Figure 1.6.

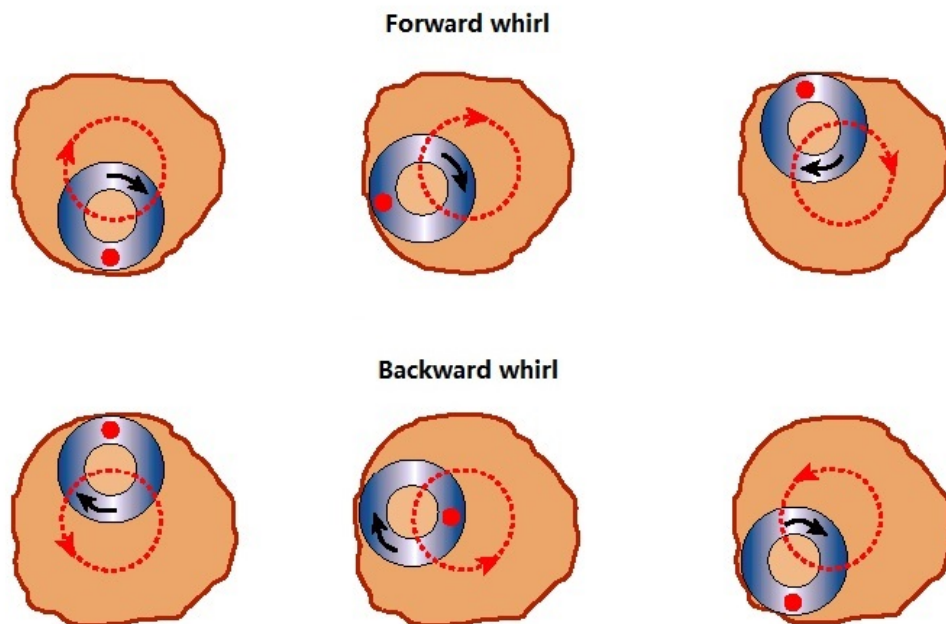


Figure 1.6: BHA whirl phenomena [11]

1.2.4 Coupled vibrations

Multiple vibration mechanisms, such as bit bounce, stick slip, forward and backward whirl, may occur simultaneously while drilling. This phenomenon significantly increases the complexity of drill-string dynamics. The initial curvature of the BHA can result in the coupling between the axial and lateral vibrations. Bit bounce can

be sometimes triggered by the large lateral vibrations of the BHA. As relating the WOB to the TOB, the drill-bit also plays an important role in drill-string vibrations coupling. The high speed it experiences during the stick slip can lead to BHA whirl phenomenon. Lateral vibrations at the BHA can be triggered by the axial vibrations at the bit. Figure 1.7 shows a summary of downhole excitation mechanisms and their corresponding influences on axial, torsional and lateral vibration modes.

Physical Mechanism	Primary Excitation	Secondary Excitation
mass imbalance	lateral	axial-torsional-lateral
misalignment	lateral	axial
three-cone bit	axial	torsional-lateral
loose drill-string	axial-torsional-lateral	
rotational walk	lateral	axial-torsional
asynchronous walk or whirl	lateral	axial-torsional
drill-string whip	lateral	axial-torsional

Figure 1.7: Drill-string vibration mechanisms, after [14]

Although the downhole vibrations are usually coupled, analyzing axial, torsional and lateral vibrations separately is crucial to securing physical integrity and minimizing risks of formulation errors [15].

1.3 Brief Introduction of the Thesis

This research work concentrates on the computer simulations of the drill-string system to predict the dynamic responses to both deterministic and random excitations.

1.3.1 Objective and significance

The main objective of this thesis is, firstly, to develop a appropriate dynamic model of the drill-string that is suitable for predicting axial, torsional and lateral vibrations. Secondly, the thesis will focus on the stick slip phenomenon of the drill-string. By simulation, the dynamic responses to both deterministic and random excitations will be clearly analyzed and discussed. This will help better understand drill-string downhole behaviors and lay a foundation for further research work.

1.3.2 Methodology

The drill-string models in the thesis are built using the finite element method. The thesis is based on Matlab simulation employing central difference and Runge-Kutta as the numerical methods. In the random case, Monte Carlo simulation and path integration methods are used to capture the probabilistic information of the response.

1.3.3 Limitations

The study is limited to vertical drilling system and the current work does not consider the geometric stiffness and the influence of the drilling fluid.

1.4 Conclusion

This chapter briefly describes the composition of a rotary drill rig system, introduces the drilling vibrations together with their subsets and consequences, and provides basic information of the thesis. In the next chapter, the literature review on drill-string will be described in detail.

Chapter 2

Literature Review

2.1 Drill-string finite element model

Recognized as one of the most powerful numerical tools for solving large-scale structures of complex geometry, the finite element method (FEM) attracted many investigators in the drill-string dynamic analysis field.

Trindade et al. [16] presented a study of the vibrations of a drill-string using a vertical slender beam. The beam was clamped on the top, pinned in the end, and its lower portion was constrained inside an outer cylinder. The beam was subject to gravity force, and geometric softening effect of its lower portion was considered in the model. In the simulations, the axial–bending coupling in the paper yielded a large number of vibro-impacts with the outer cylinder. The proper orthogonal decomposition method was employed in the paper to help better understand the non-linear coupled vibro-impact problem. The results of the paper showed that the micro-impacts and reaction forces at both ends are well presented only when using the non-linear axial-bending coupling model.

Khulief and Al-Naser [17] employed an Euler-Bernoulli beam model to represent the

whole elastic drill-string including both drillpipes and drillcollars (bottom hole assembly). In the report, the model was six degrees of freedom per node and accounted for the gyroscopic effect, the torsional-bending inertia coupling and gravity force effect. The explicit expressions of the bending/torsional inertia coupling matrices, and the gravitational axial stiffening matrices are derived. The method developed in the paper is proved to furnish a basic building block for further research of more comprehensive drilling assembly models considering wellbore/drillpipe contact, drillstring/mudflow interaction, and stick-slip at the bit.

Sampaio et al. [18] employed a geometrically non-linear model to study the coupling of axial-torsional vibrations on a drill-string. The geometrical stiffening was discussed in the paper using a non-linear finite element approximation, which accounted for large rotations and non-linear strain-displacements. The result of the paper showed that the responses of the linear and non-linear models, drill-bit rotary speed and the predictions of forces, after the first periods of stick-slip were considerably different. These observations are important in order to simulate a longtime analysis of drilling process, as well as to consider feasible control methodologies.

Pivovan and Sampaio [19] presented a finite element model considering the coupling of axial, torsional and lateral vibrations on a rotating drill-string. The drill-string model was discretized using a finite element with 12 degrees of freedom. In the simulation, the model was subjected to distributed loads due to gravity force, impacts between the drill-string and wellbore and perturbation moments at the lower end. The results showed that the influence of the geometric non-linearities in the dynamic response of the drill-strings is crucial. This influence can be observed in the calculation of reaction forces at top position as well as the time histories of radial displacements.

2.2 Bit-bounce and stick-slip vibration research

Some researchers also focus their interest on bit-bounce and stick-slip vibrations in view of their great influences on drilling performance.

Using a simplified lumped parameter model, Yigit and Christoforou [20] formulated the equations of motion of a rotary drilling system. A model that adequately captures the dynamics was used in the paper to examine the interactions between the stick-slip vibrations and bit-bounce under varying operating conditions. As can be seen in Figure 2.1, the drill-string is powered by the rotary table, which is driven by an armature controlled DC motor through a gearbox. Simulation results showed that rotational control along with axial control can effectively suppress stick-slip vibrations and bit-bounce.

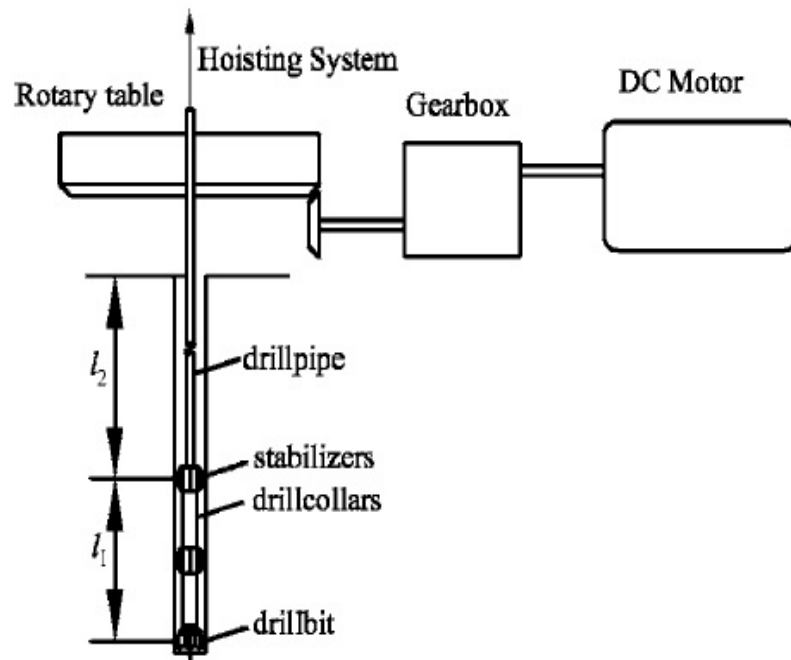


Figure 2.1: The model introduced in [20]

In their another paper [21], a fully coupled model was presented. The model accounted

for bit/formation and drill-string/borehole wall interactions as well as geometric nonlinearities. The results of the paper were in close agreement with field observations regarding stick-slip and axial vibrations. It is demonstrated by simulation results that bit motion causes torsional vibrations, which in turn excite axial and lateral vibrations resulting in bit bounce and impacts with the borehole wall. Based on optimal state feedback control, the active control strategy proposed in the paper was proved to make drill at lower speeds possible.

Van de Vrande et al. [22] proposed a systematic procedure to study the stick-slip vibrations of autonomous dynamic systems with dry friction. In their paper, the discontinuous friction forces were approximated by smooth functions. Simulation results from two block-on-belt models and a drill-string model proved that the smoothing procedure was accurate and reliable. The simplified drill-string model introduced in [22] is shown in Figure 2.2. In the paper, the drill-pipe is modeled by a linear torsional spring k . The drill-collar and drill-pipe are assumed to be rigid and modeled as the equivalent mass moment of inertia J_1 .

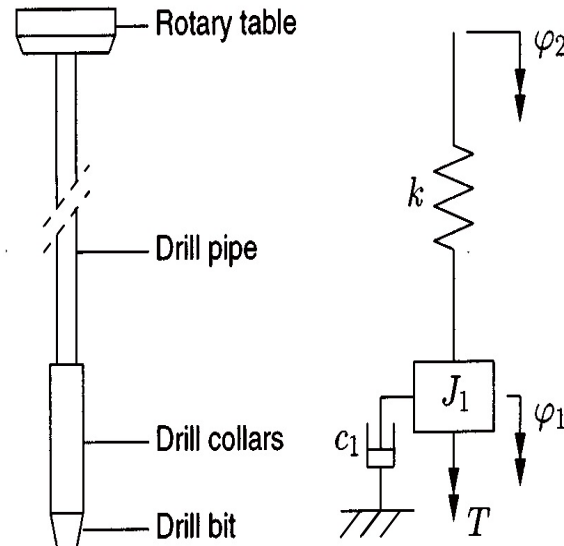


Figure 2.2: Simplified drill-string model in [22]

Navarro-López and Cortés [23] presented an n-dimensional lumped-parameter model to properly describe the stick-slip oscillation of the bit. The model also took into account the fact that the drillstring length increases as drilling operation makes progress. The torque on bit (TOB) was modeled as a combination of torques caused by dry friction and viscous damping. By changing the system parameters, such as the WOB, the motor torque and the rotary speed, bifurcations were identified and analyzed in their simulations. The mechanical model describing the torsional behaviour of a conventional drillstring in [23] is shown in Figure 2.3.

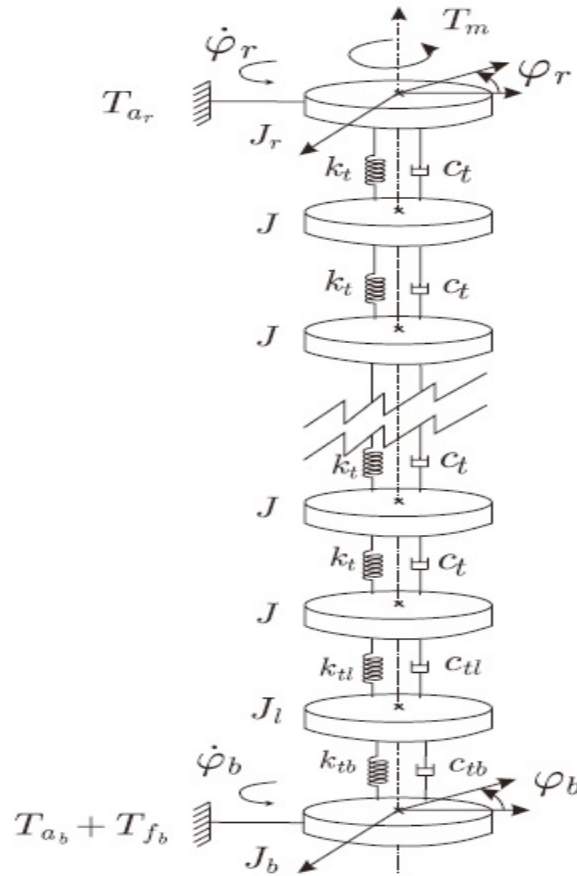


Figure 2.3: Drill-string model describing the torsional behaviour in [23]

Richard et al. [24] studied the self-excited stick-slip oscillations of a rotary drilling

system with a drag bit using a discrete axial-torsional coupled model. TOB was modeled as a combination of friction contact and cutting processes at the bit-rock interface. Figure 2.4 shows their simplified model of a drill-string system. In the figure, H_0 , Ω_0 , C , Ω , M , I , T and W represents the constant hook load, constant angular velocity, torsional stiffness of the drill-pipe, time-variant bit angular velocity, BHA mass, moment of inertia of BHA, TOB and WOB, respectively. In the simulation, the model captured stick-slip and bit-bounce behaviors under certain conditions. It was reported in the paper that the existence of self-excited vibrations and stick-slip oscillations were due to the delayed and coupled nature of the cutting process.

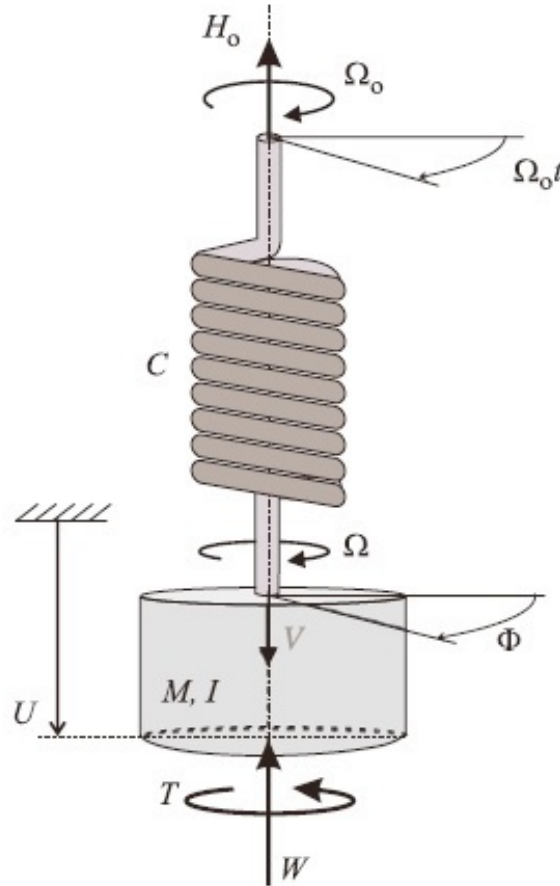


Figure 2.4: Sketch of a simplified model of the drilling system in [24]

Puebla and Alvarez-Ramirez [25] proposed an approach for suppressing stick-slip oscillations in drilling process. In their study, the drill-string was simplified as a torsional pendulum with two degrees of freedom (see Figure 2.5). The stick-slip oscillations in the paper were studied using the models of Navarro-Lopez and Suarez [26], Serrarens et al. [27] and Mihajlovic [28]. Different control strategies were simulated based on the dynamic model developed.

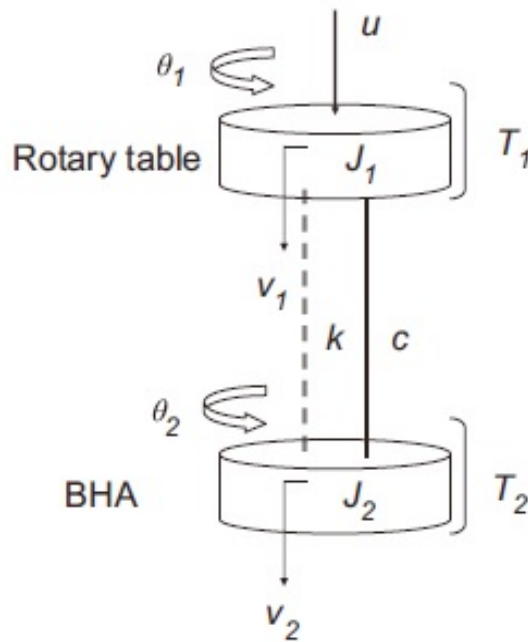


Figure 2.5: Simplified model of the drilling system in [25]

Khulief et al. [29] formulated the dynamic model of a drill-string using Lagrangian approach in conjunction with the finite element method. Torsional-bending inertia coupling, axial-bending geometric nonlinear coupling, gyroscopic effect are considered in their model. It is assumed in the paper that the WOB oscillates harmonically about its mean value. Time response of the drill-string system under stick-slip excitations was simulated and discussed. The results obtained are in excellent agreement with actual field observations and measurements.

Sarker et al. [30] presented a bond graph model of the whole drillstring including both drill pipes and drill collars, considering axial vibration, torsional vibration, and axial-torsional coupling due to bit-rock interaction. A lumped-segment approach was used to build the axial and torsional dynamic models. The developed model was subjected to its own weight, hydraulic forces due to drilling mud, an empirically treated bit-rock interaction, and top motor driving torque. The model was proved to be suitable for parametric study of the effect of table rotary speed and WOB on stick-slip vibration, and the coupling between stick-slip and bit-bounce. The paper also studied a state feedback controller that was designed based on a linear quadratic regulator (LQR) technique. It was found that this controller can effectively suppress stick-slip oscillations and make it possible to drill at lower speeds.

2.3 Downhole uncertainty research review

It is well known that randomness exists in any real system. For a drilling system, many sources of uncertainties bring randomness to the drill operation and make drill-string dynamics difficult to predict.

In the late 1950s, Bogdanoff and Goldberg [31] firstly introduced the probabilistic approach to drill-string dynamics. They modeled WOB and TOB using zero-mean normally distributed process.

Chevallier [4] investigated the lateral behaviors of nonlinear drilling assemblies subject to deterministic and random excitations. The drill-string finite element model was based on Euler-Bernoulli beam theory. The random input forces were defined by their power spectral densities, which were estimated on the bases of field data. As can be seen in Figure 2.6, in the paper, the lateral excitations applied to a BHA equipped with a tricone bit were modeled with band-limited white noise. Meanwhile,

a Kanai-Tajimi process was employed as the excitation model for a BHA with a PDC bit.

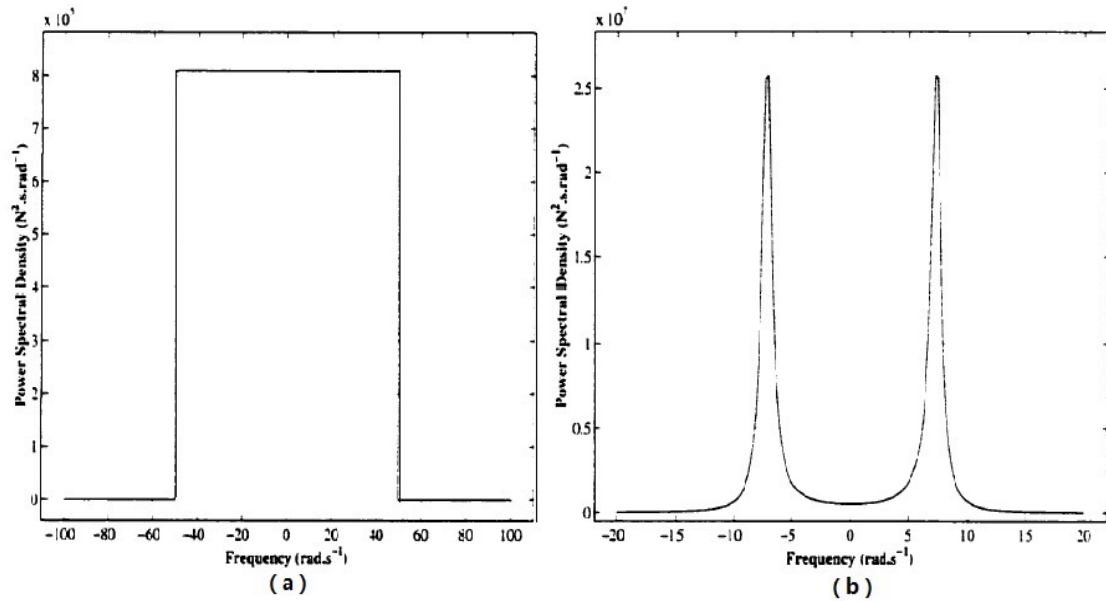


Figure 2.6: Excitation models for BHA with a tricone bit (a) and a PDC bit (b)

Ritto et al. [32] used the non-linear Timoshenko beam theory in their paper and formulated the non-linear dynamical equations by means of finite element method. This paper considered bit-rock interaction, fluid-structure interaction and impact forces. A random model was developed to describe the uncertainties in the bit-rock interaction. The results of the paper indicated that the uncertainties play a crucial role in the coupling among the axial, torsional and lateral responses.

In the paper [33], a dynamic model was proposed for the nonlinear dynamics of a horizontal drill-string. As a pioneering work, the drill-string was modeled using a bar model (tension/ compression), and was discretized by means of the finite element method. As can be seen in Figure 2.7, the model was subjected to a constant force, an oscillatory force due to the mud motor driving force, and bit-rock interaction. A random field with an exponential correlation function was employed in the paper to

model the friction between the column and the soil. Unusual stick-slip behavior in the axial direction was observed in the paper. The results were found to be similar for different excitation frequencies and different correlation lengths. But they were observed to be different for different slenderness parameters and different uncertainty levels of the random field.

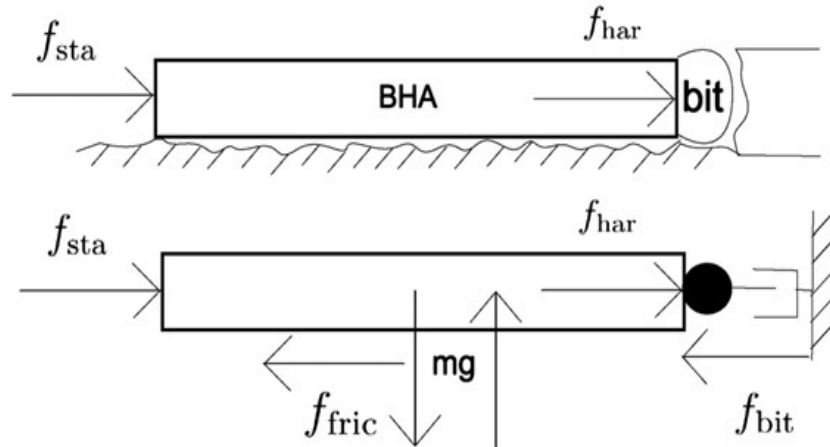


Figure 2.7: Sketch of the system analyzed in [33]

Ritto et al. [34] proposed a methodology for the robust optimization of the non-linear dynamics of a drill-string system using the finite element method. The aim of the proposed optimization problem was to maximize the expected mean rate of penetration of the drill-string, respecting the integrity limits based on the ultimate stress of the material, the damage cumulated by fatigue and the stick-slip factor. The nonparametric probabilistic approach was used to model both the uncertainties in the structure and the bit-rock interaction. The results of the paper indicated that the robust analysis gives different responses between the deterministic and random optimization analysis.

Partly due to the great complexity, research works on drill-string dynamics from the view point of random theory are relatively rare even though the random nature

has been long recognized. The refinement of the stochastic modeling and a robust optimization to maximize the performance of the system considering the uncertainties need to be studied and developed.

2.4 Remarks

Although some models are relatively simple by reducing the drill-string system to one or two degree(s) of freedom system and focusing on only one or two mode(s) of drill-string vibration [20, 24, 25], they help the researchers understand basic downhole responses and provide references to their more complicated drill-string models. As can be seen in the references, researchers used different bit-rock interaction models to analyze stick-slip vibration in drill-string [20, 22, 25, 30]. In practice, it is difficult to tell which one is the best. In this thesis, an empirical treatment of bit-rock interaction and a dry friction model are employed in Chapter 4 and Chapter 5, respectively, to model the bit-rock interaction. Chapter 5 focuses on stick-slip analysis and it is found that a dry friction model can show stick-slip phenomenon clearly. It is also very important to consider the geometric non-linearities in a drill-string model [16–19]. However, the more complex the model is, the more challenging the numerical simulation will be. Although the author of the thesis tried very hard, the results of Matlab are always mis-convergence. In the simulation, as the stiffness is time varying, the step size is also time varying, making numerical computation hard to converge. Therefore, drill-string models without considering geometric stiffness will be employed in the thesis as a basic building block for further research of more comprehensive drilling assembly models. Most of the papers mentioned in the literature review do not consider stochastic effects [16-30]. In this thesis, a multi-degree of freedom drill-string finite element model, considering stochastic effects, will be analyzed.

Chapter 3

Finite Element Model

3.1 Euler-Bernoulli Beam

The drill-string under investigation is discretized with finite element method which use Euler-Bernoulli beam theory. Using Lagrange linear shape function for the axial displacement u and twisting angle θ_u and Hermite cubic functions for the lateral deflection v and w , the displacements are represented as:

$$u = N_u q, \quad v = N_v q, \quad w = N_w q, \quad \theta_u = N_\theta q \quad (3.1)$$

where N_u , N_v , N_w and N_θ are shape function matrices, and q is the vector of nodal coordinates of the two-node finite element (see Figure 3.1), which is defined by:

$$q = \left[u_1 \ v_1 \ w_1 \ \theta_{u_1} \ \theta_{v_1} \ \theta_{w_1} \ u_2 \ v_2 \ w_2 \ \theta_{u_2} \ \theta_{v_2} \ \theta_{w_2} \right]^T \quad (3.2)$$

where u , v , w represent x -, y - and z - translational DOFs, while θ_u , θ_v and θ_w represent the rotational dofs along the x -, y - and z - axes.

By defining the element length l_e and the non-dimensional element variable $\xi = x/l_e$,

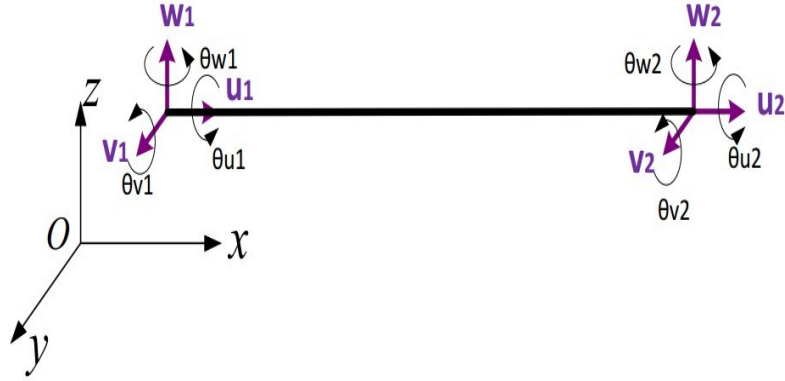


Figure 3.1: Degrees of freedom of an element

the shape function matrices are given as:

$$N_1 = 1 - \xi \quad (3.3)$$

$$N_2 = \xi \quad (3.4)$$

$$N_3 = 1 - 3\xi^2 + 2\xi^3 \quad (3.5)$$

$$N_4 = l_e \xi (1 - \xi)^2 \quad (3.6)$$

$$N_5 = \xi^2 (3 - 2\xi) \quad (3.7)$$

$$N_6 = l_e \xi^2 (\xi - 1) \quad (3.8)$$

$$N_u = \{N_1, 0, 0, 0, 0, 0, N_2, 0, 0, 0, 0, 0\} \quad (3.9)$$

$$N_v = \{0, N_3, 0, 0, 0, N_4, 0, N_5, 0, 0, 0, N_6\} \quad (3.10)$$

$$N_w = \{0, 0, N_3, 0, -N_4, 0, 0, 0, N_5, 0, -N_6, 0\} \quad (3.11)$$

$$N_\theta = \{0, 0, 0, N_1, 0, 0, 0, 0, 0, N_2, 0, 0\} \quad (3.12)$$

The expression for the linear stiffness K_e is:

$$K_e = \int_0^1 \left[\frac{EA}{l_e} N_u'^T N_u' + \frac{GJ}{l_e} N_\theta'^T N_\theta' + \frac{EI}{l_e^3} (N_v''^T N_v'' + N_w''^T N_w'') \right] d\xi \quad (3.13)$$

where N_u , N_θ , N_v and N_w are for axial, torsional and bending, respectively. The expression for the mass matrix M_e is:

$$M_e = \int_0^1 [\rho A l_e (N_u^T N_u + N_v^T N_v + N_w^T N_w) + \rho J l_e N_\theta^T N_\theta] d\xi \quad (3.14)$$

Substituting metrics 9 through 12 into equations 13 and 14, the local stiffness K_e and mass M_e for one finite element are obtained. The drill-string finite element model is based on the ideas that:

1. Using Euler-Bernoulli beam to model drill-string.
2. By dividing the drill-string into many finite elements and then assembling the local stiffness and mass matrices together, system stiffness and mass matrices can be found.
3. The number of the elements is limited by the computer calculation time and memory.

3.2 Simple Simulation

3.2.1 Model Introduction

In this section, a clamped-free hollow beam model composed of two different finite elements is built. The two finite elements are both made of steel and are both 10m in length. The cross section of the one with its left end clamped is $5.58 \times 10^{-3} m^2$. Another one is $3.65 \times 10^{-2} m^2$. In its free end, the beam is subjected to axial, torsional and lateral sinusoidal excitations. The simulation results given by Matlab built-in solver ode23t are compared with those of Abaqus, which is a software suite for finite element analysis and computer-aided engineering. The purpose of this section is to

verify the matrix built in Matlab. Because the local stiffness and mass matrices of a beam element are building blocks for the drill-string model.

After some mathematical manipulation, the equations of motion for the system can be represented in a compact matrix form as:

$$M\ddot{q}(t) + C\dot{q}(t) + Kq(t) = F(t) \quad (3.15)$$

where M , C and K are system mass, damping and stiffness matrices, respectively. The system damping is assumed to be Rayleigh damping, a linear combination of K and M as below:

$$C = \alpha M + \beta K \quad (3.16)$$

where α and β are constants to be selected.

$F(t)$ is a force vector and is extended as:

$$F(t) = \left[0 \ 0 \ 0 \ 0 \ 0 \ 0 \ 100000\sin(2t) \ 2000\sin(2t) \ 0 \ 1000\sin(2t) \ 0 \ 0 \right]^T \quad (3.17)$$

3.2.2 Simulation Results and Conclusion

For comparison purpose, the simulation results of Matlab and Abaqus are shown in Figure 3.2 to 3.7. As can be seen in these figures, the steady state simulation results given by Matlab are nearly similar to those of Abaqus, although some differences can be noticed. It can be found that the period of the responses from Abaqus is a little smaller than that from Matlab. The frequencies of the excitations are all $2rad/s$. Therefore, their periods are all π in seconds. The difference may be caused by the way they (Matlab and Abaqus) deal with π .

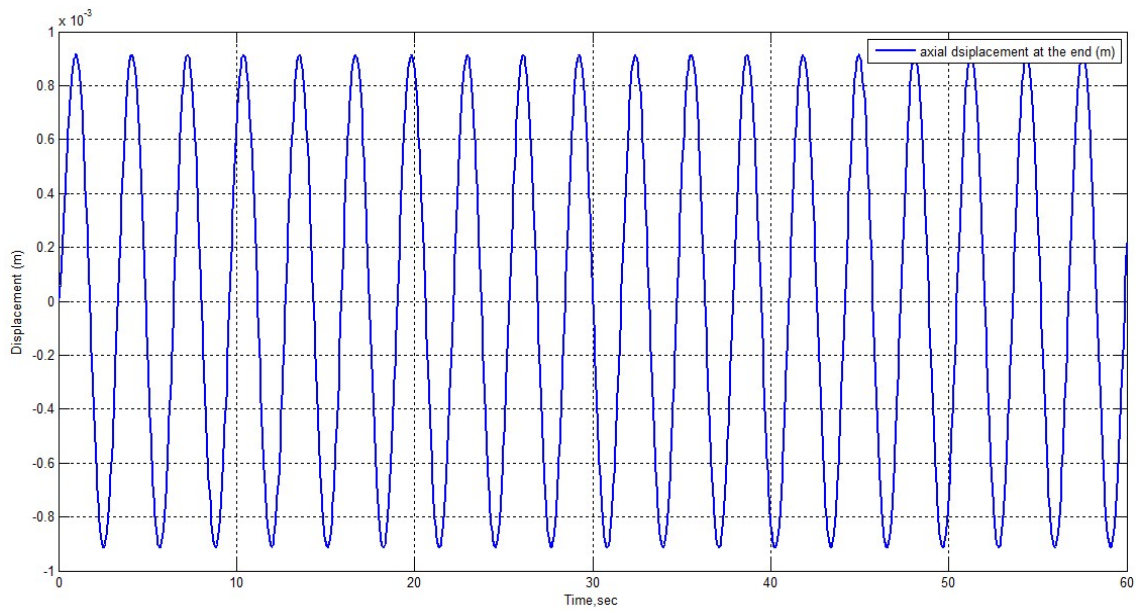


Figure 3.2: Axial displacement of the beam (Matlab Result)

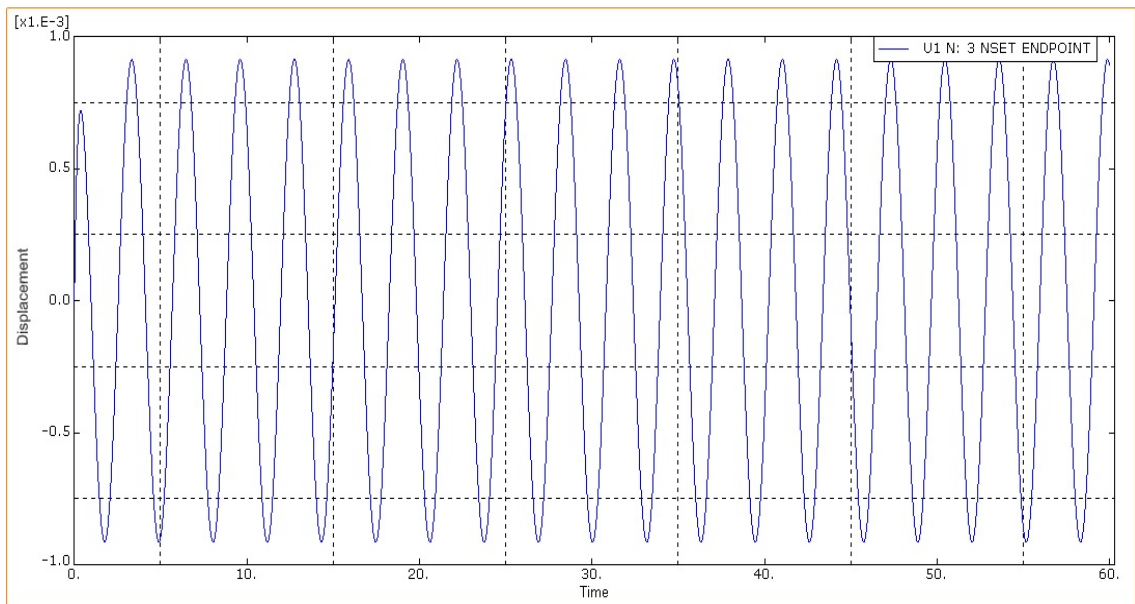


Figure 3.3: Axial displacement of the beam (Abaqus Result)

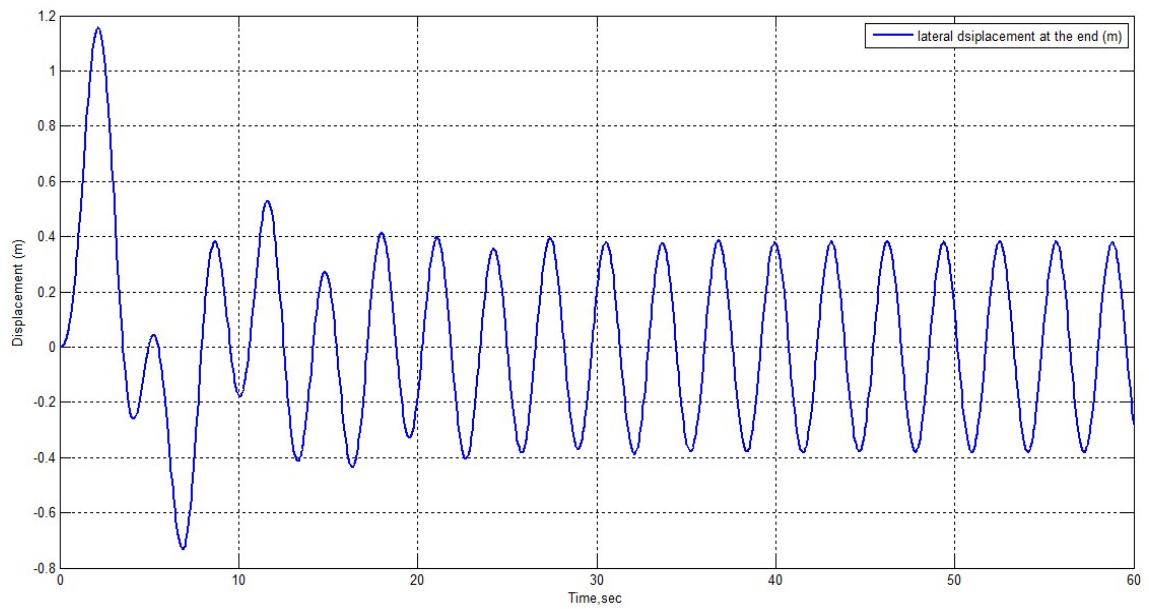


Figure 3.4: Lateral displacement of the beam (Matlab Result)

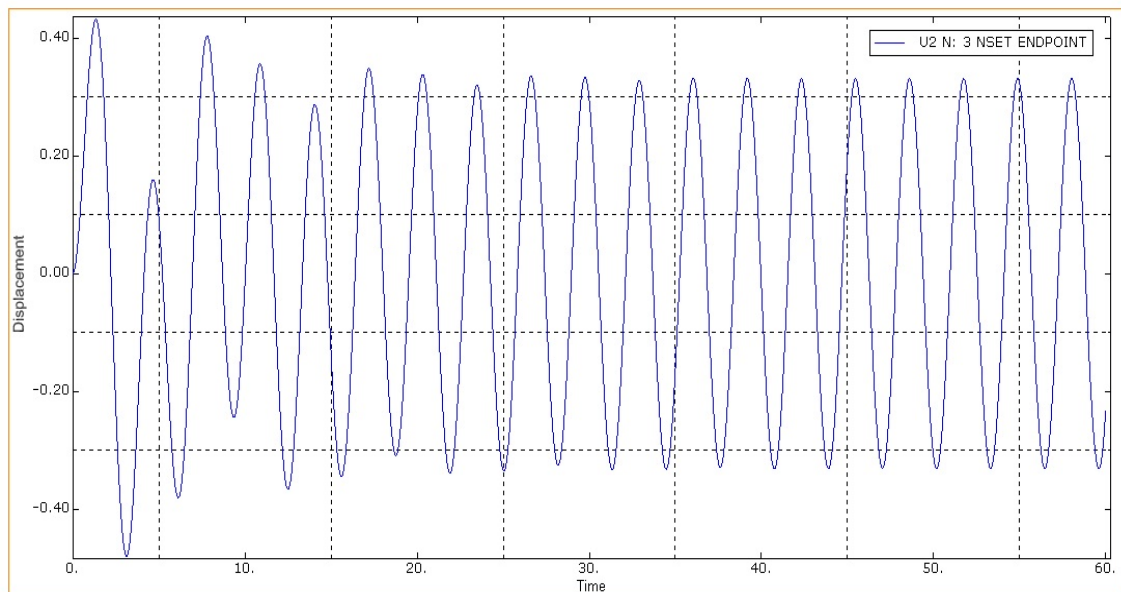


Figure 3.5: Lateral displacement of the beam (Abaqus Result)

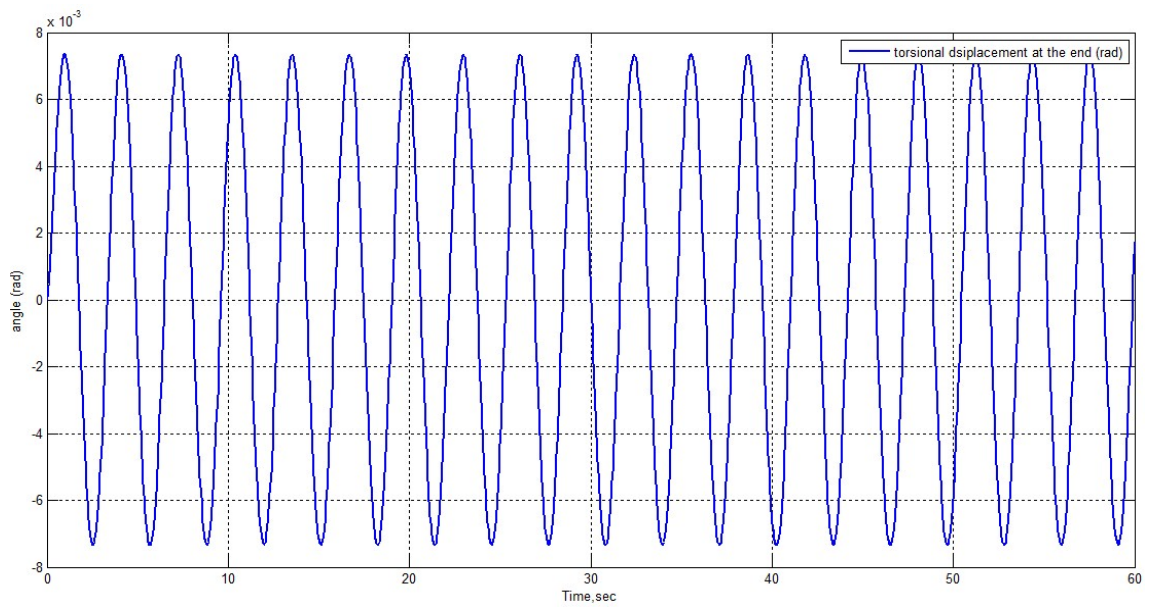


Figure 3.6: Torsional displacement of the beam (Matlab Result)

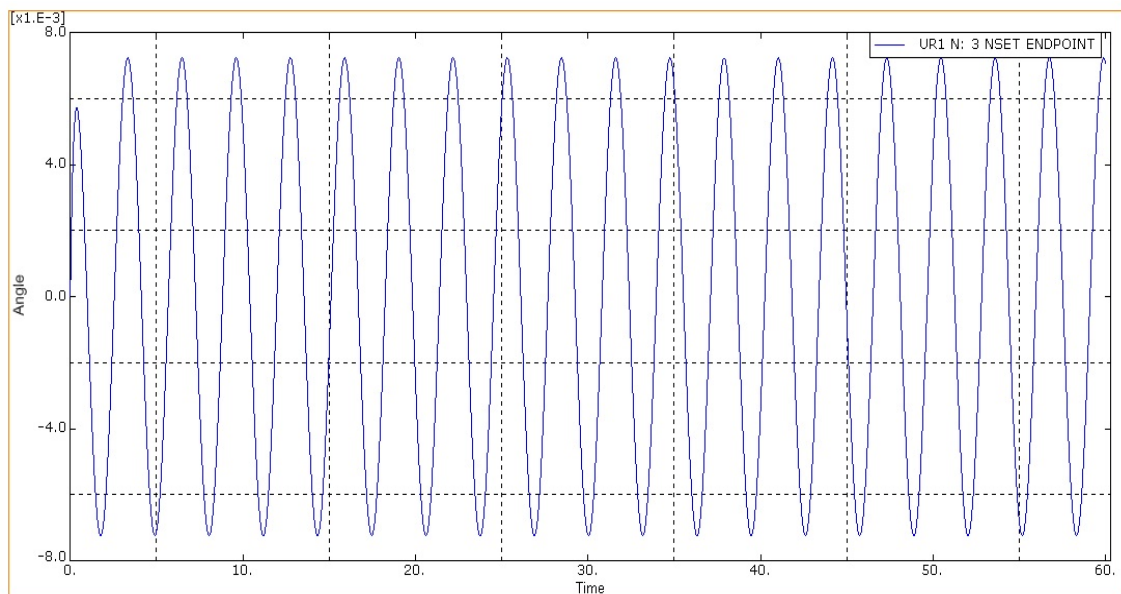


Figure 3.7: Torsional displacement of the beam (Abaqus Result)

3.3 Covariance Matrix Solution to Linear Drill-string System

For a linear multi-degree-of-freedom system subjected to Gaussian white noise excitation, the equations of the motion can be written in the matrix-vector form as:

$$M\ddot{q}(t) + C\dot{q}(t) + Kq(t) = W(t) \quad (3.18)$$

Here, the vectors $q(t)$ and $\dot{q}(t)$ have the dimension n , which is equal to the system degrees. M , C and K are symmetric and non-negative matrices with the size $n \times n$. $W(t)$ is an n -dimensional vector, containing pure random excitation. With the state vector $Y = \begin{bmatrix} q(t) & \dot{q}(t) \end{bmatrix}^T$, the system of differential equations is given as:

$$\dot{Y} = GY + F \quad (3.19)$$

where G is a $2n \times 2n$ – *matrix* assembled from the mass, stiffness and damping matrices:

$$\begin{bmatrix} 0 & I \\ -\frac{K}{M} & -\frac{C}{M} \end{bmatrix} \quad (3.20)$$

and

$$F = \begin{bmatrix} 0 & (M^{-1} \times W(t))^T \end{bmatrix}^T \quad (3.21)$$

where 0 denotes the zero matrix and I denotes the identity matrix both with size $n \times n$ in Eqn 3.20. In Eqn 3.21, 0 denotes the zero matrix with size $1 \times n$.

The covariance matrix of the state vector Y is given as:

$$R = E \begin{bmatrix} Y & Y^T \end{bmatrix} \quad (3.22)$$

The generalized cross-spectral density matrix of the white-noise excitation is given as:

$$D(t, t + \tau) = E \left[F(t) F^T(t + \tau) \right] = B\delta(\tau) \quad (3.23)$$

in which δ is the Dirac delta and B is an arbitrary cross intensity matrix of the size $2n \times 2n$. The equations of motion then yield a Lyapunov matrix equation:

$$GR + RG^T + B = \dot{R} \quad (3.24)$$

Focusing on the stationary state of the system, the state in which $B = \text{constant}$ and $\dot{R} = 0$, the Lyapunov matrix equation can be simplified as:

$$GR + RG^T + B = 0 \quad (3.25)$$

This equation can be solved by Matlab built-in solver *lyap* and R can be obtained. Now, consider a drill-string consisting of drill-pipe and drill-collar with the left end of drill-pipe clamped. The specification of the drill-string can be found in Appendix A. The drill-string is only subjected to torsional Gaussian white noise excitation with the spectral density $S_0 = 1000$.

Firstly, the drill-pipe and drill-collar are both divided into one finite element. The standard deviation of the torsional velocity at the drill-string free end is 0.1395. Then the drill-pipe and drill-collar are divided into 21 elements and 11 elements respectively. The calculated result is increased a little bit to 0.1429.

Using covariance matrix solution method, the statistical response of a linear system to random excitations can be easily obtained. However, the problem is that, in reality, the drill-string system is nonlinear. Further more, the nonlinearity of the system is sometimes so complex and so strong that statistical linearization method can not

simplify the system. As such, in the next chapter, Monte Carlo simulation is employed to investigate the behaviors of drilling assemblies subject to both deterministic and stochastic excitations.

Chapter 4

Stochastic and Deterministic Vibration Analysis on Drill-string with Finite Element Method

Using Euler-Bernoulli beam theory, a finite element model with six degrees of freedom per node is developed for a drill-string assembly in this chapter. The simplified drill-string system developed for this chapter is shown in Figure 4.1. The drill-string is driven by a DC motor on the top and is subjected to distributed loads due to its own weight as well as bit/formation interaction. The model is axial-torsional, lateral-torsional coupled. Under deterministic excitations, the model captures stick-slip behavior in drilling operation. Analysis on its negative effect on drilling performance is made, and potential mitigation measures are also discussed. In random model, the excitations to the drill-bit are modeled as combination of deterministic and random components. Monte Carlo (MC) simulation is employed to obtain the statistics of the response. Two cases of random excitation with different intensities are investigated. The results from MC simulation are compared against that from deterministic case.

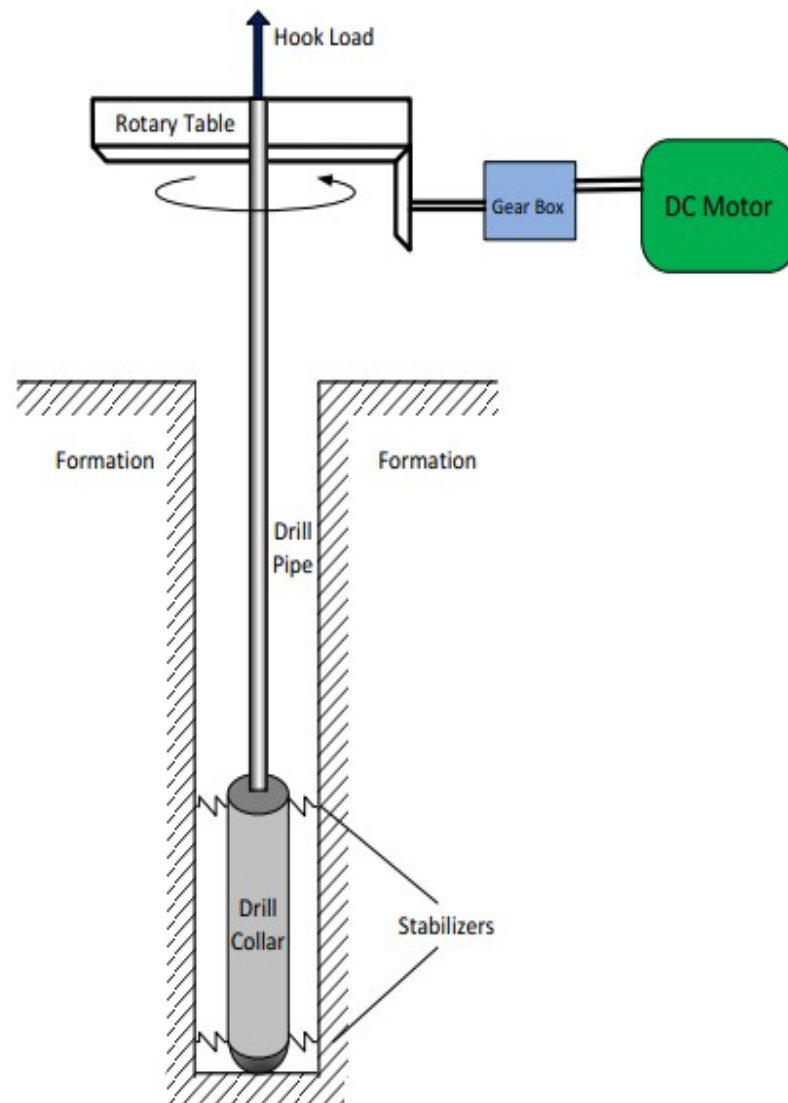


Figure 4.1: The simplified model of the system

4.1 Dynamic Model

4.1.1 Dynamic model and deterministic excitations

Considering the limitation of computer calculation time and memory, the drill-string is divided into 30 finite elements with 186 degrees of freedom at first. The drill-pipe and drill-collar respectively, is divided into 20 and 10 elements. After some mathematical manipulation, the equations of motion for the system can be represented in a compact matrix form as:

$$M\ddot{q}(t) + C\dot{q}(t) + Kq(t) = F(x, \dot{x}, \phi, \dot{\phi}, v, w, F_c, I) \quad (4.1)$$

where M , C and K are system mass, damping and stiffness matrices, respectively. $q(t)$ is the displacement vector, $F(x, \dot{x}, \phi, \dot{\phi}, v, w, F_c, I)$ is the excitation vector including WOB , TOB , $F_{\dot{\phi}}$, F_c , F_{tor} , F_g , F_h and T_{rb} . The downhole damping C is assumed to be a linear combination of K and M as below:

$$C = \alpha M + \beta K \quad (4.2)$$

where α and β are constants to be selected. In this chapter the system is assumed as underdamped which is common in engineering application.

Considering the mass and stiffness of stabilizer, M and K are given as:

$$M = M_g + A \times m \quad (4.3)$$

$$K = K_g + B \times k \quad (4.4)$$

where M_g and K_g are the global mass and stiffness matrices of the system. m and k are the mass and stiffness of the stabilizer respectively. In the model, the stabilizers

are modeled as stiff springs between the drill-collar and the borehole wall. A and B are the corresponding transformation matrices.

WOB , the weight on bit, is represented as:

$$WOB = \begin{cases} k_c(x - s) + c(\dot{x} - \dot{s}) & x \geq s \\ 0 & x < s \end{cases} \quad (4.5)$$

where x is the displacement of the bit, k_c is the formation contact stiffness, c is the rock damping coefficient and s is the elevation of the formation surface. k_c , c and s can be computed by [20, 35]

$$G_0 = \frac{E_0}{2 \times (1 + \nu)} \quad (4.6)$$

$$k_c = \frac{G_0 r_0}{1 - \nu} \quad (4.7)$$

$$c = \frac{3.4 \times r_0^2 \times \sqrt{G_0 \rho_0}}{1 - \nu} \quad (4.8)$$

$$s = s_0 \sin(\phi) \quad (4.9)$$

where E_0 , G_0 , ν , ρ_0 are determined by the property of the rock, r_0 is the foundation diameter, ϕ is bit torsional displacement.

The torque on bit (TOB) is related with WOB and cutting conditions [20], and can be calculated by:

$$TOB = WOB r_b (\mu(\dot{\phi}) + \xi_0 \sqrt{\frac{\delta_c}{r_b}}) \quad (4.10)$$

where r_b is the radius of the bit and δ_c is the depth of cut per circle:

$$\delta_c = \frac{2\pi ROP}{w} \quad (4.11)$$

ROP , representing the average rate of penetration, is given as [20]:

$$ROP = c_1 F_0 \sqrt{w} + c_2 \quad (4.12)$$

where F_0 is the difference between the total weight and the hookload, w is the average bit speed. $\mu(\dot{\phi})$ is modeled as a continuous function [20]:

$$\mu(\dot{\phi}) = \mu_0 \left(\tanh \dot{\phi} + \frac{\alpha_1 \dot{\phi}}{1 + \alpha_2 \dot{\phi}^2} + \nu \dot{\phi} \right) \quad (4.13)$$

$F_{\dot{\phi}}$ is generated by rotating unbalance, and is given as:

$$F_{\dot{\phi}} = m \dot{\phi}^2 r \quad (4.14)$$

where r is the eccentric distance.

F_c is the contact force. Depending on if the i th node is in contact with the borehole or not, it can be calculated by:

$$F_c = \begin{cases} -k_c(\sqrt{v_i^2 + w_i^2} - 0.05) & \sqrt{v_i^2 + w_i^2} \geq 0.05 \\ 0 & \sqrt{v_i^2 + w_i^2} < 0.05 \end{cases} \quad (4.15)$$

F_{tor} is the torque given by the borehole wall when the i th node is in contact with the borehole. v_i and w_i represent the lateral displacements of the drill-string on i th node. F_{tor} is simplified as:

$$F_{tor} = -\mu R k_c (\sqrt{v_i^2 + w_i^2} - 0.05) \times \text{sign}(\dot{\theta}_{u_i}) \quad (4.16)$$

where μ is a type of friction coefficient and R is the drill-collar radius. It is assumed in this chapter that the stabilizer initially contacts with the borehole wall. It is also assumed that the clearance between the borehole wall and drill-collar is 0.05 m .

F_g is the elementary load vector resulting from the gravity field:

$$F_g = \int_0^1 \rho g A l_e N_u^T d\xi + C \times mg \quad (4.17)$$

where C is the corresponding transformation matrix and l_e is the element length. N_u is the shape function matrix given in Chapter 3.

F_h is the hook load given as:

$$F_h = ratio \times Weight_{drilling\ system} \quad (4.18)$$

In this chapter, the weight of drillpipe is about 43 percent of the total weight. In order to make the drillpipe under tension and put the central point in drillcollar part, *ratio* is chosen to be larger than 0.5 in the simulations.

T_{rb} is the torque given by the rotary table. It is assumed in this chapter that the rotary table is driven by a DC motor through a gear box and T_{rb} is given as [20]:

$$L\dot{I} + R_m I + K_m n \dot{\phi}_{rt} = V_c \quad (4.19)$$

$$V_c = K_m n w_d \quad (4.20)$$

$$T_{rb} = K_m n I \quad (4.21)$$

where I is the motor current and $\dot{\phi}_{rt}$ is the speed of the rotary table. w_d is assumed to be the desired table speed in this paper.

4.1.2 Initial deformed condition

In practice, the drill-string is lowered until the bit touches the formation. WOB_{static} grows in the event of continued lowering and finally reaches the highest static value. In addition to the WOB_{static} , the drill-string is also subjected to distributed loads due to its own weight and constant hookload at the top position. Therefore, the equation of motion for the system is written as:

$$M\ddot{q} + C\dot{q} + Kq = F_g + F_h + WOB_{static} \quad (4.22)$$

Notice that F_g , F_h and WOB_{static} are all time-invariant. *Ratio* is chosen to be 0.6. Using Matlab solver ode23t, the initial deformed condition q_0 is obtained, which will be used as the initial condition in the further simulations. From the value of q_0 , it is clear that entire drillpipe and nearly 20 percent of the drillcollar is under tension. The percentage of the drillcollar can be changed by chosen different *ratio*. As mentioned above, in order to make the central point in drillcollar part, *ratio* is chosen to be larger than 0.5 in the simulations.

4.1.3 Model simplification

Firstly, it is assumed in the chapter that stabilizer can effectively suppress lateral vibrations. Secondly, considering that the drillpipe is under tension, geometric stiffening effect will make it difficult to bend. Therefore, lateral degrees of freedom of drillpipe can be neglected. The stiffness and mass matrices for drillpipe elements are

simplified as:

$$K_{pipe} = \begin{bmatrix} \frac{EA}{le} & 0 & -\frac{EA}{le} & 0 \\ 0 & \frac{GJ}{le} & 0 & -\frac{GJ}{le} \\ -\frac{EA}{le} & 0 & \frac{EA}{le} & 0 \\ 0 & -\frac{GJ}{le} & 0 & \frac{GJ}{le} \end{bmatrix} \quad (4.23)$$

$$M_{pipe} = \begin{bmatrix} \frac{\rho Al}{3} & 0 & \frac{\rho Al}{6} & 0 \\ 0 & \frac{\rho Jl}{3} & 0 & \frac{\rho Jl}{6} \\ \frac{\rho Al}{6} & 0 & \frac{\rho Al}{3} & 0 \\ 0 & \frac{\rho Jl}{6} & 0 & \frac{\rho Jl}{3} \end{bmatrix} \quad (4.24)$$

The total degrees of freedom of the model are reduced to 106 after this simplification.

4.2 Simulation Setup and Results

4.2.1 Deterministic results

In this chapter, a drill-string with the specification similar to the one used in Ref.[36] is considered. The specification of the drill-string can be found in Appendix A. Based on the model developed, simulation is firstly carried out for deterministic case. The simulation results in the case when the desired table speed is 15 rad/s (142.2 rpm) and *ratio* is 0.6, are shown in Figure 4.2. It can be seen that the bit rotary speed experiences large fluctuations in this case. The rotation of the bit is slowed down to nearly zero at some points and then increased to as high as 30 rad/s (284.5 rpm) at some other points. This phenomenon, as mentioned in the introduction, is known as stick-slip oscillation. An effective measure to mitigate the stick-slip in drilling operation is to increase RPM once it is detected. Figure 4.3 shows the simulation

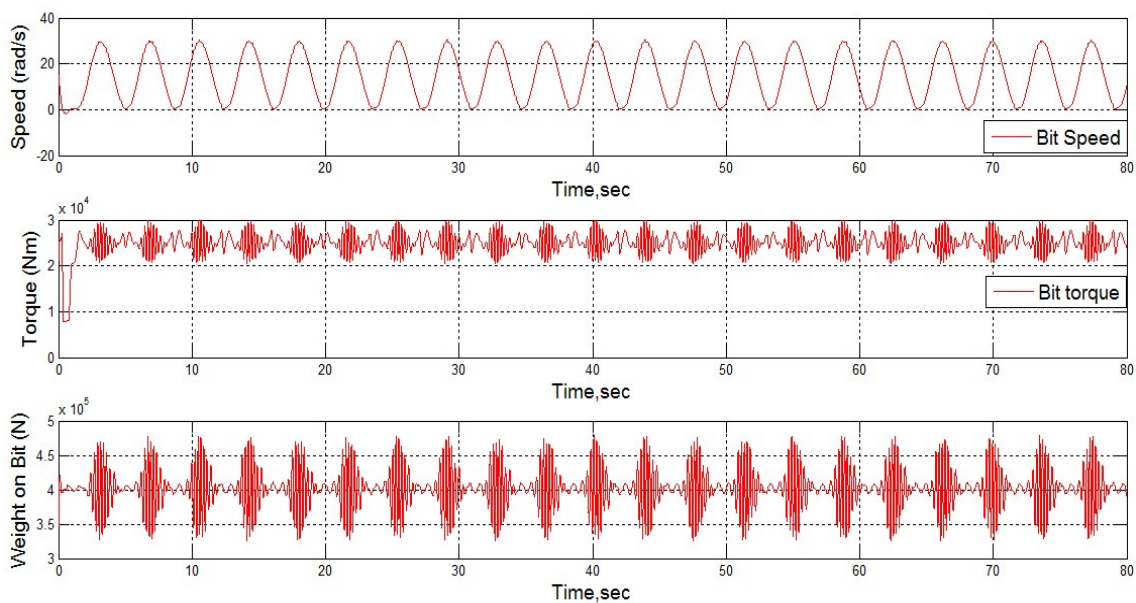


Figure 4.2: Desired table speed is 15 rad/s and stick-slip is detected

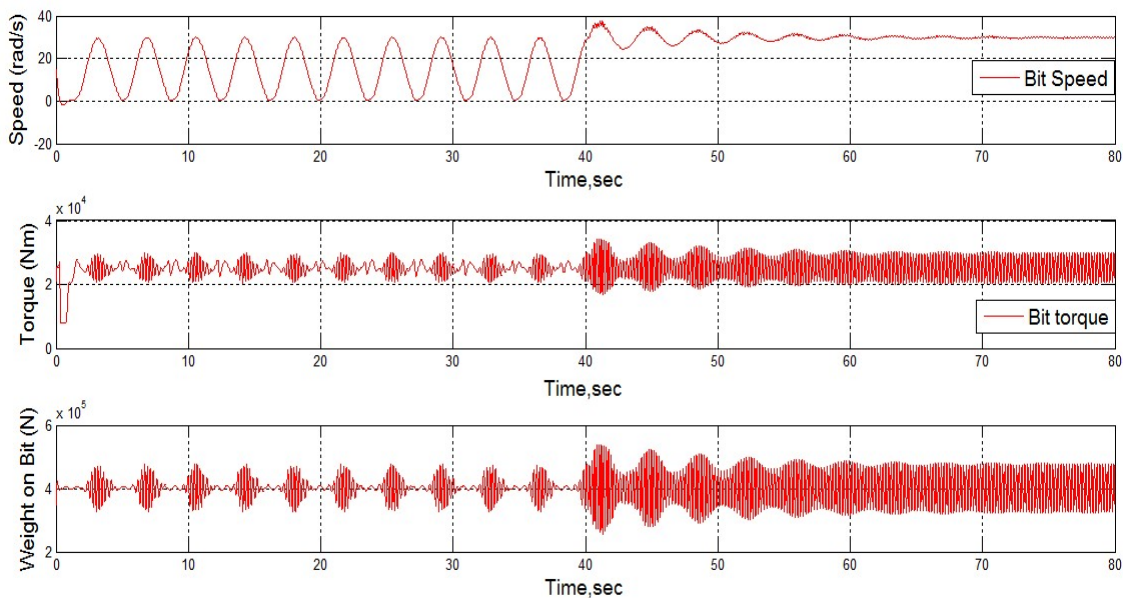


Figure 4.3: Increasing desired table speed from 15 rad/s to 30 rad/s

results when the desired table speed is increased from 15 rad/s to 30 rad/s (*ratio* is still 0.6). As can be seen, stick-slip is effectively eliminated at this table speed. The bit remains in contact with the formation and no bit-bounce can be found. *WOB* fluctuates around the static value ($4 \times 10^5 \text{ N}$) and the maximum amplitude remains nearly unchanged. After increasing the desired table speed from 15 rad/s to 30 rad/s , the bit rotary speed experiences large fluctuations at the beginning and then decays gradually. The reason for this may be that the torque given by the *DC* motor can overcome *TOB* and the vibrations are reduced due to damping.

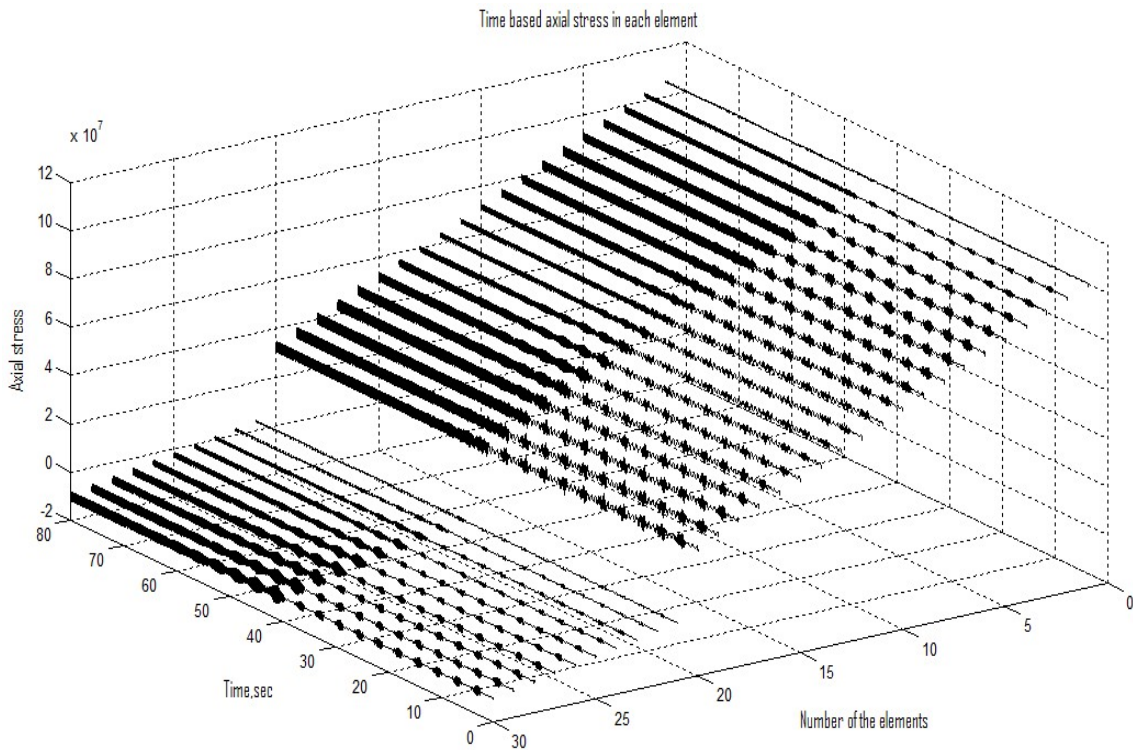


Figure 4.4: Time-based axial stress of each element

Figure 4.4 describes the time-based axial stress of each element before and after 40s. As can be seen in the figure, in the simulation, element 1 to 23 are under tension and the other elements are under compression. By setting the *ratio* to 0.6, the central

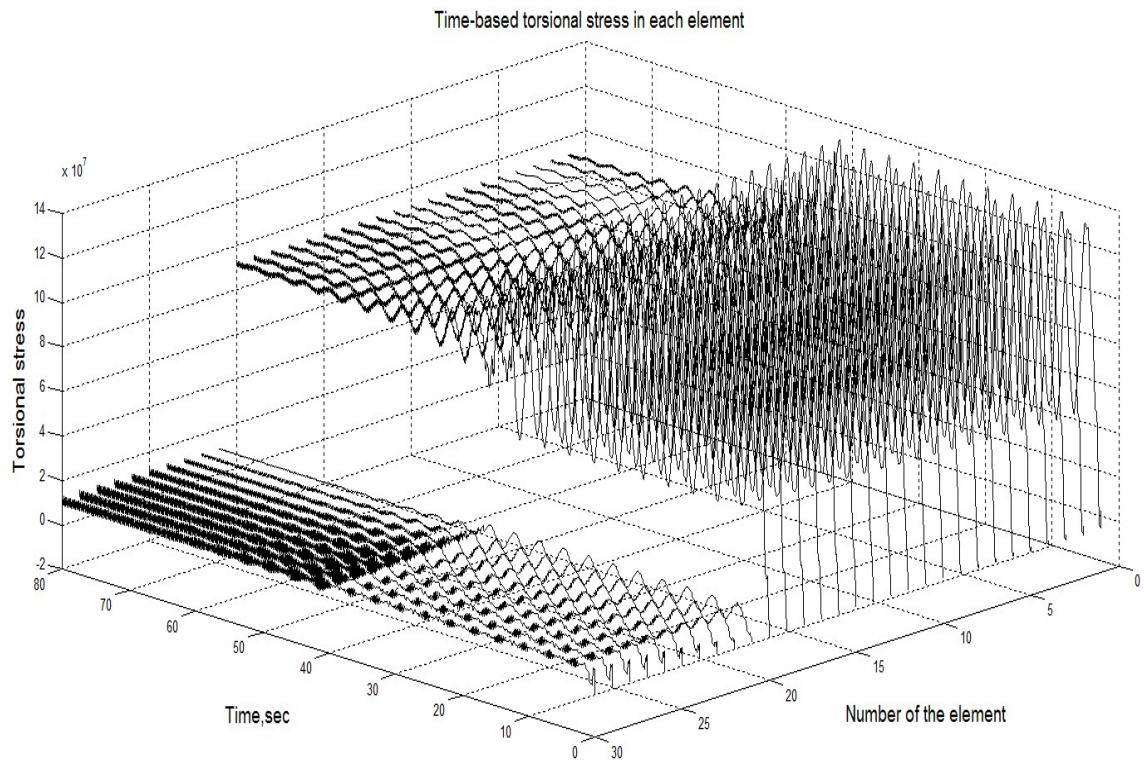


Figure 4.5: Time-based torsional surface stress of each element

point is successfully located in drillcollar part. Figure 4.5 describes the time-based torsional surface stress of each element before and after 40s. Element 20 is the last element of drillpipe and element 21 is the beginning element of dillcollar. Considering the cross sectional area of the later is 5.5 times larger than that of the former, the sudden change of the surface stress from element 20 to element 21 is reasonable. It can be seen that, when stick-slip happens, surface stress of the drillpipe also experiences large fluctuations. This phenomenon, if frequently happens, may enlarge surface cracks and cause premature failure of the drillpipe.

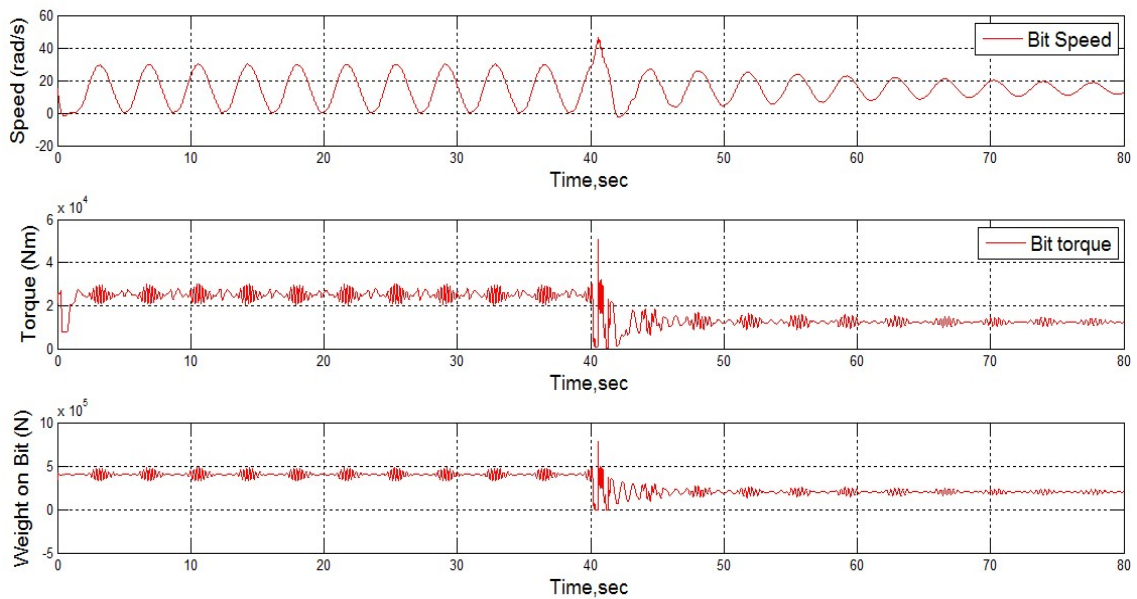


Figure 4.6: Increasing *ratio* from 0.6 to 0.8

According to equation 24, *WOB* influences *TOB*; the magnitude of *WOB* directly affects bit torsional oscillations. Therefore, reducing *WOB* by increasing *ratio* may help relieve the stick-slip problem. Figure 4.6 shows the simulation results when the *ratio* is increased from 0.6 to 0.8 and the desired table speed is kept as 15 *rad/s*. It can be seen that stick-slip problem is alleviated after increasing *ratio*. However, it is

also noticed that *WOB* is decreased by nearly 50 percent. Largely decreasing *WOB* will inevitably have negative influences on drilling efficiency, which may not be useful in the practice.

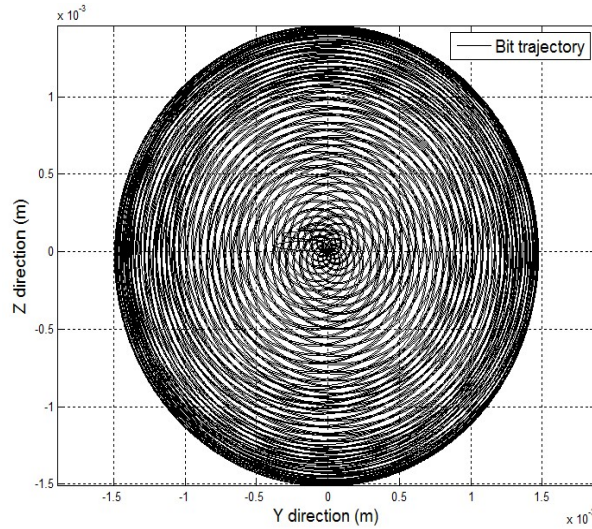


Figure 4.7: Bit trajectory when desired table speed is 15 rad/s

Figure 4.7 describes the bit trajectory when desired table speed is 15 rad/s . In the model, the bit has the same 0.05 m clearance with the borehole as does the collars. Rotating unbalance of the stabilizer leads to lateral vibrations, which excite bit in the lateral direction. The magnitude of the lateral vibrations depends on rotary speed, according to equation 28. When stick-slip happens, bit rotary speed periodically vibrates; therefore, bit trajectory is nearly evenly distributed in Figure 4.7. The denser part of Figure 4.8 represents the bit trajectory at the steady state when the desired table speed is 30 rad/s . As mentioned above, at the speed of 30 rad/s , large fluctuations quickly die out and the magnitude of the bit trajectory ranges from 1 to $1.5 \times 10^{-3} \text{ m}$ due to slight vibrations. It is pretty clear that the maximum deviation of the bit in Figure 4.7 is about $1.5 \times 10^{-3} \text{ m}$. Without stick-slip, the maximum deviation should be significantly less. Therefore, stick-slip vibration may not only

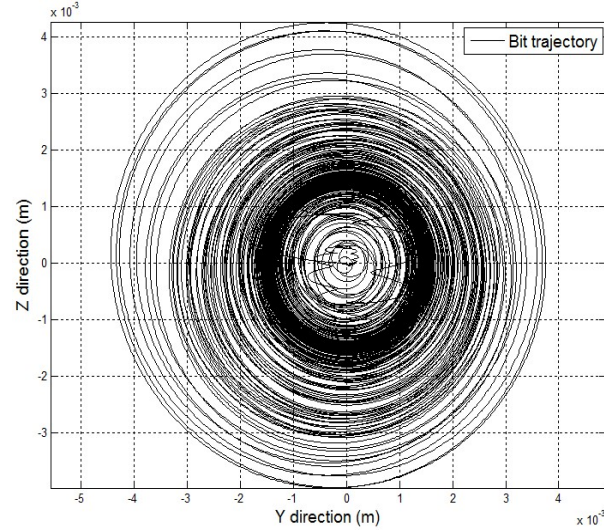


Figure 4.8: Bit trajectory when desired table speed is 30 rad/s

largely decrease ROP and cause fatigue failure of bit cutting elements, but also may lead to severe bit deviation and cause hole enlargement.

4.2.2 Monte Carlo Simulation for Random Case

According to Equations 4.5 to 4.13, the excitations of the drilling system, especially for WOB and TOB, depend on the displacement and speed vectors. The expressions of the excitations are too complex and statistical linearization is not applicable. Due to the nonlinearity of the system, spectral matrix solution method and covariance matrix solution method cannot be used directly either. Therefore, Monte Carlo simulation is employed in this chapter to investigate the behaviors of drilling assemblies subject to both deterministic and stochastic excitations. In the simulation, the desired table speed is 30 rad/s and *ratio* is 0.6. The equation of motion for the system is given as:

$$M\ddot{q}(t) + C\dot{q}(t) + Kq(t) = F(x, \dot{x}, \phi, \dot{\phi}, v, w, F_c, I) + Nw(t) \quad (4.25)$$

where $w(t)$ is assumed to be a stationary Gaussian white noise with zero mean and spectral intensity S_0 . N is a constant transformation matrix which inputs $w(t)$ to bit torsional degree of freedom. The stochastic excitation term compensates for phenomena that are not considered in bit-rock interaction.

Eqn 4.25 is valid for any given time instant q_i . Using the central difference method, the acceleration and velocity vectors at time t_i can be written as [37]:

$$\dot{q}_i = \frac{1}{2\Delta t}(q_{i+1} - q_{i-1}) \quad (4.26)$$

$$\ddot{q}_i = \frac{1}{\Delta t^2}(q_{i+1} - 2q_i + q_{i-1}) \quad (4.27)$$

Time step Δt depends on the maximum natural frequency w_n of the system. Δt is set to be 0.0002 in the simulation by considering:

$$\Delta t < \frac{2\pi}{w_n} \times \frac{1}{10} \quad (4.28)$$

By substituting equations 4.26 and 4.27 into equation 4.25, and rearranging the terms one has [37]:

$$q_{i+1} = \Delta t^2 N_1 F_i + N_2 q_i + N_3 q_{i-1} \quad (4.29)$$

with

$$F_i = f(x, \dot{x}, \phi_i, \dot{\phi}_i, v_i, w_i, F_c, I_i) + N \times w(t_i) \quad (4.30)$$

and

$$N_1 = [M + \frac{1}{2}\Delta t C]^{-1} \quad (4.31)$$

$$N_2 = N_1[2M - \Delta t^2 K] \quad (4.32)$$

$$N_3 = N_1[\frac{1}{2}\Delta t C - M] \quad (4.33)$$

M , K , C are all constant at each time step. x_i , \dot{x}_i , ϕ_i , $\dot{\phi}_i$, v_i , w_i and I_i are required to obtain F_i . However, Eqn 4.26 can not be used directly here to calculate \dot{x}_i and $\dot{\phi}_i$. To solve this problem, velocity vectors at time t_i are calculated in terms of:

$$\dot{q}_i = \dot{q}_{i-1} + \ddot{q}_{i-1}\Delta t \quad (4.34)$$

with

$$\ddot{q}_{i-1} = M^{-1}[F_{i-1} - C\dot{q}_{i-1} - Kq_{i-1}] \quad (4.35)$$

$f(I_i)$ is given as:

$$f(I_i) = T_{rb_i} = K_m n I_i \quad (4.36)$$

$$I_i = \frac{1}{L} \times (2\Delta t V_c - 2\Delta t n K_m \dot{\phi}_{i-1} - 2R_m I_{i-1} \Delta t + L I_{i-2}) \quad (4.37)$$

According to Eqn 4.30, the continuous time white noise excitation needs to be discretized in the simulation. It is achieved by using [38]:

$$w(t_i) = \sqrt{\frac{2\pi S_0}{\Delta t}} U_i \quad (4.38)$$

where random variables U_i are normal distributed variables with zero mean and unit standard deviation.

In the simulation, U_i is generated by the computer at each step. F_i is determined at time step t_i and therefore q_{i+1} can be calculated using Eqn 4.29. For each sample, the computational procedure can be described as below:

1. Initially set uniform q_0 , \dot{q}_0 , I_0 and I_{-1} for all the samples.
2. Compute $f(x_0, \dot{x}_0, \phi_0, \dot{\phi}_0, v_0, w_0, F_c, I_0)$ and $w(t_0)$, and then assemble F_0 .
3. Compute \ddot{q}_0 using equation $\ddot{q}_0 = M^{-1}[F_0 - C\dot{q}_0 - Kq_0]$.

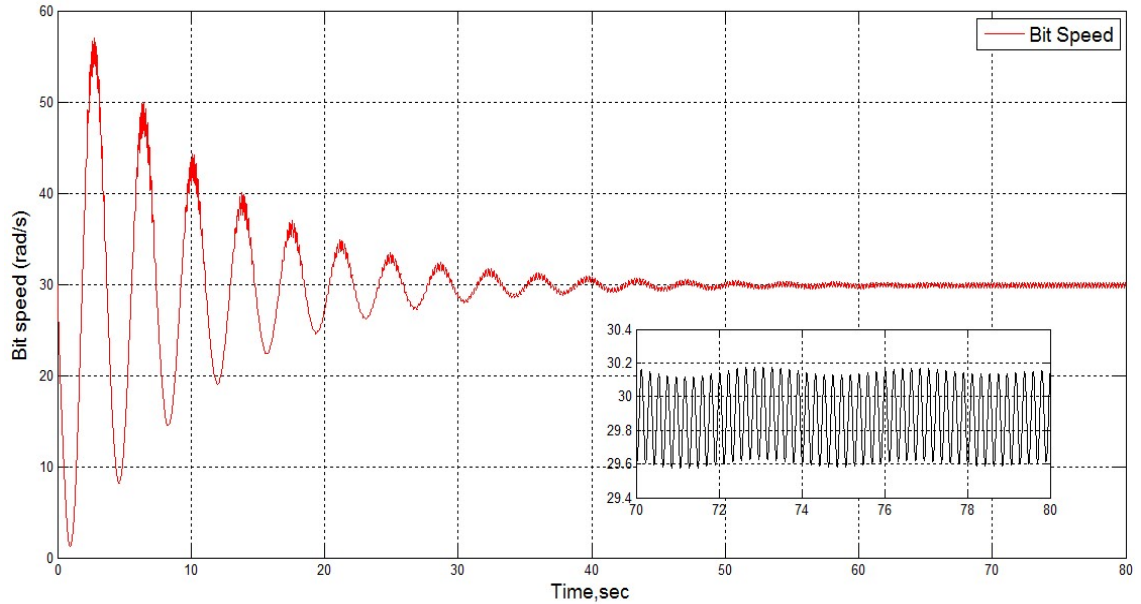


Figure 4.9: System response under deterministic excitation

4. Compute q_{-1} using equation $q_{-1} = q_0 - \Delta t \dot{q}_0 + \frac{\Delta t^2}{2} \ddot{q}_0$.
5. Start with $i = 0$.
6. Find q_{i+1} using Eqn 4.29.
7. Compute I_{i+1} using \dot{q}_i , I_i , I_{i-1} and Eqn 4.37, compute $f(I_{i+1})$.
8. Compute \dot{q}_{i+1} using Eqn 4.34.
9. Store q_{i+1} , \dot{q}_{i+1} , q_i , I_{i+1} and I_i .
10. Compute $f(x_{i+1}, \dot{x}_{i+1}, \phi_{i+1}, \dot{\phi}_{i+1}, v_{i+1}, w_{i+1}, F_c, I_{i+1})$ and $w(t_{i+1})$, and then assemble F_{i+1} .
11. Compute \ddot{q}_{i+1} using $\ddot{q}_{i+1} = M^{-1}[F_{i+1} - C\dot{q}_{i+1} - Kq_{i+1}]$.
12. $i = i + 1$.

Repeat step 6 to 12 until $i > N$. N marks the last step of the calculation. If the intensity of white noise $w(t_i)$ is set to zero, it corresponds to the deterministic case. The deterministic case can also be solved by Runge-Kutta method using Matlab build-in solver. Simulation results from these two methods are in excellent agreement, and are almost indistinguishable. This fact provides a verification to each method.

4.2.3 Random Response Statistics

Field test data have long recognized the random nature of down-hole vibration. However, the huge diversity and uncertainty in drilling, such as formation, resonance, dill-string well bore contact etc, make it almost impossible to determine work-for-all random intensity. In this chapter, two different power spectral densities are considered simply for comparison purpose.

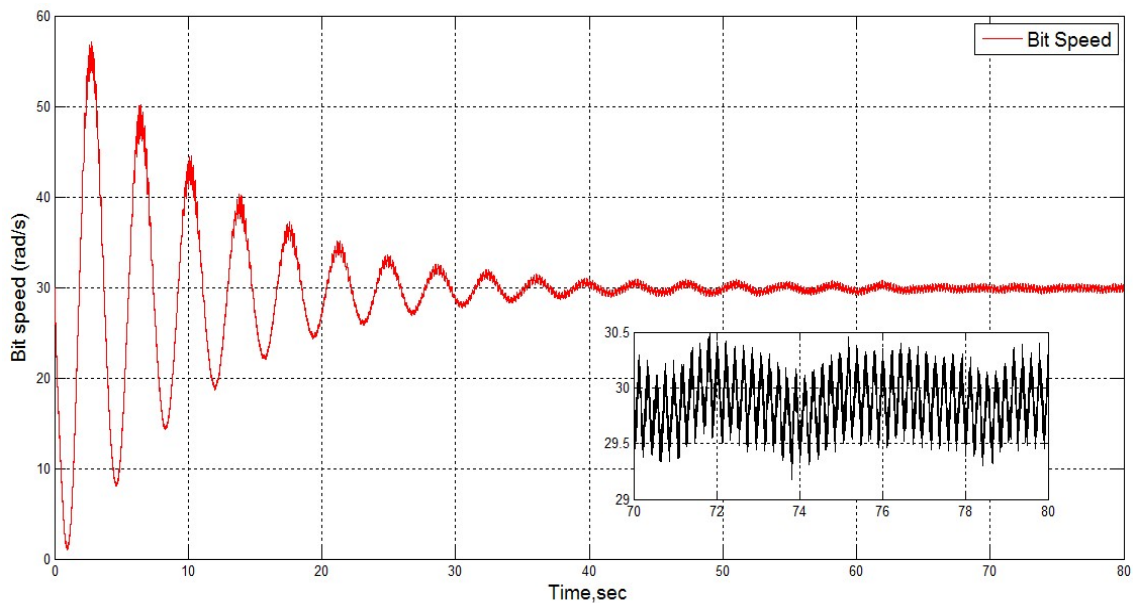


Figure 4.10: System response with white noise ($S_0 = 200$)

Figure 4.10 and 4.11 represent sample realizations of the response under deterministic excitation and a random noise with power spectral density of 200 and 2000

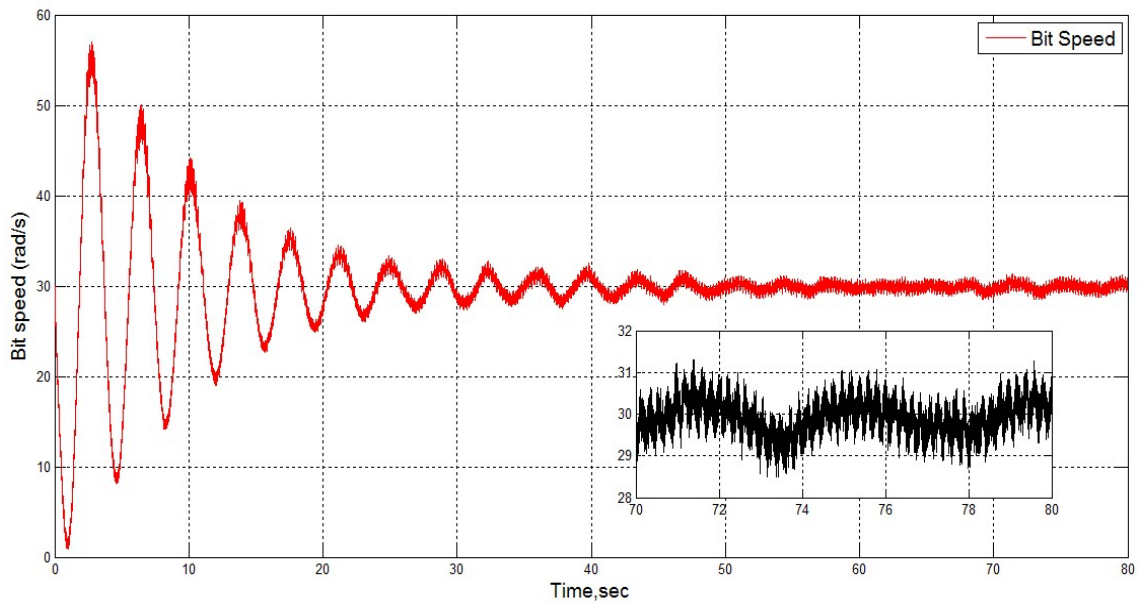


Figure 4.11: System response with white noise ($S_0 = 2000$)

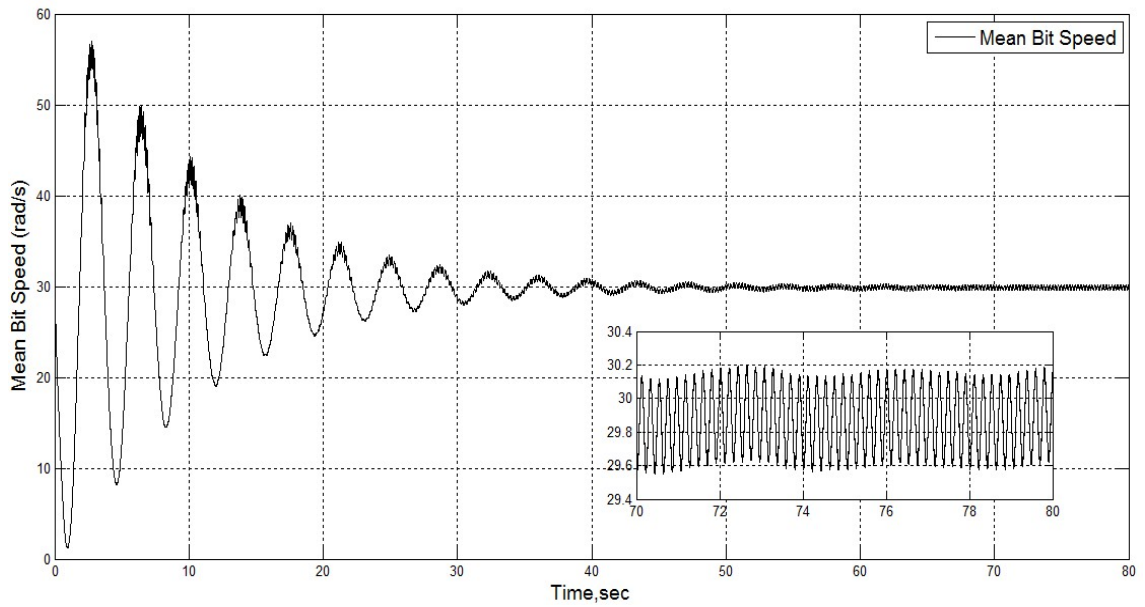


Figure 4.12: Mean bit speed (MC, $S_0 = 200$)

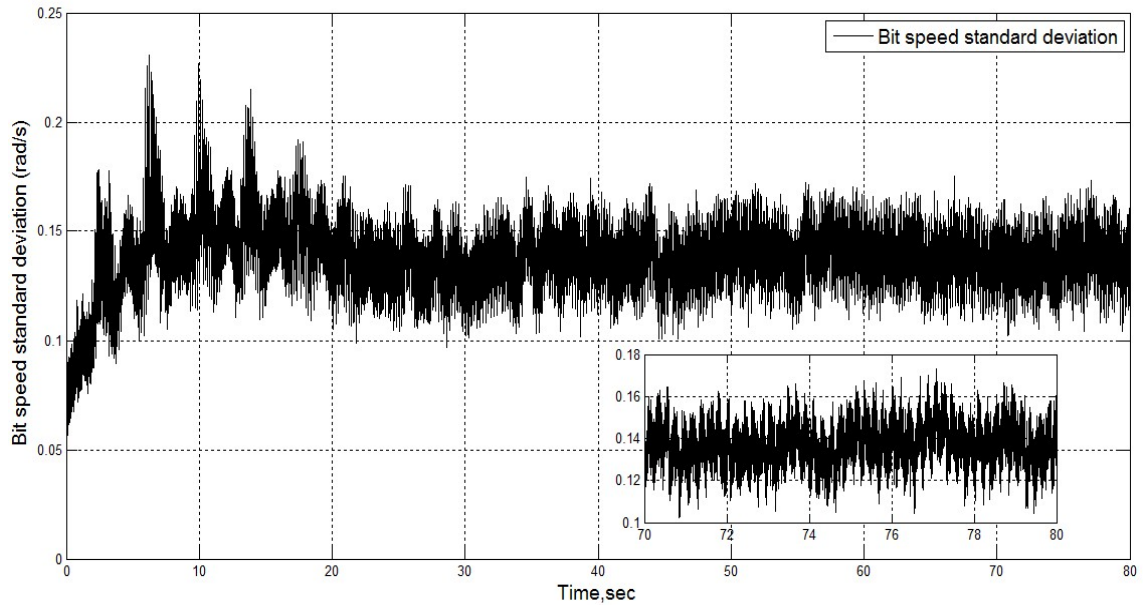


Figure 4.13: Bit speed standard deviation (MC, $S_0 = 200$)

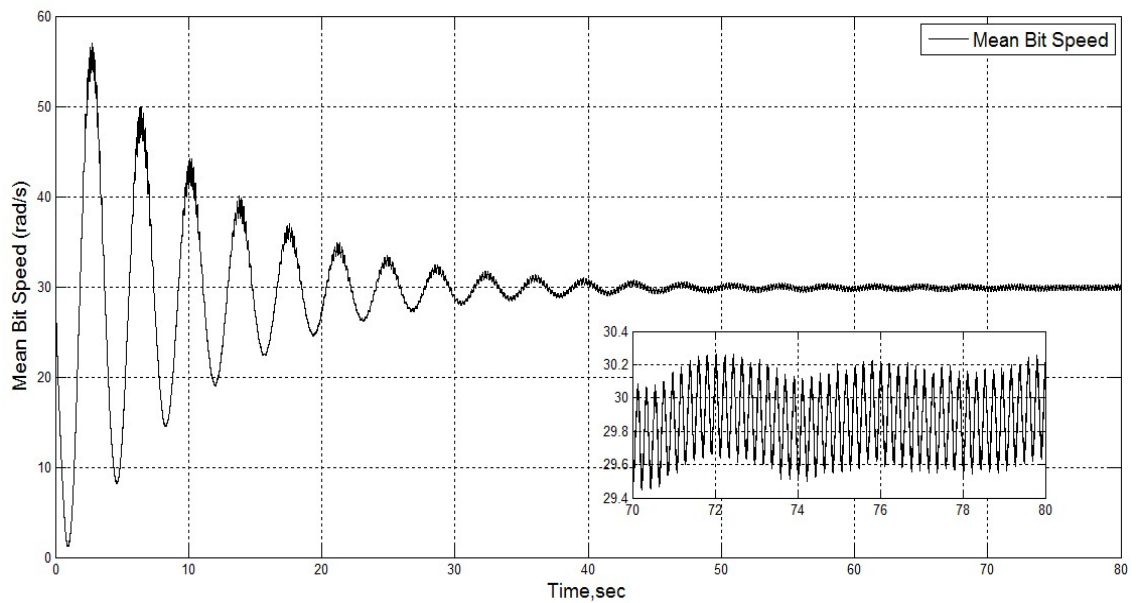


Figure 4.14: Mean bit speed (MC, $S_0 = 2000$)

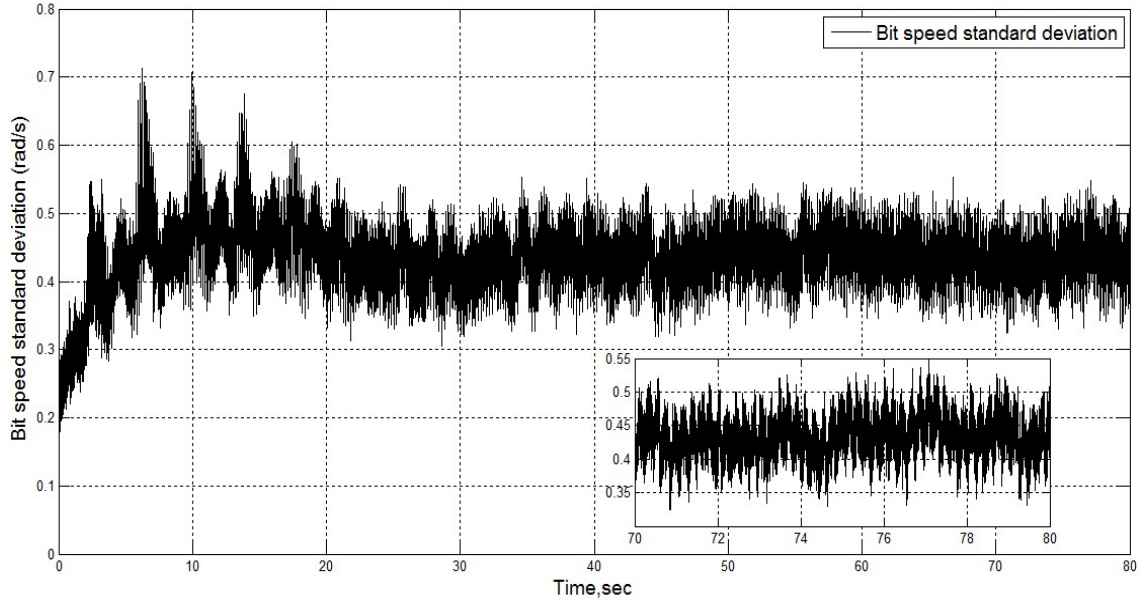


Figure 4.15: Bit speed standard deviation (MC, $S_0 = 2000$)

respectively. It can be seen that when the random intensity is low (Figure 4.10), the deterministic component is dominant in the response; while with increasing random intensity, the random part of the response becomes more obvious in Figure 4.11. Also for comparison, the response with only deterministic excitation with desired table speed of 30 rad/s , is given in Figure 4.9 as well. The mean of the response with $S_0 = 200$ is given in Figure 4.12. It can be seen the mean is almost the same with the deterministic response in Figure 4.9. This is because the random excitation is assumed as zero-mean and stochastic influence ($S_0 = 200$) is limited. Figure 4.13 and 4.15 show bit speed standard deviation results with the power spectral density of 200 and 2000 respectively. The unsmooth vibrations are considered due to the limited simulation samples and system's high natural frequencies. Please see the supportive explanation in Appendix B. Another possible reason may be that, the axial-torsional and lateral-torsional couplings combined with changing excitations (depend on the displacement and speed vectors) lead to time variant stiffness in the model.

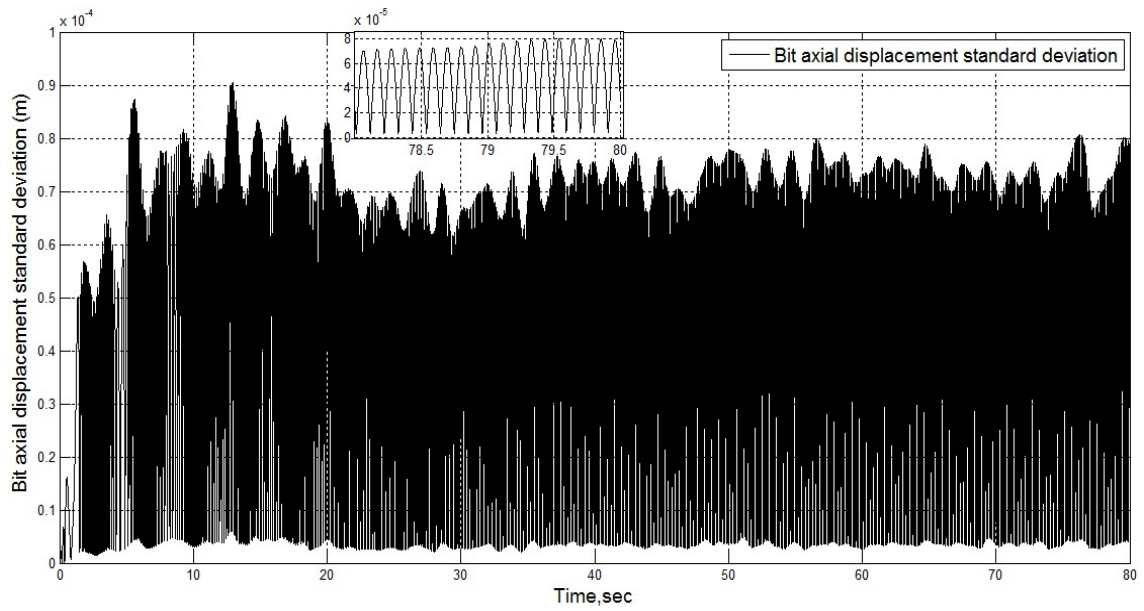


Figure 4.16: σ for bit axial displacement (MC, $S_0 = 200$)

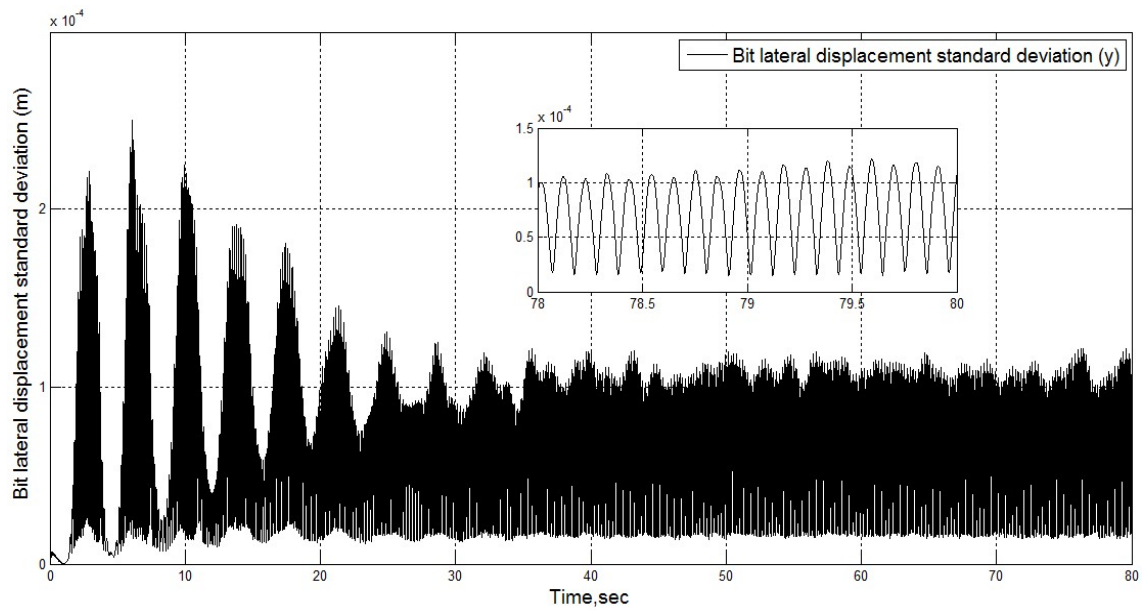


Figure 4.17: σ for bit y direction (MC, $S_0 = 200$)

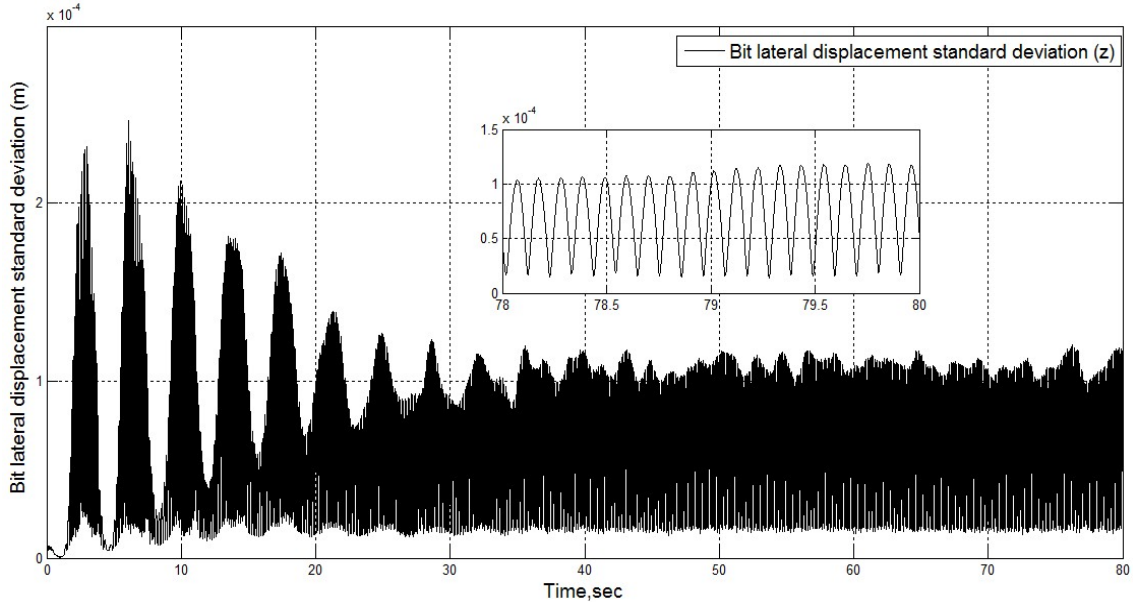


Figure 4.18: σ for bit z direction (MC, $S_0 = 200$)

Due to the many degrees of freedom and the very short time step Δt required in the simulation, the Monte Carlo simulation is very time and computer memory consuming. Precise result is difficult to obtain because of the limited 100 samples. Although the conclusions are not imprecise, they are still convincing. As can be seen in Figures 4.13 and 4.15, the corresponding standard deviations fluctuate around 0.14 and 0.45 at the steady state. Figure 4.16 represents the standard deviation of bit axial displacement. Although the magnitude (10^{-4}) is small, it definitely exceeds the numerical error and therefore it is considered due to the axial-torsional coupling. Without axial – torsional coupling, the standard deviation of axial displacement should be zero under the deterministic axial excitation. The inside figure shows that the standard deviation fluctuates around $4 \times 10^{-5}m$. Figure 4.17 and 4.18 describe the standard deviations of the bit lateral displacement caused by lateral-torsional coupling. It seems that, for the drill-string model presented in the paper, torsional random excitation has equivalent influences in bit y and z directions. Similar result is observed when the

spectral intensity is 2000.

4.3 Conclusion Remarks

Using a finite element model with six degrees of freedom per node, this chapter investigates the dynamic behaviors of a drill-string subject to both deterministic and random excitations. The model is axial-torsional, lateral-torsional coupled. MC simulation, in combination with a modified central difference method, is employed in obtaining the response statistics. The main conclusions drawn from this chapter are as below:

1. Stick-slip vibration happens under certain conditions, and it can be effectively mitigated by increasing the table speed.
2. Rotating unbalance may lead to severe bit deviation and cause hole enlargement.
3. Axial-torsional and lateral-torsional couplings introduce random components into drill-string axial and lateral directions.

The current work does not consider the geometric stiffness and the influence of the drilling mud. Work on more complicated model, which is nonlinear and consider the hydrodynamic forces, is on the way.

Chapter 5

Stick-slip Analysis of a Drill-string under Deterministic and Stochastic Circumstances

This chapter focuses on drill-string torsional vibration and its stick-slip analysis. A finite element model of the drillstring with inclusion of both deterministic and random excitations is developed. Simulation is carried out under certain parameters and it is shown that in deterministic case the torsional vibration may exhibit stick-slip. With change of some parameters, bifurcation and chaos of the system are observed. In the random case, Monte Carlo simulation is used to capture the probabilistic information of the response.

It is assumed in this chapter that the drill-string is clamped on the top and the ground rotates at a constant speed. Therefore, the drill-string is driven by TOB in the dynamic model. The simplified model of the system discussed in this chapter is shown in Figure 5.1

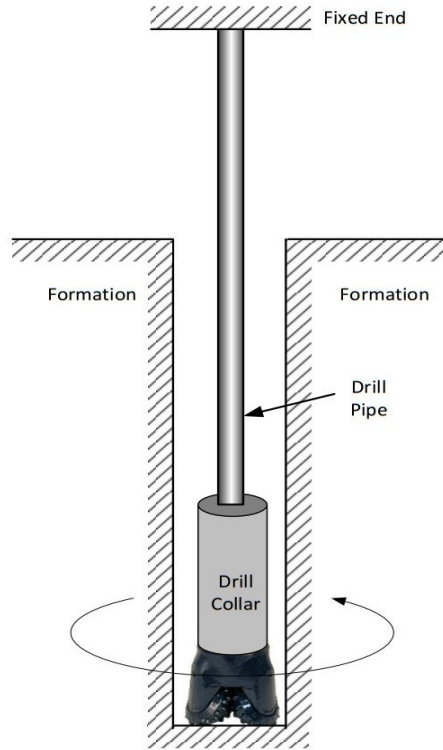


Figure 5.1: The simplified model of the system

5.1 Dynamic Model

5.1.1 Finite Element Model

Because this chapter only focuses on drill-string torsional vibration, the drill-string is discretized into finite element model only using Lagrange linear shape function for the twisting angle ϕ . Thus, the displacements are represented as:

$$\phi = N \cdot q \quad (5.1)$$

where N , is the shape function matrix, and q is the vector of nodal coordinates of the two-node finite element, which is defined by:

$$q = \{\phi_1 \quad \phi_2\}^T \quad (5.2)$$

By defining the element length l_e and the non-dimensional element variable $\xi = x/l_e$, the shape function matrix is given as:

$$N = \{1 - \xi, \quad \xi\} \quad (5.3)$$

The expression for the local stiffness K_e is:

$$K_e = \int_0^1 \frac{GJ}{l_e} N'^T N' d\xi \quad (5.4)$$

The expression for the local mass matrix M_e is:

$$M_e = \int_0^1 \rho J l_e N^T N d\xi \quad (5.5)$$

where G is the shear modulus, J is the polar moment of inertia of drill-string cross section. J and l_e both have two different values for drillpipe and drillcollar. Substituting Eqn 5.3 into Eqn 5.4 and Eqn 5.5, the local stiffness K_e and mass M_e are

obtained:

$$K_e = \begin{bmatrix} \frac{GJ}{l_e} & -\frac{GJ}{l_e} \\ -\frac{GJ}{l_e} & \frac{GJ}{l_e} \end{bmatrix} \quad (5.6)$$

$$M_e = \begin{bmatrix} \frac{\rho J l_e}{3} & \frac{\rho J l_e}{6} \\ \frac{\rho J l_e}{6} & \frac{\rho J l_e}{3} \end{bmatrix} \quad (5.7)$$

By assembling the local stiffness and mass matrices respectively, system's global mass and stiffness matrices can be obtained. In this paper, the drill-string is divided into 30 elements: 20 elements for drillpipe section and 10 elements for drillcollar section. Considering the boundary condition on the top, the drill-string finite element model contains 30 degrees of freedom in total.

5.1.2 Dynamic Equation

After some mathematical manipulation, the equations of motion for the system can be represented in a compact matrix form as:

$$M\ddot{q}(t) + C\dot{q}(t) + Kq(t) = F(\dot{\phi}) + F(t) + F \quad (5.8)$$

where M , C and K are the system global mass, damping and stiffness matrices, respectively, $q(t)$ is the displacement vector. $F(\dot{\phi})$, $F(t)$ and F together represent the excitations. The downhole damping C is assumed to be a linear combination of K and M in this chapter as below:

$$C = \alpha M + \beta K \quad (5.9)$$

where α and β are constants to be selected. In the chapter the system is assumed as underdamped which is common in engineering application.

$F(\dot{\phi})$ represents the dry friction, which is considered in two different forms in the chapter [23]:

$$Model\ 1 : F(\dot{\phi}) = \begin{cases} WOB \cdot r_b \cdot u_1 & 0 \leq V - \dot{\phi}_{bit} < e \\ WOB \cdot r_b \cdot u_2 & V - \dot{\phi}_{bit} \geq e \end{cases} \quad (5.10)$$

$$Model\ 2 : F(\dot{\phi}) = \begin{cases} WOB \cdot r_b \cdot u_1 & 0 \leq V - \dot{\phi}_{bit} < e \\ WOB \cdot r_b \cdot u_3 & V - \dot{\phi}_{bit} \geq e \end{cases} \quad (5.11)$$

where WOB is the constant weight on bit, which is about 40 percent of the total drill-string weight, r_b is the radius of the bit, V is the constant rotary speed of the ground, e is the narrow band separating the stick and slip situations, which is given as 0.01, u_1 is the static friction coefficient, which is originally set to be 0.3, u_2 and u_3 are two different kinetic friction coefficients, u_2 is constant (0.21) and u_3 is formulated as [23]:

$$u_3 = u_2 + (u_1 - u_2)exp(-|V - \dot{\phi}_{bit}|) \quad (5.12)$$

$F(t)$ and F simulate the torque during the bit cutting actions. F is constant and $F(t)$ is given as:

$$F(t) = 5000 \cdot \sin(\omega \cdot t) \quad (5.13)$$

where ω is the frequency of the harmonic excitation.

It is assumed in the chapter that the drill-string is clamped on the top and the ground rotates at a constant speed. Therefore, the drill-string is driven by TOB in the simulation. Given the fact that the deterministic representation of the excitation above is not able to fully define the complex excitation mechanism in drilling, a

random excitation can be added to the model as:

$$M\ddot{q}(t) + C\dot{q}(t) + Kq(t) = F(\dot{\phi}) + F(t) + F + W(t) \quad (5.14)$$

where $W(t)$ is a stationary Gaussian white noise with zero mean and spectral intensity S_0 .

5.2 Solution Strategy

Central difference method is employed as the numerical method. Time step Δt depends on the maximum natural frequency ω_n of the system. Δt is determined in the simulation by considering:

$$\Delta t < \frac{2\pi}{\omega_n} \times \frac{1}{10} \quad (5.15)$$

The continuous time white noise excitation in Eqn 6.16 is discretized in the simulation by using [38]:

$$W(t_i) = \sqrt{\frac{2\pi S_0}{\Delta t}} U_i \quad (5.16)$$

where random variables U_i are normal distributed with zero mean and unit standard deviation.

It is assumed in the chapter that stick-slip happens when:

$$|V - \dot{\phi}_{t_i}| < e \quad (5.17)$$

where $\dot{\phi}_{t_i}$ is the speed of the bit at t_i . Assuming ϕ_1 and ϕ_2 are angular displacements of the drill-string last element at t_s . It is defined in the simulation that the stick is

interrupted when:

$$torque = \frac{G \cdot J}{l_e} \cdot (-\phi_1 + \phi_2) \quad (5.18)$$

$$torque > F(\dot{\phi}_{t_s}) + F(t_s) + F + (W(t_s)) \quad (5.19)$$

5.3 Results from Deterministic Excitations

5.3.1 Stick-slip

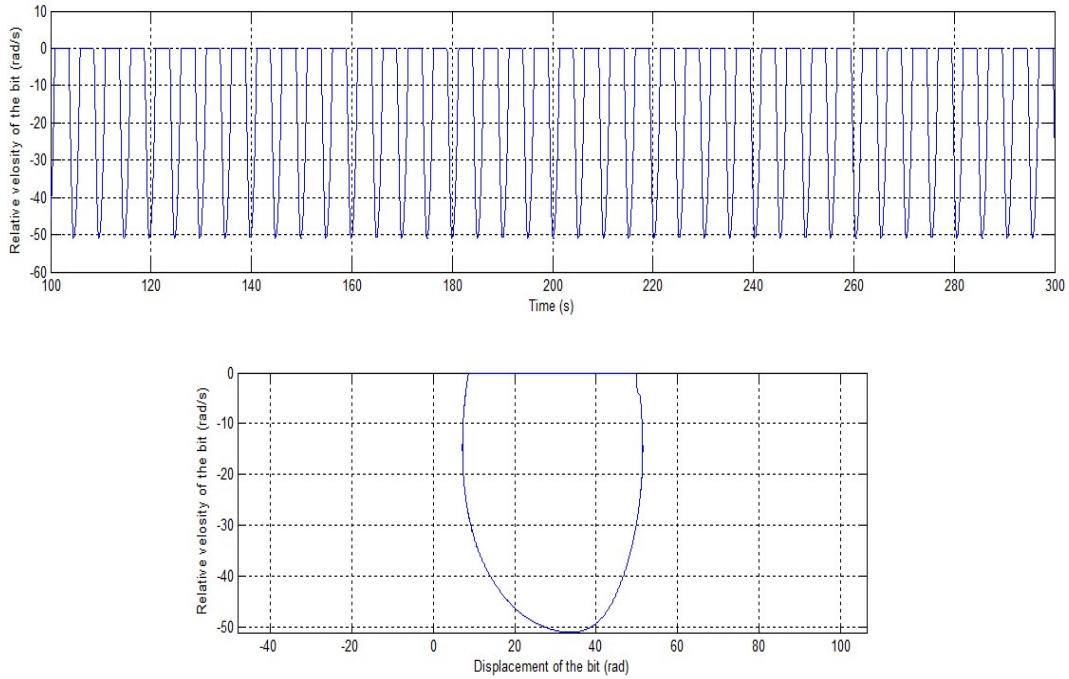


Figure 5.2: Stick-slip is detected in model 1

In this chapter, a drill-string with the specification similar to the one used in Ref.[36] is considered. The specification of the drillstring can be found in Appendix A. As mentioned above, the drill-string is clamped on the top and driven by a constant rotating ground at the end. Therefore, the stick-slip happens when the relative speed

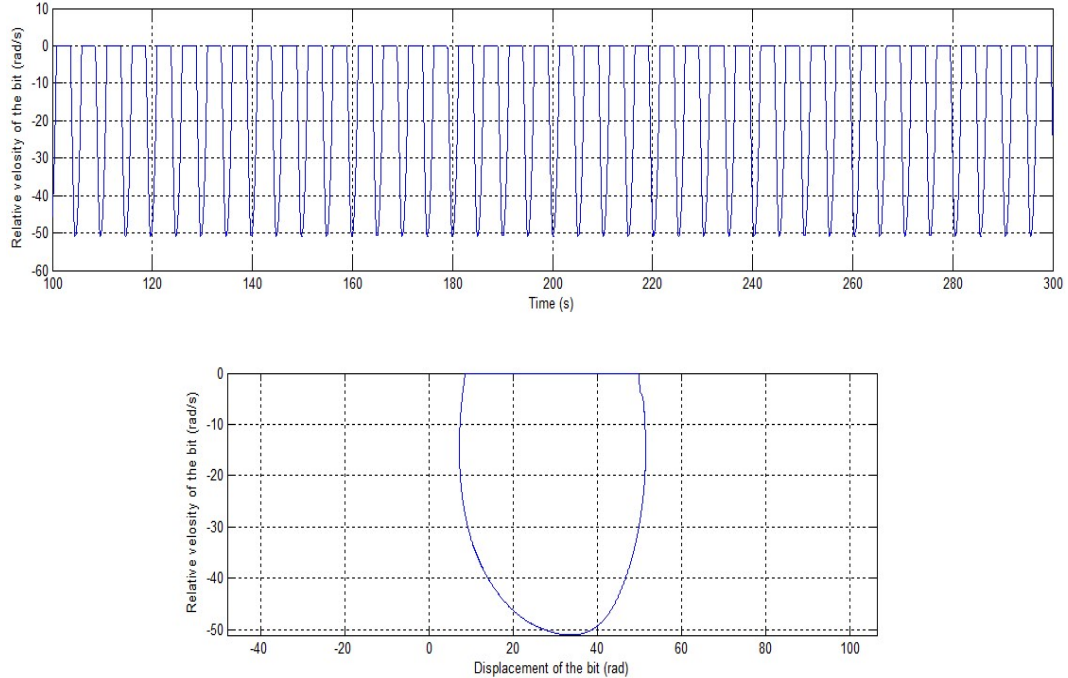


Figure 5.3: Stick-slip is detected in model 2

between the bit and the ground reaches zero or becomes pretty close to zero. The simulation result with a ground speed of 15 rad/s (142.2 rpm) is shown in Figure 5.2. The frequency of the harmonic excitation in Eqn 6.6 is given as 5 rad/s and the dry friction is calculated using model 1. As can be seen in the phase plane, while the bit sticks, the displacement of the bit keeps increasing. This status continues until the torque calculated from Eqn 5.18 becomes larger than the TOB (without random excitation). After that, the relative bit speed is increased to as high as 52 rad/s (493.1 rpm). It is clear that the trajectory of the bit has only one period in this case. During the process, the drill-string experiences severe torsional vibrations. Figure 5.3 shows the similar result when the dry friction is calculated using model 2. Further investigations indicate that model 1 and model 2 show some differences in capturing the bifurcation and chaos of the system. Their differences will be reported in future publications. Model 2 is used in the following simulations.

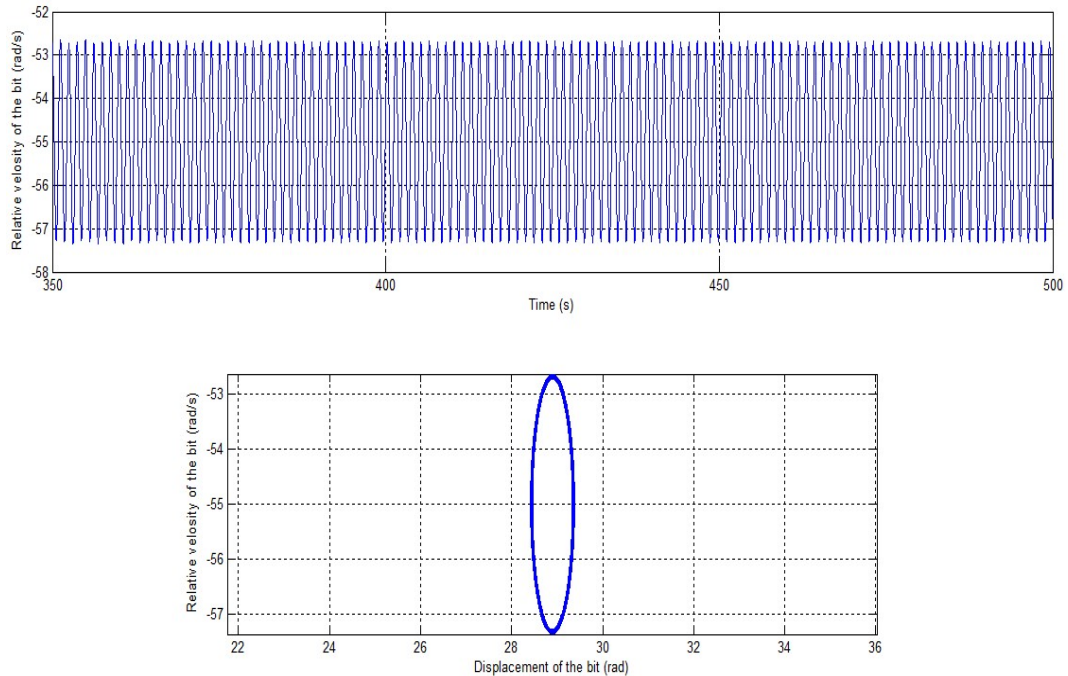


Figure 5.4: Stick-slip is eliminated by increasing the ground speed to 55 rad/s

An effective measure to mitigate the stick-slip in drilling operation is to increase rotation per minute (RPM) once it is detected. Figure 5.4 shows the simulation results when the ground speed is increased from 15 rad/s to 55 rad/s with all other parameters unchanged. As can be seen, stick-slip is effectively eliminated and the bit speed experiences small fluctuations due to harmonic excitation.

5.3.2 Bifurcation and Chaos

Bifurcation and chaos mark the sudden change of the motion in mechanical system. It is found in the simulations that the system response is very sensitive to the changes of the parameters. By changing the static friction coefficient u_1 from 0.3 to 0.2 and the kinetic friction coefficient u_2 from 0.21 to 0.14, the friction coefficients induced bifurcation is detected and is described in Figure 5.5 as a double periodic motion. Frequency induced bifurcation is also discovered by changing the frequency of the

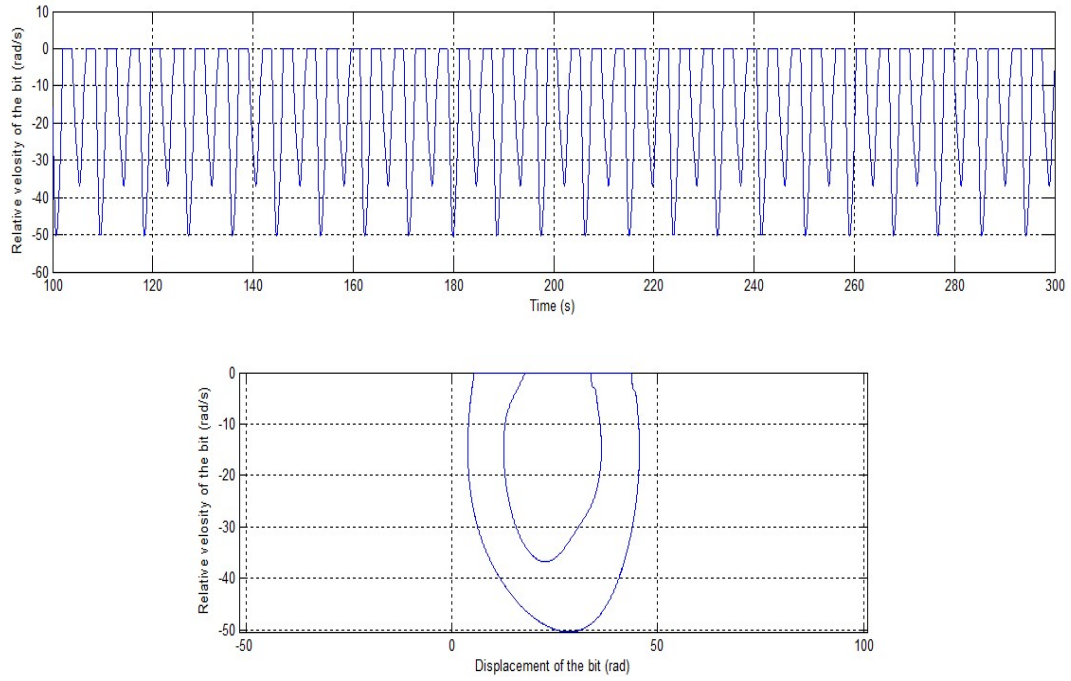


Figure 5.5: Friction coefficients induced bifurcation

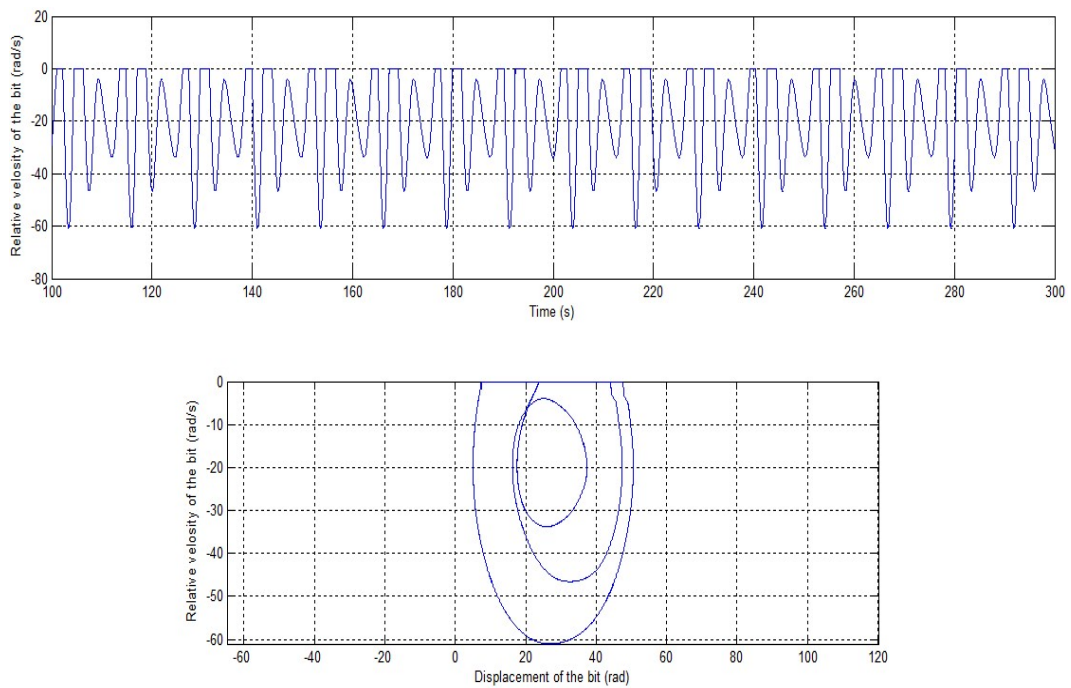


Figure 5.6: Frequency induced bifurcation

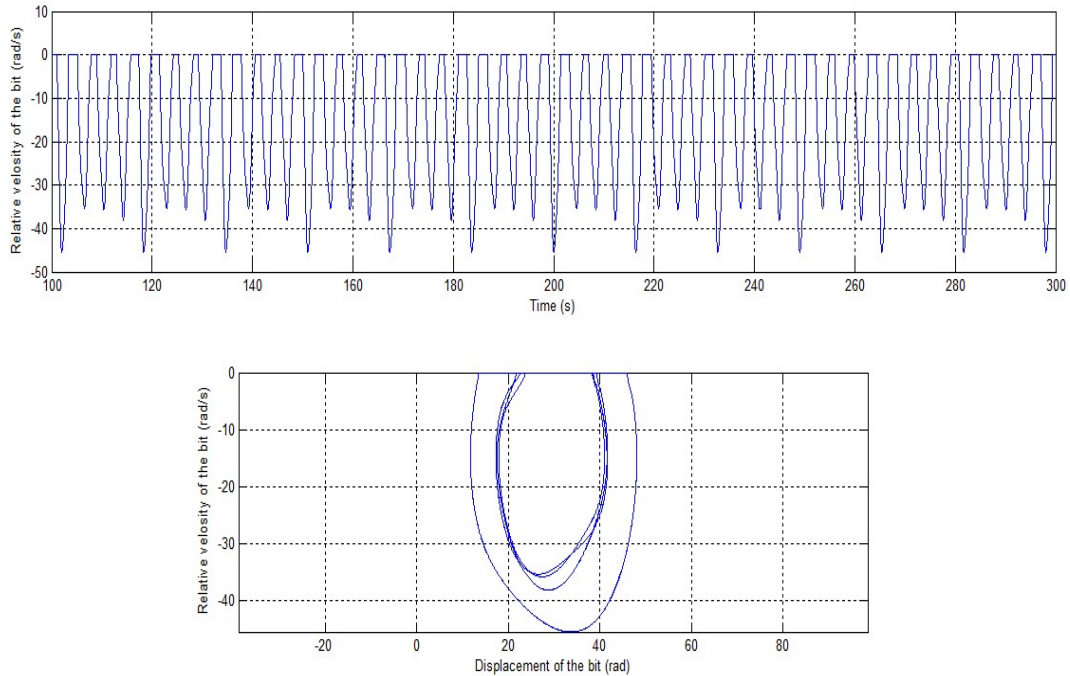


Figure 5.7: Damping induced bifurcation

harmonic excitation from 5 rad/s to 2 rad/s while the ground speed is 20 m/s . As can be seen in Figure 5.6, a three-period motion is observed. It is also noticed that the bifurcation develops into chaos as the frequency becomes smaller. In addition to the excitation induced bifurcations, some researchers reported damping induced bifurcations in their reports [39]. This phenomenon is also detected in the simulation. By changing α and β both from 0.01 to 0.03, the damping induced bifurcation is captured and the corresponding four periodic motion is described in Figure 5.7.

Closely related to bifurcations, chaos is a special kind of motion which is unique to non-linear oscillation systems. It marks the behavior of a system that is inherently unpredictable. Observed from the simulations, many changes in the parameters lead to chaotic responses. The example listed here is a result of changing both friction coefficients and harmonic excitation frequency. As can be seen in Figure 5.8 (phase plane), the clearances between the bit trajectories definitely exceeds the numerical

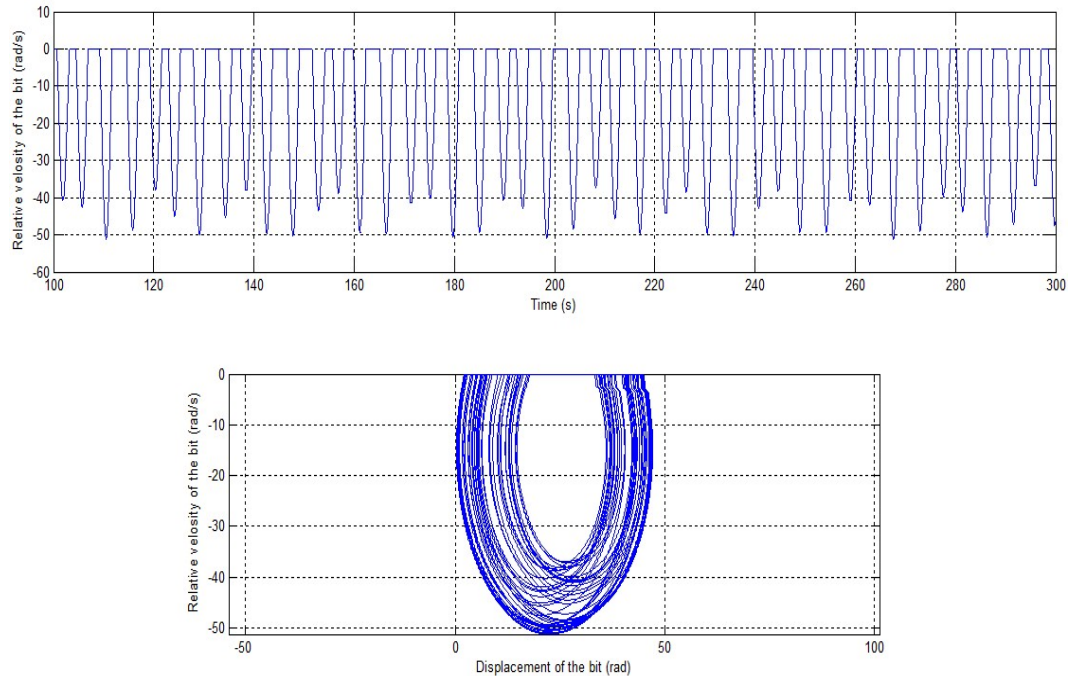


Figure 5.8: Chaos is detected when u_2 is 0.14, u_1 is 0.2 and w is 1 rad/s

error and therefore it is considered to be chaotic behaviors. Bifurcation and chaos will inevitably bring complexity to drill-string system and make down-hole dynamic responses difficult to predict.

5.4 Results Considering Random Components

The dynamic equation of the system is nonlinear and random in nature. Several methods are available for solving nonlinear random dynamics systems, including Monte Carlo (MC) method, statistic linearization, various closure methods, stochastic averaging method and direct integration methods. Given the highly complexity and the many degrees of freedom, MC is chosen in this chapter. The sample size is set to be 200 and the simulation results between 180 s and 200 s are recorded in the simulation. Although field test data has long recognized the random nature of down-hole vibration,

no data have been reported on the strength of the randomness in public literature. In the simulation of this chapter, the power spectral density is set to be $S_0 = 20$ which may not be realistic in real drilling operation. However, this does not affect the significance of the study. More realistic strength of the randomness in the excitation can be obtained through future tests.

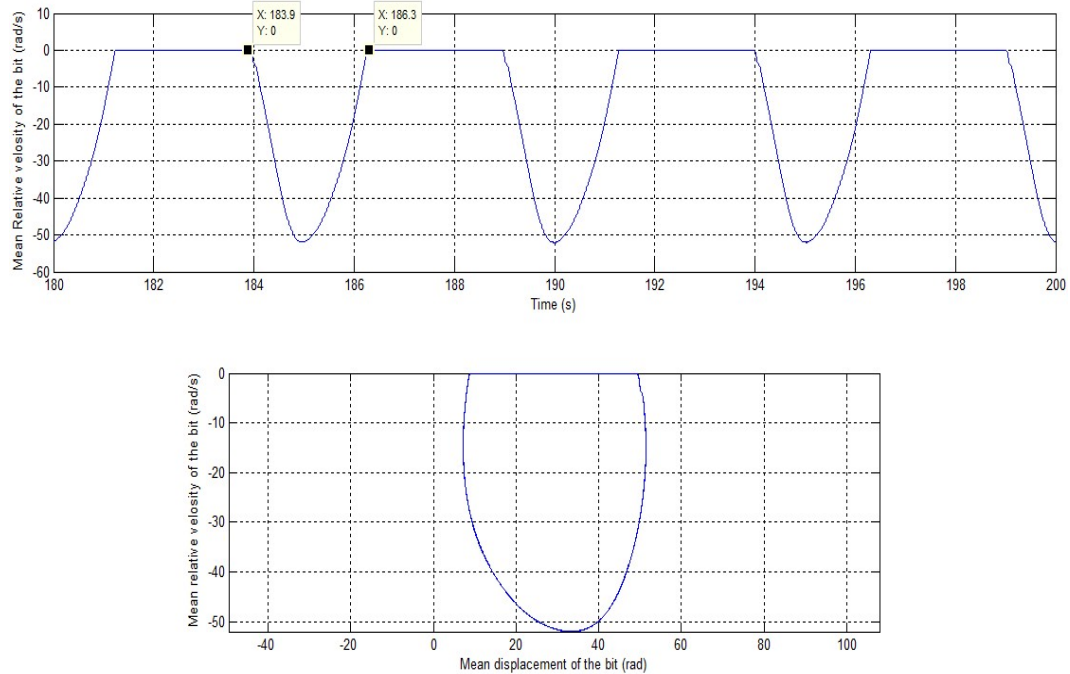


Figure 5.9: Mean relative bit speed (rad/s) and the corresponding phase plane

The mean relative speed and the corresponding phase plane are shown in Figure 5.9. As expected, the mean response is similar to that in deterministic case. The phase plane indicates a one-period stick-slip motion in this case. The two representative points indicating the leave and entry of the stick stage are $t = 183.9s$ and $t = 186.3s$ respectively.

As for each sample, these two representative times vary around the mean result. Also the single line phase plane curve in deterministic case becomes diffusive curves which stay around the mean one in random case. This can be clearly seen in Figure 5.10.

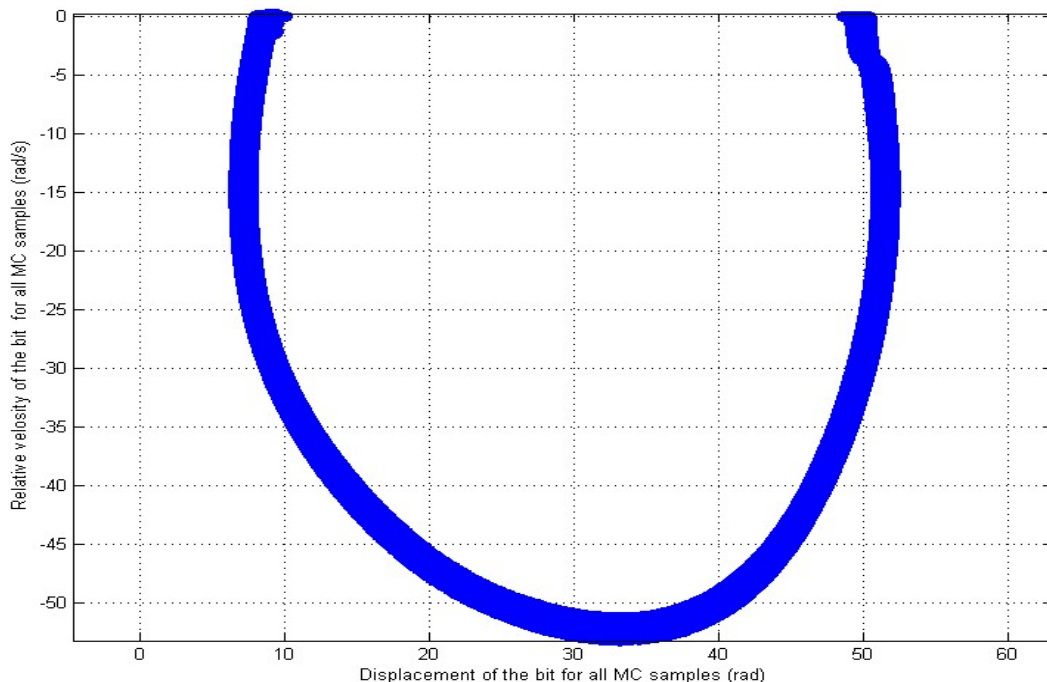


Figure 5.10: Phase plane for all MC samples

Statistics are also made among the MC simulation samples. The probability distribution in this case is presented in Figure 5.11. The marginal probabilistic density at the two representative points are shown in Figure 5.12. It can be seen that the distribution is pretty similar to a normal distribution except with the tail parts. Obviously this deviation of the tail part from normal is caused by the nonlinear nature of the problem. It is expected that with increase of nonlinearity this deviation would become more noticeable.

5.5 Conclusions

Using a finite element model with 30 degrees of freedom in total, this chapter investigates the stick-slip behavior of a drill-string subject to both deterministic and random excitations. Stick-slip behaviors and chaos are captured under certain condi-

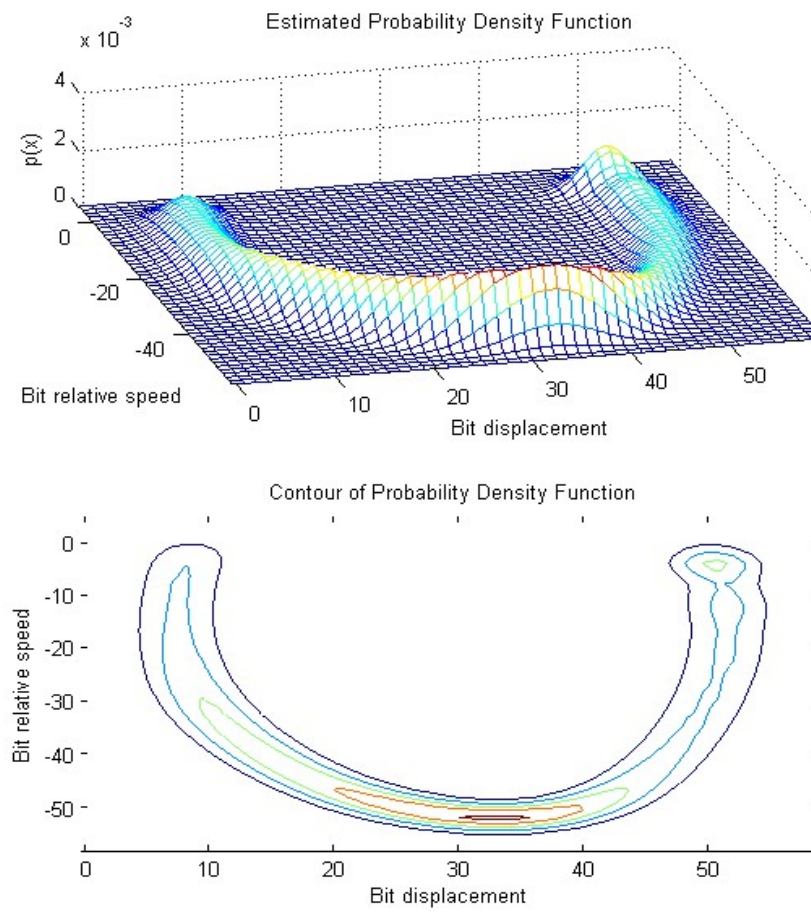


Figure 5.11: Probability density estimate of the bit

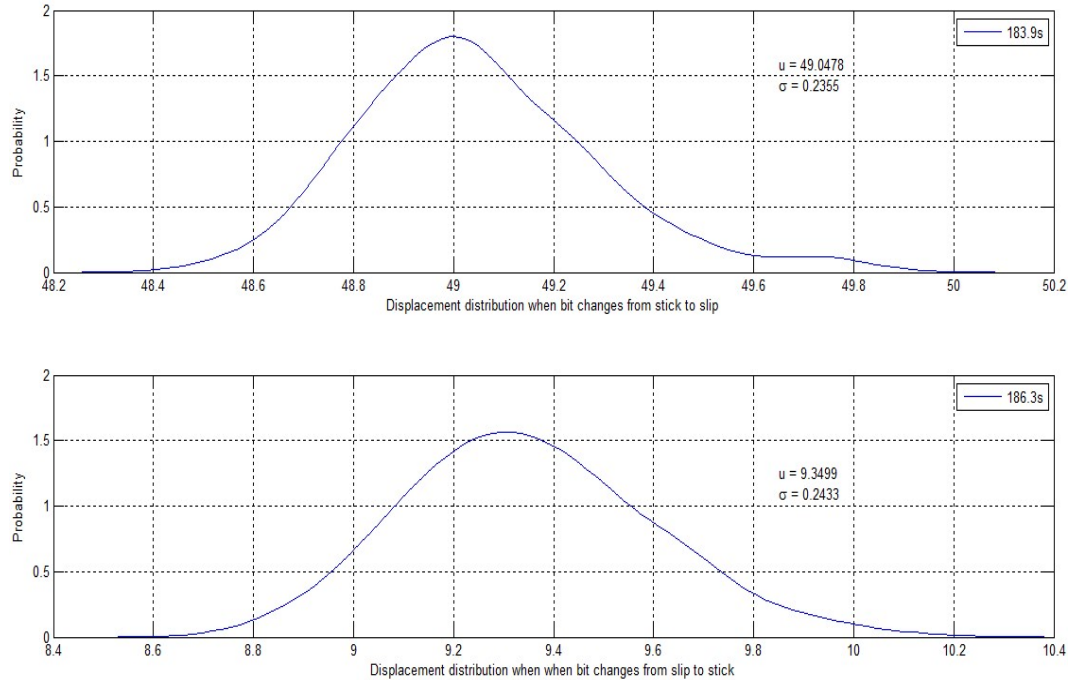


Figure 5.12: Probability density estimate of the bit displacements when bit changes between stick and slip

tions in the deterministic simulation. Under random excitation, the system response becomes scattered around its mean. Correspondingly, the phase plane curve becomes scattered around the mean in an area. The probabilistic density obtained from the simulation shows that the distribution is quite similar to normal with exception to the tail part. It is expected that the non-normal phenomenon will become more obvious with increase of the nonlinear effect in the dynamic model.

Chapter 6

Stick-slip Analysis of a Drill-string Using Path Integration

This chapter continues to investigate the drill-string stick-slip response to deterministic and random excitations. To this end, a simple one degree of freedom system is built and path integration method is employed. Although the system becomes relatively simple, path integration method will give a precise description of the probability distribution of the response, which is a very useful information in stochastic analysis. Furthermore, this information will also lay a good foundation for drill-string reliability analysis. Figure 6.1 shows the simplified model of the system.

6.1 Dynamic Model

After some mathematical manipulation, the equation of motion for the system can be represented as:

$$M\ddot{q}(t) + C\dot{q}(t) + Kq(t) = F(\dot{\phi}) + F(t) + F \quad (6.1)$$

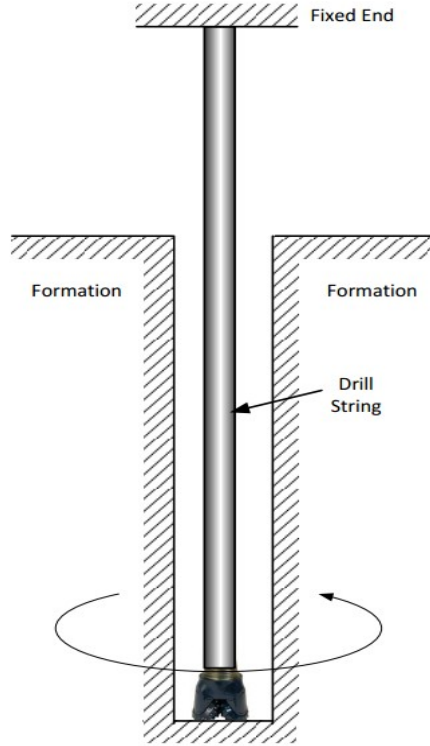


Figure 6.1: The simplified model of the system

where M , C and K are the system mass, damping and stiffness matrices, respectively, $q(t)$ is the displacement. $F(\dot{\phi})$, $F(t)$ and F together represent the excitations. The downhole damping C is assumed to be a linear combination of K and M . M , K and C are calculated in this chapter as below:

$$M = \rho \cdot J \cdot l \quad (6.2)$$

$$K = \frac{G \cdot J}{l} \quad (6.3)$$

$$C = \alpha M + \beta K \quad (6.4)$$

where α and β are constants to be selected. In the chapter the system is assumed as underdamped which is common in engineering application. l is the total length of the drill-string system. ρ is the drill-string density, G is the drill-string shear modulus

and J is the polar moment of inertia of the cross section.

$F(\dot{\phi})$ represents the dry friction, which is considered in the form as: [23]:

$$F(\dot{\phi}) = \begin{cases} WOB \cdot r_b \cdot u_1 & 0 \leq V - \dot{\phi}_{bit} < e \\ WOB \cdot r_b \cdot u_2 & V - \dot{\phi}_{bit} \geq e \end{cases} \quad (6.5)$$

where WOB is the constant weight on bit, which is about 40 percent of the total drill-string weight. r_b is the radius of the bit. V is the constant rotary speed of the ground. e is the narrow band separating the stick and slip situations, which is given as 0.01. u_1 is the static friction coefficient, which is originally set to be 0.3. u_2 is the kinetic friction coefficient, which is 0.21.

$F(t)$ and F simulate the torque during the bit cutting actions. F is constant and $F(t)$ is given as:

$$F(t) = 5000 \cdot \sin(\omega_0 \cdot t) \quad (6.6)$$

where ω_0 is the frequency of the harmonic excitation.

6.2 System Dimensionless

In order to make the system dimensionless, it is convenient to introduce the following parameters:

$$x = \frac{q(t)}{20} \quad (6.7)$$

$$\omega = \sqrt{\frac{K}{M}} \quad (6.8)$$

$$\tilde{t} = \omega t \quad (6.9)$$

$$k = \frac{K}{M\omega^2} \quad (6.10)$$

$$c = \frac{C}{M\omega} \quad (6.11)$$

$$\tilde{\omega} = \frac{\omega_0}{\omega} \quad (6.12)$$

$$f_0 = \frac{WOB \cdot r_b \cdot u_1}{M\omega^2} \quad (6.13)$$

$$f_1 = \frac{WOB \cdot r_b \cdot u_2}{M\omega^2} \quad (6.14)$$

$$f_2 = \frac{F(\tilde{t})}{M\omega^2} \quad (6.15)$$

For simplicity, \tilde{t} and $\tilde{\omega}$ are replaced with t and ω respectively in the rest of the chapter. Given the fact that the deterministic representation of the excitation above is not able to fully define the complex excitation mechanism in drilling, a random excitation can be added to the model as:

$$\ddot{x}(t) + c\dot{x}(t) + kx(t) = f + f_2 + rW(t) \quad (6.16)$$

where $W(t)$ is a stationary Gaussian white noise with zero mean and unit spectral intensity, f is equal to f_0 in the slip case and is increased to f_1 in the stick case. The stick-slip response of the dimensionless system under deterministic excitations is shown in Figure 6.2. Compared with its counterpart in chapter 5, the maximum ve-

locity and displacement of the system are largely decreased due to the nondimensionalized method. By shrinking the system, the calculation efficiency of path integration will be improved.

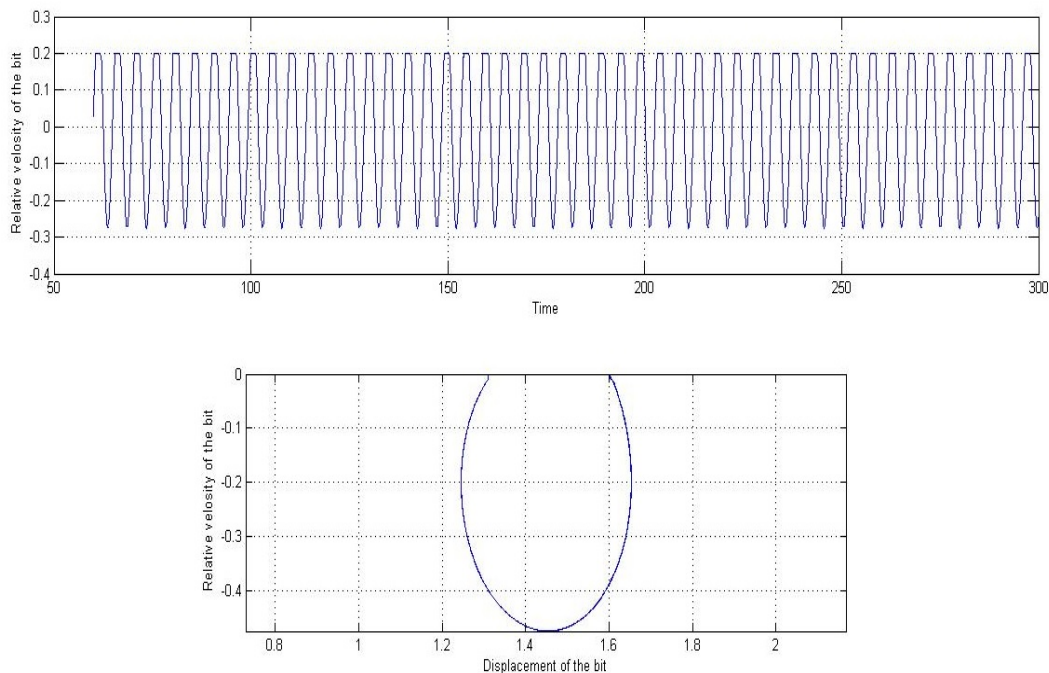


Figure 6.2: Stick-slip response after making the system dimensionless

6.3 Path Integration

6.3.1 Brief introduction

Path integration is a numerical procedure which describes the evolution of the probability density function (PDF) of a Markov process in time from an initial condition. The Markov process is a short memory process. That is, the probability of the event (x_i, t_{i-1}) conditional on the past history $(x_{i-1}, t_{i-1}; \dots; x_0, t_0)$ depends only on the most

recent past event (x_{i-1}, t_{i-1}) [40]. The conditional probability of the process satisfies:

$$p(x_i, t_i | x_{i-1}, t_{i-1}; \dots; x_0, t_0) = p(x_i, t_i | x_{i-1}, t_{i-1}) \quad (6.17)$$

Therefore, the probability density at i step $p(x_i, t_i)$ can be calculated as the integration of the product of previous step probability density $p(x_{i-1}, t_{i-1})$ and transition probability density $q(x_i, t_i | x_{i-1}, t_{i-1})$:

$$p(x_i, t_i) = \int_R q(x_i, t_i | x_{i-1}, t_{i-1}) p(x_{i-1}, t_{i-1}) dx_{i-1} \quad (6.18)$$

With a given initial probability density and transition probability density at each step, the probability density at i step can be calculated by the stepwise algorithm from the initial step as [41]:

$$p(x_i, t_i) = \int_R q(x_i, t_i | x_{i-1}, t_{i-1}) dx_{i-1} \int_R q(x_{i-1}, t_{i-1} | x_{i-2}, t_{i-2}) dx_{i-2} \dots \int_R q(x_2, t_2 | x_1, t_1) dx_1 \int_R q(x_1, t_1 | x_0, t_0) p(x_0, t_0) dx_0 \quad (6.19)$$

In path integration, the transition PDF $q(x_i, t_i | x_{i-1}, t_{i-1})$ is assumed to be Gaussian within a short time interval. Several expressions exist in the literature for the short time Gaussian transition PDF [42–44]. In this chapter, the transition PDF is modeled as [44]:

$$q(x_i, \dot{x}_i, t_i | x_{i-1}, \dot{x}_{i-1}, t_{i-1}) = \frac{1}{2\pi\sigma_{x_i}\sigma_{\dot{x}_i}\sqrt{1-\rho^2}} \exp\left\{-\frac{z}{2(1-\rho^2)}\right\} \quad (6.20)$$

where

$$z = \frac{(x_i - u_{x_i})^2}{\sigma_{x_i}^2} - \frac{2\rho(x_i - u_{x_i})(\dot{x}_i - u_{\dot{x}_i})}{\sigma_{x_i}\sigma_{\dot{x}_i}} + \frac{(\dot{x}_i - u_{\dot{x}_i})^2}{\sigma_{\dot{x}_i}^2} \quad (6.21)$$

ρ is the correlation coefficient calculated as:

$$\rho = \frac{\sigma_{x_i \dot{x}_i}}{\sigma_{x_i} \sigma_{\dot{x}_i}} \quad (6.22)$$

6.3.2 Numerical procedure

In practice, the numerical path integration is carried out within a reduced state space range, assuming that the probability evolution outside this range is negligible [41]. To precisely calculate the probability evolution step by step, the Gauss-Legendre based algorithm will be employed. The essential features of it will be illustrated for a two-dimensional system. In this case, the typical step of probability evolution from t_{i-1} to t_i is discretized into the following composite Gauss-Legendre quadrature as follows:

$$p(X_{kl}^{(i)}, t_i) = \delta_x \delta_y \sum_{m=1}^M \sum_{n=1}^N c_{mn} p(X_{mn}^{(i-1)}, t_{i-1}) q(X_{kl}^{(i)}, t_i | X_{mn}^{(i-1)}, t_{i-1}) \quad (6.23)$$

$$X_{kl}^{(i)} = \begin{bmatrix} x_k^{(i)} \\ \dot{x}_l^{(i)} \end{bmatrix}, k = 1, 2, \dots, M, \text{ and } l = 1, 2, \dots, N$$

where M and N are the number of quadrature points in x and \dot{x} direction respectively, c_{mn} is the calculation weight for each $X_{mn}^{(i-1)}$. In this case, x and \dot{x} axes are evenly distributed into $\frac{M}{2}$ and $\frac{N}{2}$ sub-intervals respectively. Each sub-interval has two Gauss quadrature points. Therefore, c_{mn} is equal to 1. δ_x is the half length of the sub-interval along x axis and δ_y is the half length of the sub-interval along \dot{x} axis. For two Gauss points in the interval (x_a, x_b) , their positions are calculated as [41]:

$$\begin{aligned} x_1 &= x_a + 0.211375(x_b - x_a) \\ x_2 &= x_b - 0.211375(x_b - x_a) \end{aligned} \quad (6.24)$$

6.3.3 Calculation method for purely slip case

In this case, it is assumed that stick phenomenon barely happens. Therefore, the system is simplified to a linear system and the equation of motion of the system is written as:

$$\ddot{x}(t) + c\dot{x}(t) + kx(t) = f_0 + f_2 + rW(t) \quad (6.25)$$

Figure 6.3 describes the trajectory of the bit at its steady state in the simulation.

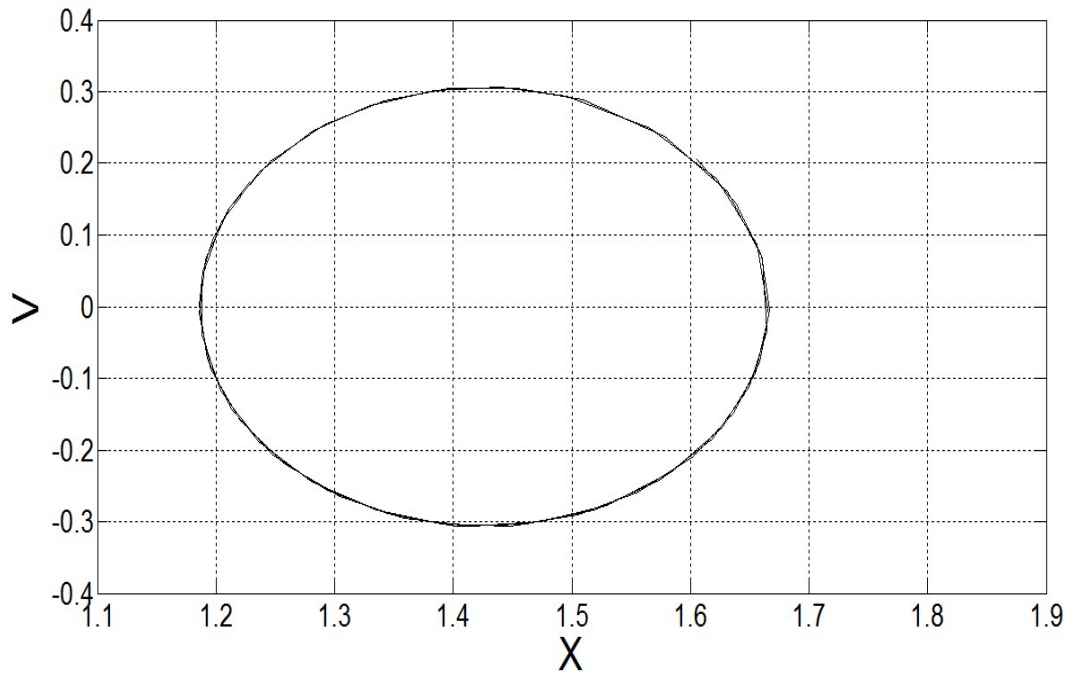


Figure 6.3: The figure for describing purely slip case

Using moment equations proposed by Sun and Hsu [43], the mean u , standard deviation σ and correlation coefficient ρ can be obtained at each time step t_i to calculate the transition PDF. The first and second order moments derived from Eq 6.25 are

expressed as [44]:

$$\dot{m}_{01} = -cm_{01} - km_{10} + f_0 + f_2 \quad (6.26)$$

$$\dot{m}_{10} = m_{01} \quad (6.27)$$

$$\dot{m}_{11} = -cm_{11} - km_{20} + m_{02} + m_{10} \cdot (f_0 + f_2) \quad (6.28)$$

$$\dot{m}_{02} = -2cm_{02} - 2km_{11} + r^2 + 2m_{01} \cdot (f_0 + f_2) \quad (6.29)$$

$$\dot{m}_{20} = 2m_{11} \quad (6.30)$$

where $m_{ij} = E[x^i \dot{x}^j]$, the ensemble average of $x^i \dot{x}^j$. The initial probability density function is represented as:

$$p(x_0, \dot{x}_0) = \frac{1}{2\pi\sigma_{x_0}\sigma_{\dot{x}_0}} \exp \left\{ -\frac{(x_0 - u_{x_0})^2}{2\sigma_{x_0}^2} - \frac{(\dot{x}_0 - u_{\dot{x}_0})^2}{2\sigma_{\dot{x}_0}^2} \right\} \quad (6.31)$$

where $u_{x_0} = 1.6$, $u_{\dot{x}_0} = 0$, $\sigma_{x_0}^2 = 0.01$, $\sigma_{\dot{x}_0}^2 = 0.01$.

The moment equations are solved by Matlab built-in solver ode45 in the simulation. Simulation step is set to be $\frac{T}{4}$. The state space is taken as $[0.8, 2.0] \times [-0.6, 0.6]$ with 15×30 evenly distributed subintervals. With four Gauss quadrature points in each subinterval, there are totally 30×60 points in the state space.

6.3.4 Calculation method for stick-slip case

The equation of motion of the system in stick-slip case is written as:

$$\ddot{x}(t) + c\dot{x}(t) + kx(t) = f + f_2 + r_1W(t) \quad (6.32)$$

where f is equal to f_0 in the slip case and is increased to f_1 in the stick case.

The way to calculate the mean u , standard deviation σ and correlation coefficient ρ at each time step t_i depends on the transfer path (4 cases), which can be clearly seen

in Figure 6.4:

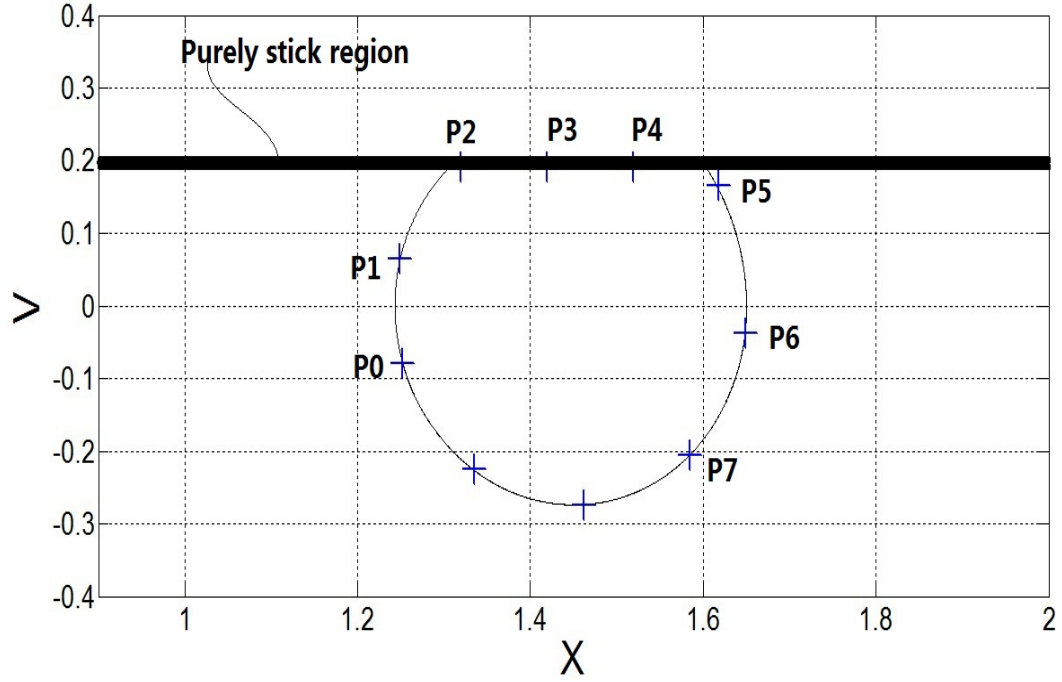


Figure 6.4: The figure for explaining calculation method for stick-slip case

1. Case 1: P_0 to P_1 , slip to slip

In this case, due to the perturbation of Gaussian white noise, the probability at P_0 will be distributed around P_1 . The deviations between random response and deterministic result are calculated as:

$$\sigma_{x_i}^2 = \frac{G_0}{4\xi\omega_0^3} \left\{ 1 - e^{-2\xi\omega_0\Delta t} \left[\frac{\omega_0^2}{\omega_d^2} + \frac{\xi\omega_0}{\omega_d} \sin 2\omega_d\Delta t - \frac{\xi^2\omega_0^2}{\omega_d^2} \cos 2\omega_d\Delta t \right] \right\} \quad (6.33)$$

$$\sigma_{\dot{x}_i}^2 = \frac{G_0}{4\xi\omega_0} \left\{ 1 - e^{-2\xi\omega_0\Delta t} \left[\frac{\omega_0^2}{\omega_d^2} - \frac{\xi\omega_0}{\omega_d} \sin 2\omega_d\Delta t - \frac{\xi^2\omega_0^2}{\omega_d^2} \cos 2\omega_d\Delta t \right] \right\} \quad (6.34)$$

$$\sigma_{x\dot{x}_i} = \frac{G_0}{2\omega_d^2} e^{-2\xi\omega_0\Delta t} \sin^2 \omega_d\Delta t \quad (6.35)$$

with

$$G_0 = 2\pi r_1 \quad (6.36)$$

$$\xi = \frac{c}{2\sqrt{k}} \quad (6.37)$$

$$\omega_0 = \sqrt{k} \quad (6.38)$$

$$\omega_d = \omega_0 \sqrt{1 - \xi^2} \quad (6.39)$$

where Δt equals to the simulation time step.

In the chapter 6.3.3, the moment equation method is employed to calculate the mean and variance step by step. In stick-slip case, the situation becomes more complicated and this method is not applicable. Therefore, the response mean is obtained by Matlab built-in solver ode45 and variance is calculated by equations 6.33 through 6.35.

2. Case 2: P_1 to P_2 , slip to stick

In this case, it is assumed that the probability at P_1 will be transported to P_2 . The random excitation does influence the system and therefore there should be a probability distribution around P_1 . However, the method to properly describe this distribution is not found in the literature. The author tried many methods and this one was thought to be the best.

3. Case 3: P_2 to P_3 , stick to stick

In this case, the probability at P_2 will be transported to P_3 in the calculation. Based on the assumption that random excitation has no influence on the drill-string when stick happens, the probability of $P(P_3 | P_2)$ is 1.

4. Case 4: P_4 to P_5 , stick to slip

The moment it leaves stick, the drill-string will be under random excitation. The deviations between random response and deterministic result can be calculated using equations in case 1 with different Δt for different points. However, simulation results indicate that some really short Δt will lead to small standard deviations. Because of it, in order to precisely describe the probability distribution, the state space needs to be divided into much smaller subintervals. This is time and memory consuming for the simulation. Therefore, in this case, Δt also equals to the simulation time step.

Assume the coordinate of P_5 is (1.62, 0.18). The probability distribution of P_5 may pass the purely stick region (see Figure 6.4). If the probability at point (1.62, 0.21) is 0.01, this probability will be moved downward to the point (1.62, 0.20) and relocated in the purely stick region.

The initial probability density function is also represented as:

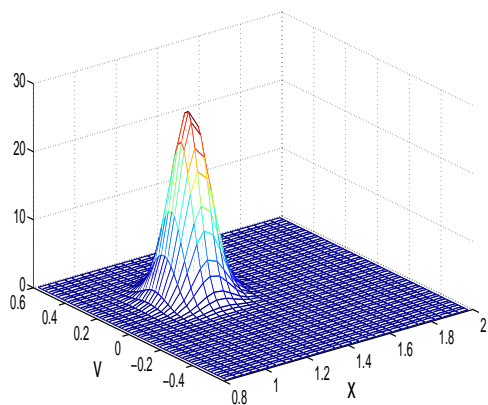
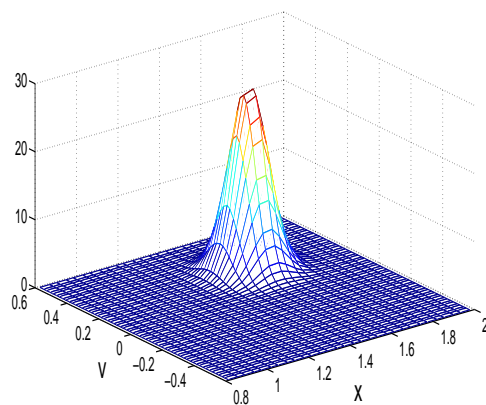
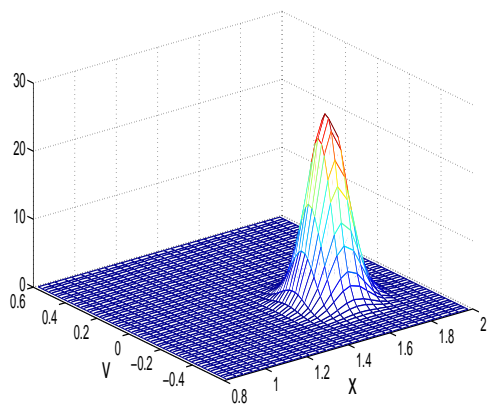
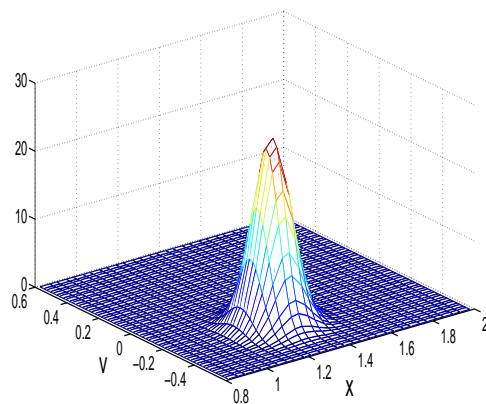
$$p(x_0, \dot{x}_0) = \frac{1}{2\pi\sigma_{x_0}\sigma_{\dot{x}_0}} \exp \left\{ -\frac{(x_0 - u_{x_0})^2}{2\sigma_{x_0}^2} - \frac{(\dot{x}_0 - u_{\dot{x}_0})^2}{2\sigma_{\dot{x}_0}^2} \right\} \quad (6.40)$$

where $u_{x_0} = 1.2967$, $u_{\dot{x}_0} = -0.1832$, $\sigma_{x_0}^2 = 0.006$, $\sigma_{\dot{x}_0}^2 = 0.006$.

In the simulation, the time step implementing in the above process should be carefully considered. In the practice, large time step may lead to the increasing of computation error and the real transition PDF may significantly deviate from the normal assumption. While if it is too short, the computation would be time-consuming. Therefore, simulation step is set to be $\frac{T}{10}$ for the calculation of stick-slip case. The state space of this case is taken as $[0.5, 2.5] \times [-0.8, 0.6]$ with 75×70 evenly distributed subintervals. With four Gauss quadrature points in each subinterval, there are totally 150×140 points in the state space.

6.4 Simulation Results

6.4.1 Simulation results of purely slip case

(a) $9\frac{1}{4}T$ (b) $9\frac{2}{4}T$ (c) $9\frac{3}{4}T$ 

(d) 10 T

Figure 6.5: Evolution of probability density at (a) $9\frac{1}{4}T$; (b) $9\frac{2}{4}T$; (c) $9\frac{3}{4}T$; (d) $10T$.

In this case, the period of the deterministic response is about $4.92s$ and the response reaches its steady-state before $6T$. The probability density distributions at $9\frac{1}{4}T$, $9\frac{2}{4}T$, $9\frac{3}{4}T$ and $10T$ are shown in Figure 6.5 and their corresponding contours are described in Figure 6.6. For comparison purpose, the deterministic results of the displacement

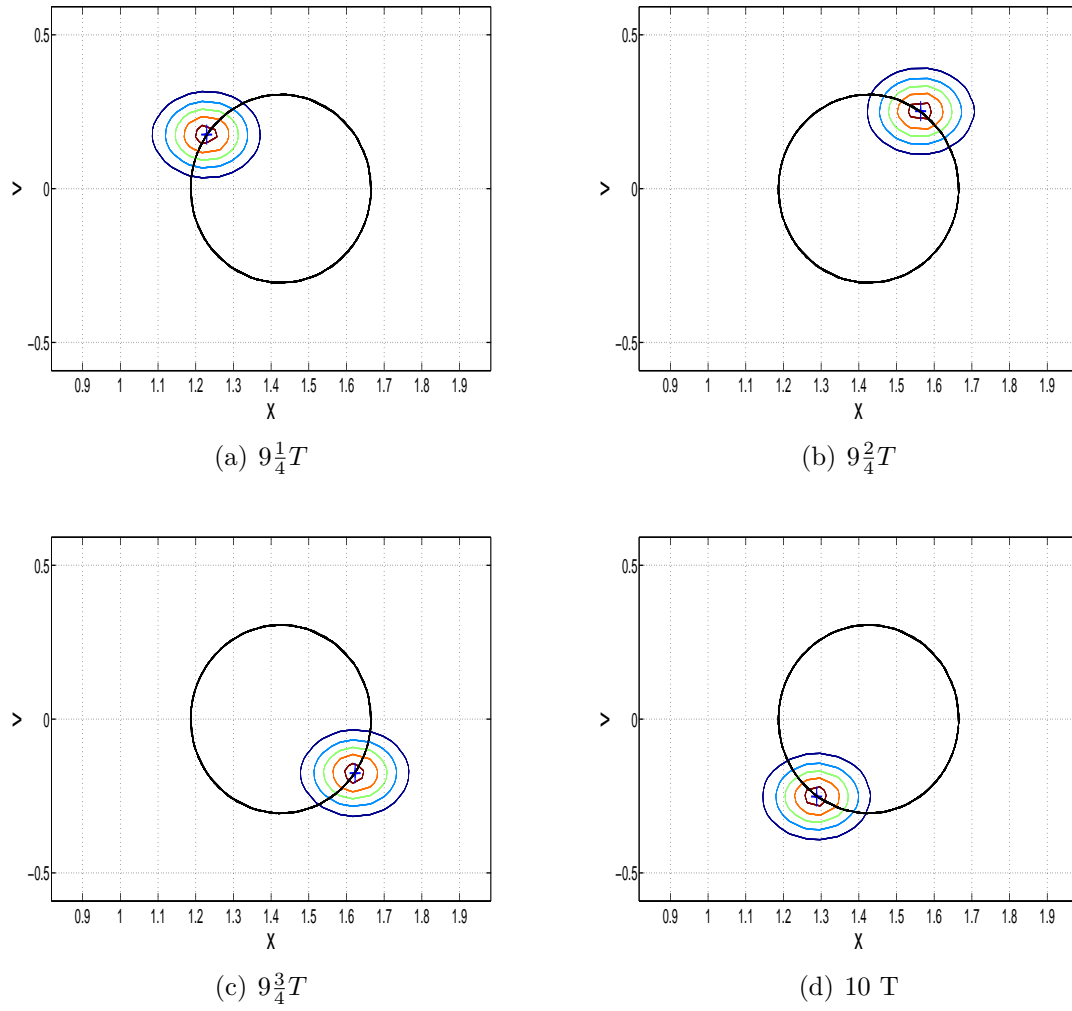


Figure 6.6: Contour of the corresponding probability density distribution

Table 6.1: Deterministic results of x and v

Time	Displacement	Velocity
$9\frac{1}{4}T$	1.229	0.1758
$9\frac{2}{4}T$	1.564	0.2519
$9\frac{3}{4}T$	1.623	-0.1757
$10T$	1.288	-0.2518

and velocity at the corresponding time spot, which are listed in Table 6.1, are marked with "+" in the Figure 6.6. It can be seen clearly that these "+" marks stay very close to the centers of probability density distributions. The black circle in the figure depicts the phase plane of the drill-bit under deterministic excitation at the steady state.

As can be seen in Figure 6.6, because of the perturbation of Gaussian white noise, the probability density distributions of random response are distributed around the deterministic results. The simulation results of purely slip case present good agreements between random and deterministic responses, indicating the capability of path integration method in random analysis.

6.4.2 Simulation results of stick-slip case

In this case, the period of the deterministic response is about $5s$ and the response reaches its steady-state before $4T$. The probability density distributions from P_0 to P_7 (see Figure 6.4) are described in Figure 6.7 and Figure 6.9. Their corresponding contours are described in Figure 6.8 and Figure 6.10, where the phase plane of the drill-bit under deterministic excitation at the steady state is also depicted. The probability of slip and stick from P_0 to P_7 are listed in Table 6.2. The total probability is about 0.19% higher than 1. This is considered due to the numerical calculation error.

As can be seen in the figures, the points stay very close to the centers of probability density distributions. Figure 6.7(b) describes the probability distribution at P_1 . The highest probability density is not around P_1 . This is because the region representing stick is very narrow. As the point changing from slip to stick, the probability density in this region becomes extremely high. Actually, from Table 6.2, the probability of P_1 at slip is 0.9021. This result, to some degree, matches to the response of the system under deterministic excitations. From the figures and the table, when drill-string sticks, the

probability located in the stick region is very high and is distributed like Gaussian. From P_2 to P_4 , the corresponding probability distribution seems alike, especially P_3 and P_4 . This result matches to the assumption that the random excitation has no influence on the drill-string and therefore the probability distribution is almost locked when stick happens.

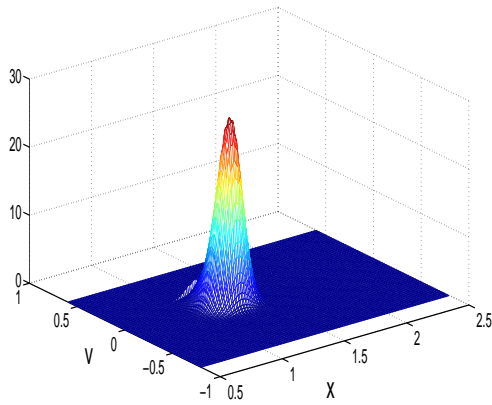
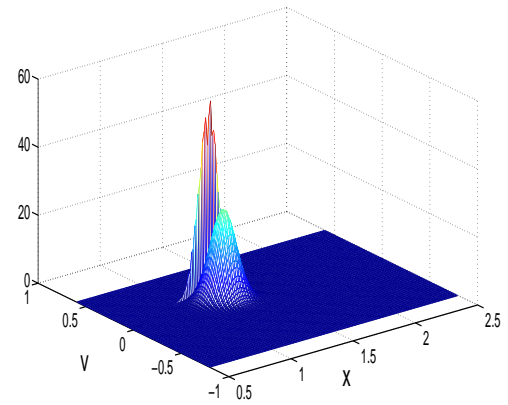
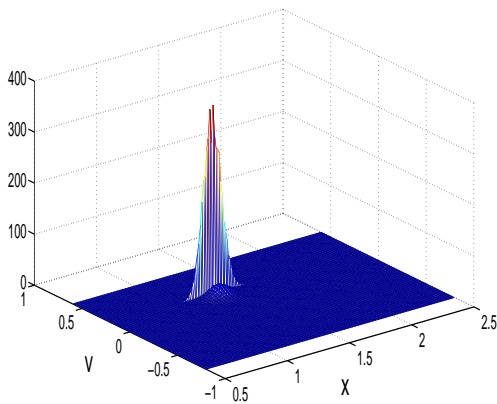
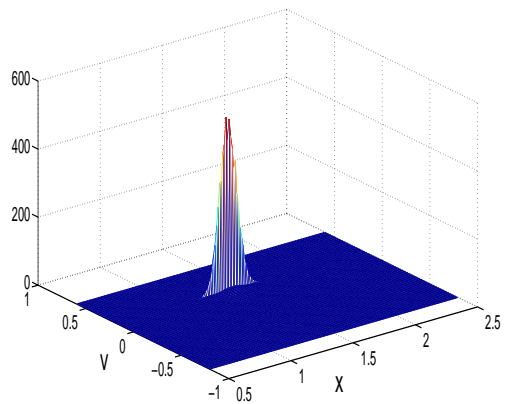
(a) Probability distribution at P_0 (b) Probability distribution at P_1 (c) Probability distribution at P_2 (d) Probability distribution at P_3

Figure 6.7: Evolution of probability density at (a) P_0 ; (b) P_1 ; (c) P_2 ; (d) P_3 .

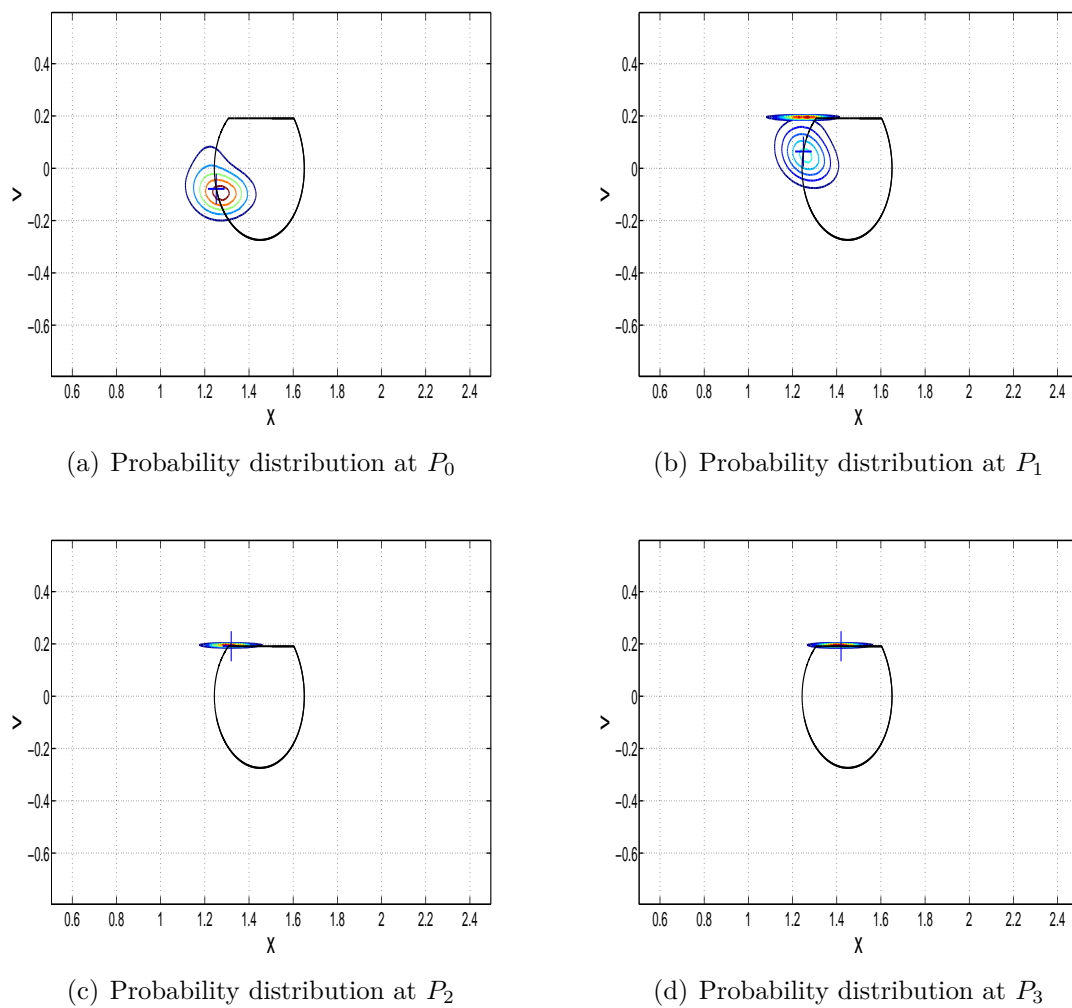
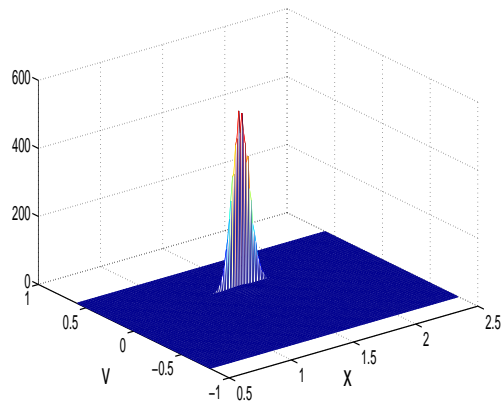
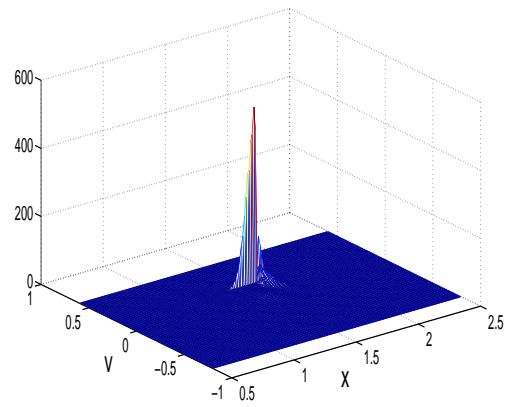
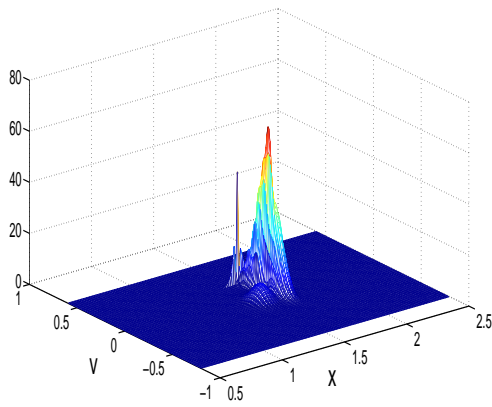
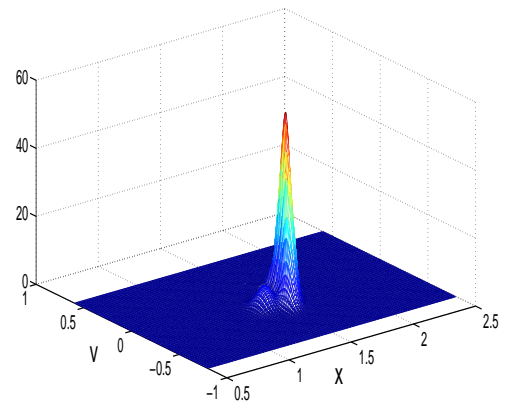


Figure 6.8: Contour of the corresponding probability density distribution

(a) Probability distribution at P_4 (b) Probability distribution at P_5 (c) Probability distribution at P_6 (d) Probability distribution at P_7 Figure 6.9: Evolution of probability density at (a) P_4 ; (b) P_5 ; (c) P_6 ; (d) P_7 .

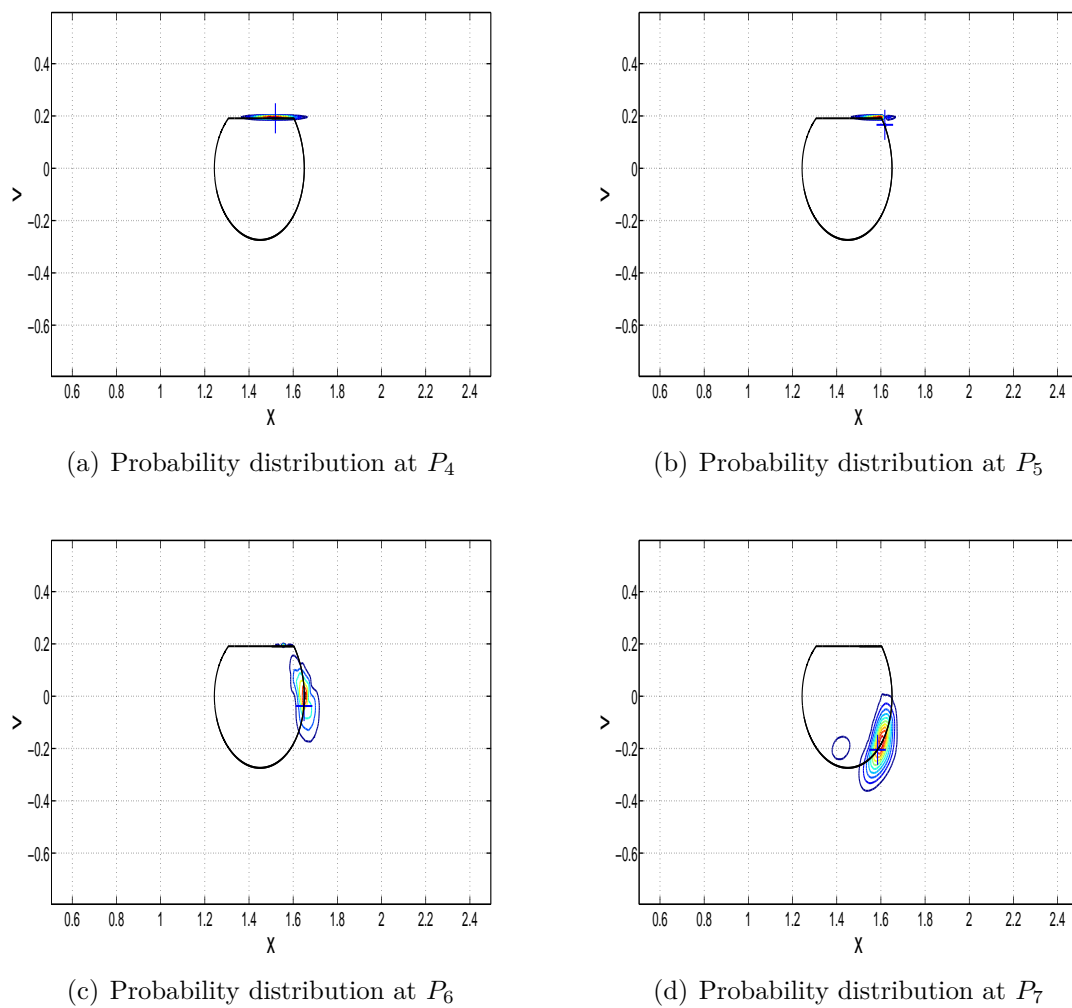


Figure 6.10: Contour of the corresponding probability density distribution

Table 6.2: Probability of slip and stick at each point

Point	Slip	Stick
P_0	0.9978	0.0041
P_1	0.9021	0.0999
P_2	0.3876	0.6144
P_3	0.1654	0.8366
P_4	0.1562	0.8458
P_5	0.5159	0.4860
P_6	0.9850	0.0169
P_7	1.0017	0.0002

6.5 Conclusions

This chapter investigates the stick-slip response of the simplified drill-string system under harmonic and white noise excitations. The PDF evolutions of the response is examined with path integration method which assumes the response transition PDF is Gaussian within a short time interval. The results of path integration match well to those of deterministic cases.

Chapter 7

Conclusion and Recommendations

7.1 Achievements

1. A finite element model of the drill-string that is suitable for predicting axial, torsional and lateral vibrations is built using Euler-Bernoulli beam theory in the thesis. The model is axial-torsional coupled due to bit/formation interaction and lateral-torsional coupled due to drill-string/borehole interaction.
2. The response of the drill-string to both deterministic and random excitations is paid much attention to in the thesis. Simulation is carried out under certain parameters and it is shown that in deterministic case the torsional vibration may exhibit stick-slip. With change of some parameters, bifurcation and chaos of the system are observed. In the random case, the probabilistic information of the response is captured by using Monte Carlo simulation and path integration method. The results of path integration match well to those of deterministic cases.
3. A method that calculates the probability density distribution of the stick-slip response is firstly proposed in the thesis.

7.2 Recommendations for Future Work

1. This thesis is limited to vertical drilling system. Currently, most of the oilwells are non-vertical. The geometric stiffness and the influence of the drilling fluid are not considered in the current work. The number of the finite elements are limited and therefore the model may not describe the drill-string dynamic response precisely. A model that considering these factors is required.
2. Drill-string stick-slip behavior is studied in the thesis. In the future, comprehensive studies on the mechanical behaviors of bit-rock interaction under different types of drill-bits are required.
3. Drill-string random vibration research is a promising topic. In the thesis, Monte Carlo simulation and path integration are employed to investigate the behaviors of drilling assemblies subject to both deterministic and stochastic excitations. However, path integration is not suitable for multi-degree of freedom system and Monte Carlo also has its limitations. In order to analyze drilling random dynamic, more advanced methods need to be developed.

Bibliography

- [1] Aadnøy, Bernt Sigve., 2009. *Advanced Drilling and Well Technology, Society of Petroleum Engineers.*
- [2] Dareing, Don W., 2012. *Mechanics of Drillstrings and Marine Risers.* ASME Press.
- [3] Wikipedia. (n.d.). *Drilling rig.* In WIKIPEDIA. Retrieved Oct 20, 2013, from <http://www.encapgroup.com/drilling/>.
- [4] Chevallier, A, 2001. “Nonlinear stochastic drilling vibrations”. Ph.D. Thesis, Rice University, USA. See also URL <http://hdl.handle.net>.
- [5] Wikipedia. (n.d.). *A tricone bit.* In WIKIPEDIA. Retrieved Oct 20, 2013, from http://ffden-2.phys.uaf.edu/211_fall2010.web.dir/Jared_Boerger/Technique.html.
- [6] Wikipedia. (n.d.). *A PDC bit.* In WIKIPEDIA. Retrieved April 7, 2014, from <http://varelintl.com/Oil-and-Gas-Home/PDC-Drill-Bits/ToughDrill-Bits/>.
- [7] Discovery Drilling Funds. (n.d.). *Anatomy of a Land Based Drilling Rig - Hoisting System.* In Discovery Drilling Funds. Retrieved Oct 21, 2012, from <http://www.drillingfunds.com/hoisting.html>.

- [8] Azar, J. J., & Samuel, G. R. (2007). *Drilling engineering*. PennWell Books.
- [9] Occupational Safety and Healthy Administration. *Blowout preventers*. In Oil and Gas Well Drilling and Serving eTool. Retrieved Oct 22, 2013, from https://www.osha.gov/SLTC/etools/oilandgas/drilling/wellcontrol_bop.html.
- [10] Wikipedia. (n.d.). *Measurement while drilling*. In WIKIPEDIA. Retrieved Oct 22, 2013, from http://en.wikipedia.org/wiki/Measurement_while_drilling.
- [11] Ashley, DK., McNary, XM., Tomlinson, JC., 2001. “Extending BHA life with multi-axis vibration measurements”. *SPE/IADC drilling conference*.
- [12] Skaugen, E., 1987. “The Effects of Quasi-Random Drill Bit Vibrations Upon Drillstring Dynamic Behavior”. *SPE Annual Technical Conference and Exhibition*.
- [13] Vandiver, Kim., Nicholson, James., Shyu, Rong-Juin., 1990. “Case studies of the bending vibration and whirling motion of drill collars”. *SPE Drilling Engineering*, **5**, pp. 282–290.
- [14] Besaisow, Amjad and Payne, Mike., 1988. “A study of excitation mechanisms and resonances inducing bottomhole-assembly vibrations”. *SPE drilling engineering*, **3**(1), pp. 93–101.
- [15] Chin, Wilson C., 1994. “Wave Propagation in Petroleum Engineering: Modern Applications to Drillstring Vibrations, Measurement-while-drilling, Swab-surge, and Geophysics”. *Gulf Publishing Company*.
- [16] Trindade, M. A., Wolter, C., and Sampaio, R., 2005. “Karhunen–Loève decomposition of coupled axial/bending vibrations of beams subject to impacts”. *Journal of Sound and Vibration*, **279**(3), pp. 1015–1036.

- [17] Khulief, Y. A., Al-Naser, H., 2005. “Finite element dynamic analysis of drill-strings”. *Finite elements in analysis and design*, **41**(13), pp. 1270–1288.
- [18] Sampaio, R., Piovan, M. T., and Venero Lozano, G., 2007. “Coupled axial/torsional vibrations of drill-strings by means of non-linear model”. *Mechanics Research Communications*, **34**(5), pp. 497–502.
- [19] Piovan, M. T., Sampaio, R., 2006. “Non Linear Model for Coupled Vibrations of Drill-strings”. In *III European Conference on Computational Mechanics*, January, pp. 1751–1765.
- [20] Yigit, A. S., Christoforou, A. P., 2006. “Stick-slip and bit-bounce interaction in oil-well drillstrings”. *Journal of Energy Resources Technology*, **128**, pp. 268–274.
- [21] Christoforou, A. P., Yigit, A. S., 2003. “Fully coupled vibrations of actively controlled drillstrings”. *Journal of Sound and Vibration*, **267**(5), pp. 1029–1045.
- [22] Van de Vrande, B.L., Van Campen, D.H., and De Kraker, A., 1999. “An approximate analysis of dry-friction-induced stick-slip vibrations by a smoothing procedure”. *Nonlinear Dynamics*, **19**(2), pp. 159–171.
- [23] Navarro-López, Eva M., Cortés, Domingo, 2007. “Avoiding harmful oscillations in a drillstring through dynamical analysis”. *Journal of Sound and Vibration*, **307**(1), pp. 152–171.
- [24] Richard, Thomas., Gernay, Christophe., and Detournay, Emmanuel., 2007. “A simplified model to explore the root cause of stick-slip vibrations in drilling systems with drag bits”. *Journal of Sound and Vibration*, **305**(3), pp. 432–456.
- [25] Puebla, Hector., Alvarez-Ramirez, Jose., 2008. “Suppression of stick-slip in drill-

- strings: A control approach based on modeling error compensation”. *Journal of Sound and Vibration*, **310**(4), pp. 881–901.
- [26] E.M. Navarro-Lopez, and R. Suarez-Cortez., 2004. “Practical approach to modelling and controlling stick-slip oscillations in oilwell drillstrings”. *Control Applications, 2004. Proceedings of the 2004 IEEE International Conference on*, **2**, pp. 1454–1460.
- [27] Serrarens, AFA., Van de Molengraft, MJG., Kok, JJ., Van den Steen, L., 1998. “ H_∞ control for suppressing stick-slip in oil well drillstrings”. *Control Systems, IEEE*, **18**(2), pp. 19–30.
- [28] N. Mihajlovic, 2005. “Torsional and Lateral Vibrations in Flexible Rotor Systems with Friction”. Ph.D. Thesis, Eindhoven University of Technology, The Netherlands.
- [29] Khulief, Y. A., Al-Sulaiman, F. A., and Bashmal, S., 2007. “Vibration analysis of drillstrings with self-excited stick–slip oscillations”. *Journal of Sound and Vibration*, **299**(3), pp. 540-558.
- [30] Mejbahul Sarker, Md., Rideout, D Geoff., Butt, Stephen D., 2012. “Dynamic Model of an Oilwell Drillstring with Stick-Slip and Bit-Bounce Interaction”. *10th International Conference on Bond graph Modeling and Simulation*.
- [31] Bogdanoff, J. L., Goldberg, J. E., 1961. “A New Analytical Approach to Drill Pipe Breakage II”. *Journal of Engineering for Industry*, **83**, pp. 101.
- [32] Ritto, T. G., Soize, C., and Sampaio, R., 2009. “Non-linear dynamics of a drill-string with uncertain model of the bit–rock interaction”. *International Journal of Non-Linear Mechanics*, **44**(8), pp. 865-876.

- [33] Ritto, TG., Escalante, MR., Sampaio, Rubens., Rosales, MB., 2012. “Drill-string horizontal dynamics with uncertainty on the frictional force”. *Journal of Sound and Vibration*, **332**, pp. 145-153.
- [34] Ritto, TG., Soize, Christian., Sampaio, R., 2010. “Robust optimization of the rate of penetration of a drill-string using a stochastic nonlinear dynamical model”. *Computational Mechanics*, **45**(5), pp. 415–427.
- [35] Gazetas, G., 1983. “Analysis of machine foundation vibrations: state of the art”. *International Journal of Soil Dynamics and Earthquake Engineering*, **2**(1), pp. 2-42.
- [36] Yigit, A. S., Christoforou, A. P., 2000. “Coupled torsional and bending vibrations of actively controlled drillstrings”. *Journal of Sound and Vibration*, **234**(1), pp. 67-83.
- [37] To, C. W. S., Liu, M. L., 2000. “Large nonstationary random responses of shell structures with geometrical and material nonlinearities”. *Finite elements in analysis and design*, **35**(1), pp. 59-77.
- [38] Bucher, C., 2009. *Computational Analysis of Randomness in Structural Mechanics*, Vol. 3 of *Structures and Infrastructures Book Series*. CRC Press. Chap. 4, pp. 112.
- [39] Gaus, Nicole., and Proppe, Carsten., 2011 “Bifurcation Analysis of Stochastic Non-smooth Systems”. *Symposium on Nonlinear Stochastic Dynamics and Control*, pp. 201–209.
- [40] Sun, Jian-Qiao., 2006 *Stochastic dynamics and control*, Vol. 4 of *Monograph Series on Nonlinear Science and Complexity* Elsevier Press. Chap. 3, pp. 48.

- [41] Yu, JS., Cai, GQ., Lin, YK., 1997 “A new path integration procedure based on Gauss-Legendre scheme”. *International journal of non-linear mechanics*, **32**(4), pp. 759–768.
- [42] Naess, Arvid., Kolnes, F.E., Mo, Eirik., 2007 “Stochastic spur gear dynamics by numerical path integration”. *Journal of Sound and Vibration*, **302**(4), pp. 936–950.
- [43] Sun, JQ and Hsu, CS t., 1990 “The generalized cell mapping method in nonlinear random vibration based upon short-time Gaussian approximation”. *Journal of applied mechanics*, **57**(4), pp. 1018–1025.
- [44] Yu, JS and Lin, YK., 2004 “Numerical path integration of a non-homogeneous Markov process”. *International Journal of Non-Linear Mechanics*, **39**(9), pp. 1493–1500.
- [45] Sun, Jian-Qiao., 2006 *Stochastic dynamics and control*, Vol. 4 of *Monograph Series on Nonlinear Science and Complexity* Elsevier Press. Chap. 8, pp. 132.

Appendix A

In the paper, a drill-string similar to the one used in Ref.[36] is considered. The specification of the drillstring is listed as follows:

Table 7.1: Drill-string data.

	Drillpipe	Drillcollar
Length	1,000 <i>m</i>	200 <i>m</i>
Outer diameter	0.127 <i>m</i>	0.2286 <i>m</i>
Inner diameter	0.095 <i>m</i>	0.0762 <i>m</i>
Drillstring density	7850.0 <i>kg/m</i> ³	
Elastic modulus	210×10^9 <i>N/m</i> ²	
Shear modulus	7.6923×10^{10} <i>N/m</i> ²	

Appendix B

Consider a single-degree-of freedom (SDOF) system, a spring-mass oscillator, subject to an external random loading $W(t)$. The motion of the system is given by the following stochastic differential equation:

$$m\ddot{X} + c\dot{X} + kX = W(t) \quad (7.1)$$

where m is the mass, k is the spring constant, and c is the damping coefficient. $W(t)$ is assumed to be a stationary Gaussian white noise with zero mean and spectral intensity S_0 . The steady state standard deviation of the response is well known as [45]:

$$\sigma_x = \sqrt{\frac{\pi S_0}{2\xi\omega_n^3 m^2}} \quad (7.2)$$

where $\omega_n = \sqrt{\frac{k}{m}}$ is the resonant frequency and $\xi = \frac{c}{2\omega_n m}$ is the damping ratio.

Firstly, set $m = 1$, $c = 0.1$, $k = 1$ and $S_0 = 1$. Figure 7.1 represents the statistic responses obtained from stochastic central difference method presented by [37] and Monte Carlo simulation (1000 samples). As can be seen in Figure 7.1, standard deviations given by these two methods at steady state are both about 5.6. This value is supported by equation 7.2. Therefore, Monte Carlo simulation and stochastic central difference method are proved to be reliable.

Secondly, increase k from 1 to 100 and keep other parameters unchanged. Simulation

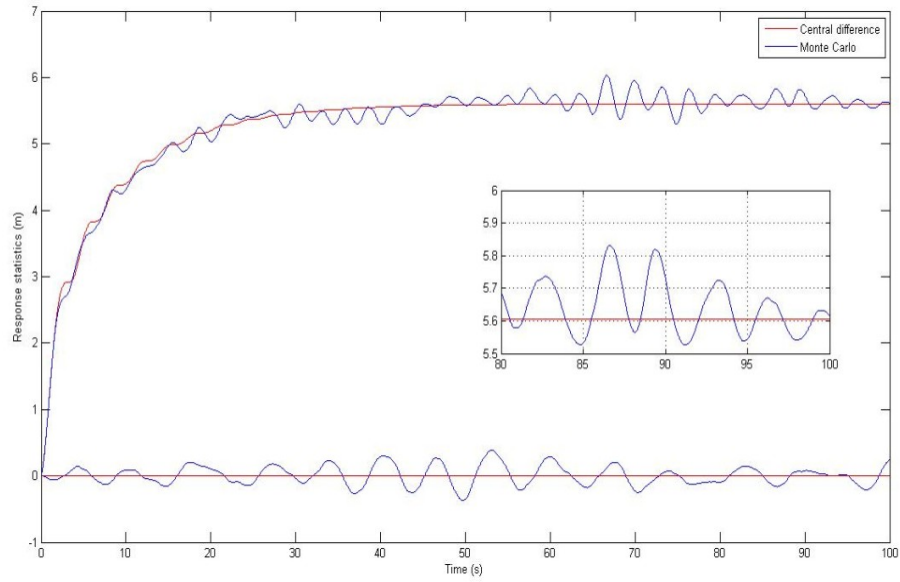


Figure 7.1: Monte Carlo simulation and stochastic central difference method result1

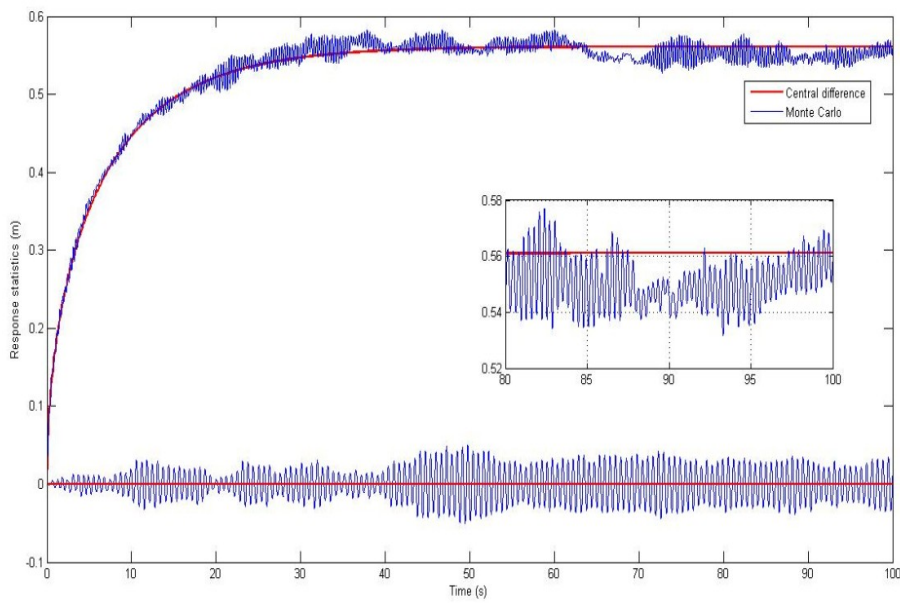


Figure 7.2: Monte Carlo simulation and stochastic central difference method result2

results are also in excellent agreement with the theory. Interestingly, as can be seen in Figure 7.2, the results of Monte Carlo simulation vibrate violently.

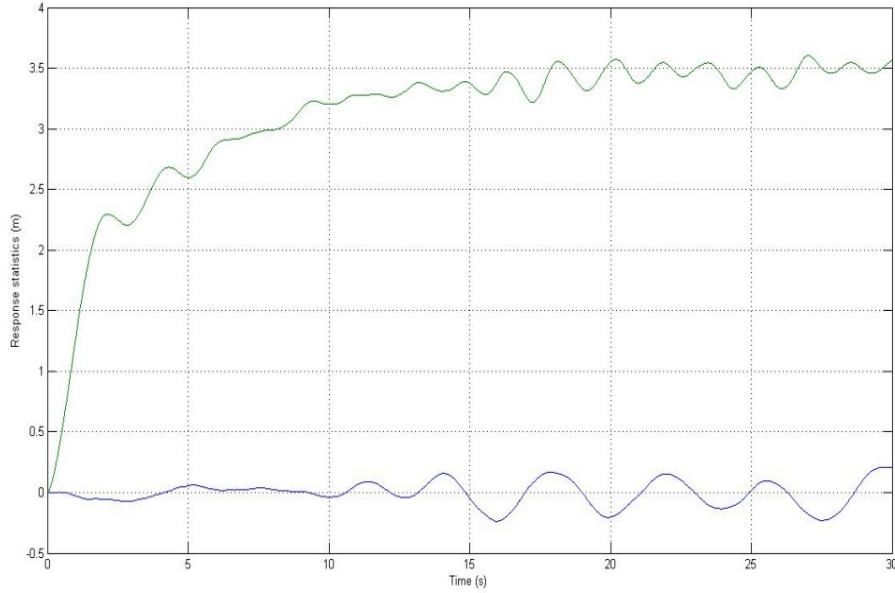


Figure 7.3: Monte Carlo simulation of duffing oscillator ($k = 1$)

In another example, consider a duffing oscillator given by [38]:

$$m\ddot{X} + c\dot{X} + k(X + \alpha X^3) = W(t) \quad (7.3)$$

with $m = 1$, $c = 0.1$, $k = 1$ (initial value), $\alpha = 0.05$ and spectral density $S_0 = 1$.

In Monte Carlo simulation (1000 samples), severe vibrations are also detected after only increasing the spring constant to $100 N/m$. The corresponding results are shown in Figure 7.3 and 7.4. Figure 7.5 indicates that the simulation result is largely improved after increasing simulation samples from 1000 to 10000. According to Figure 7.5, vibration amplitudes are weakened and the result becomes better. Several conclusions can be drawn from the above two examples:

1. Monte Carlo simulation may be very sensitive to the nature frequency of the

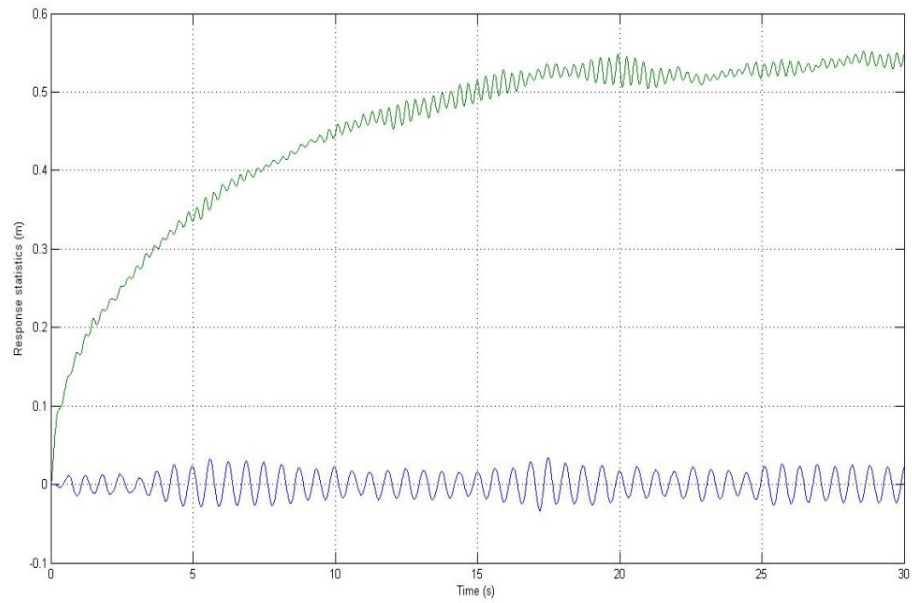


Figure 7.4: Monte Carlo simulation of duffing oscillator ($k = 100$)

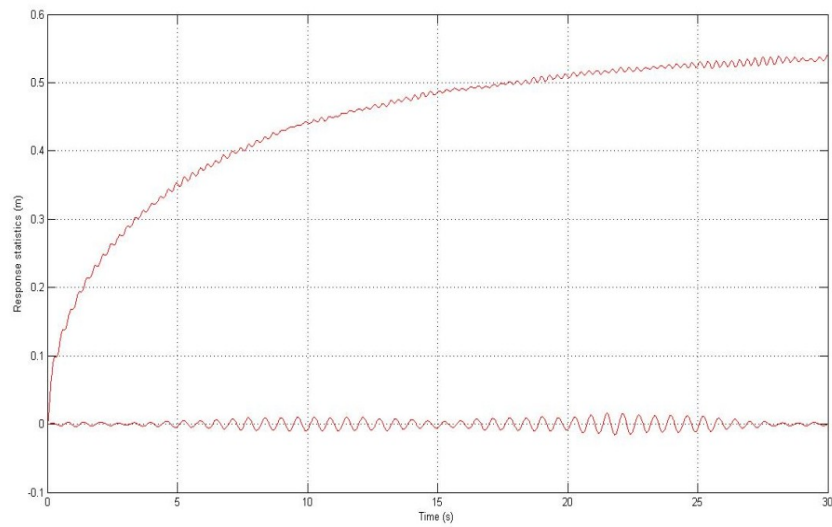


Figure 7.5: Monte Carlo simulation of duffing oscillator ($k = 100$, sample = 10000)

system.

2. The characteristic detected may exist in both linear and nonlinear systems.
3. The higher the nature frequency, the severer the vibration.
4. Increasing experimental samples can help improve the simulation results.

Considering the model employed in chapter 4 has high torsional natural frequencies, the conclusions can be used as supportive explanations for the standard deviation results presented in chapter 4.